

**Editor-in-Chief B.E.Paton**

**Editorial board:**

Yu.S.Borisov	V.F.Khorunov
A.Ya.Ishchenko	I.V.Krivtsun
B.V.Khitrovskaya	L.M.Lobanov
V.I.Kyrian	A.A.Mazur
S.I.Kuchuk	Yatsenko
Yu.N.Lankin	I.K.Pokhodnya
V.N.Lipodaev	V.D.Poznyakov
V.I.Makhenko	K.A.Yushchenko
O.K.Nazarenko	A.T.Zelnichenko
I.A.Ryabtsev	

**International editorial council:**

N.P.Alyoshin	(Russia)
U.Diltey	(Germany)
Guan Qiao	(China)
D. von Hofe	(Germany)
V.I.Lysak	(Russia)
N.I.Nikiforov	(Russia)
B.E.Paton	(Ukraine)
Ya.Pilarczyk	(Poland)
G.A.Turichin	(Russia)
Zhang Yanmin	(China)
A.S.Zubchenko	(Russia)

**Promotion group:**

V.N.Lipodaev, V.I.Lokteva  
A.T.Zelnichenko (exec. director)

**Translators:**

A.A.Fomin, O.S.Kurochko,  
I.N.Kutianova, T.K.Vasilenko

**Editor:**

N.A.Dmitrieva  
Electron gallery:  
D.I.Sereda, T.Yu.Snegiryova

**Address:**

E.O. Paton Electric Welding Institute,  
International Association «Welding»,  
11, Bozhenko str., 03680, Kyiv, Ukraine

Tel.: (38044) 200 82 77

Fax: (38044) 200 81 45

E-mail: journal@paton.kiev.ua

http://www.nas.gov.ua/pwj

URL: www.rucont.ru

State Registration Certificate  
KV 4790 of 09.01.2001

**Subscriptions:**

**\$324**, 12 issues per year,  
postage and packaging included.  
Back issues available.

All rights reserved.  
This publication and each of the articles  
contained herein are protected by copyright.  
Permission to reproduce material contained in  
this journal must be obtained in writing from  
the Publisher.  
Copies of individual articles may be obtained  
from the Publisher.

## CONTENTS

### SCIENTIFIC AND TECHNICAL

*Kyrian V.I., Dvoretzky V.I. and Malgin M.G.* Calculation of local stresses in welded joint zones of large-sized space structures ..... 2

*Ternovoj E.G. and Bondarev A.A.* Electron beam welding of thick-wall shells of aluminium AMg6 and M40 alloys ..... 6

*Kharchenko G.K., Ustinov A.I., Falchenko Yu.V., Petrushinets L.V., Grigorenko S.G., Kostin V.A. and Gurienko V.P.* Vacuum diffusion welding of  $\gamma$ -TiAl intermetallic alloy to 12Kh18N10T steel ..... 12

*Lukashenko A.G., Melnichenko T.V. and Lukashenko D.A.* Laser welding of sheet stainless steel by modulated radiation ..... 15

*Olabode M., Kah P. and Martikainen J.* Experimental review of the welding metallurgy of high-strength aluminium alloy 7025-T6 ..... 20

*Borisova A.L., Borisov Yu.S., Astakhov E.A., Murashov A.P., Burlachenko A.N. and Tsymbalistaya T.V.* Heat-protecting properties of thermal spray coatings containing quasi-crystalline alloy of the Al-Cu-Fe system ..... 31

### INDUSTRIAL

*Paton B.E., Kaleko D.M., Bulatsev A.R. and Shulym V.F.* Capacitor-discharge stud welding in vacuum ..... 37

*Poleshchuk M.A., Matveev I.V. and Bovkun V.A.* Fields of application of magnetic-pulse welding (Review) ..... 42

*Pantelejmonov E.A.* Equipment for heat treatment of welded joints on pipelines ..... 47

Theory and technology of submerged-arc welding ..... 51

News ..... 19, 50



# CALCULATION OF LOCAL STRESSES IN WELDED JOINT ZONES OF LARGE-SIZED SPACE STRUCTURES

V.I. KYRIAN, V.I. DVORETSKY and M.G. MALGIN

E.O. Paton Electric Welding Institute, NASU, Kiev, Ukraine

An approach to calculation of local stresses in zones of welded joints on structures has been developed. The approach is based on introducing absolutely rigid bodies (ARB) in the form of plane sections into the calculation model. According to plane section hypothesis, ARB provides an adequate transfer of external force effects from one fragment model to another, and permits local distribution of stresses in the zones of the welded joints to be investigated, taking into account the 3D work of the entire structure, thus providing a qualitatively new tool to allow for service loading of elements in evaluation of fatigue life.

**Keywords:** *large-sized space structures, welded joints, local stresses, finite-element method, finite-element model, absolutely rigid body, calculation*

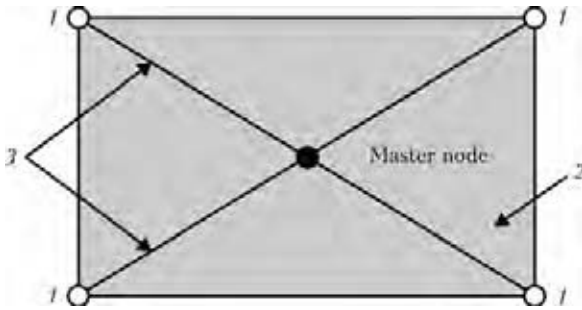
At determination of the level and repeatability of stresses in welded connections it is highly important to take into account the 3D work of the structure. The main method of 3D analysis of the stress-strain state (SSS) of structural connection and elements is the finite-element method (FEM) which allows approximating any deformed body by a model, consisting of a certain type of finite elements (FE). In mathematical terms calculation is reduced to solving a system of equations of equilibrium, consistency of deformations and physical equations.

At calculation evaluation of welded connection SSS it is necessary to adequately reflect the nature of element interaction in structural stress raiser zones with welded joint geometry. Therefore, it is necessary to approximate the entire structure by 3D FE. It is extremely difficult to perform calculations with such a detailed approximation of all the components and elements. Such calculations require application of high-power computers and are performed in exceptional cases. In common engineering practice calculation of local stresses in welded connections of metal structures of industrial buildings and engineering constructions is related to their separation into individual fragments and stage-by-stage analysis of SSS [1]. The welded structure is first considered as a rod model with specified loads and fastening conditions. Then a fragment with the studied welded connection is separated from the rod model of the entire structure and it is represented as shell FE. After calculation of a fragment from shell FE, the welded connection is separated from it, and is represented by 3D FE. Calculation of the latter gives volume distribution of SSS of each structural element present in it. In such cases, basic and quite difficult to implement is the need to establish at transition from one calculation model of a fragment to another one (with a more complex approximation), the boundary conditions in the form of nodal ties and external force impacts derived in calculation of previous fragment SSS. The complexity is increased in the case of structure operation under alternating

loading, leading to a change of the nature of interaction of structural elements of welded connections. In order to adequately represent the influence of external alternating impacts on SSS in the analyzed points of welded connection at different loading schematics, it is necessary to develop new boundary conditions for each calculation model of a fragment. This makes it more difficult to perform structure design, and analysis of the level and nature of stress variation in individual elements of welded connection at the same initial conditions (specifying the design characteristics, design loads and their comparison criteria).

At the same time, in calculations of building structures, in particular, concrete, such an FE as an absolutely rigid body (ARB) is used, which allows creating a rigid constraint between models of fragments, consisting of various FE types [2, 3]. It is used for transfer of information on SSS from one part of structure model to another one. Used as ARB is one of the structural (connecting) elements, as a result of which the entire structure is considered as one calculation model. The idea of ARB application in the form of structural elements is quite good and well-proven at rather simple forms of transition: combining the model of a column of industrial buildings with the model of covering plate from plate FE; combining rod models of ribs of bridge structure beams with the roadway slab from plate FE, etc. At evaluation of welded connection SSS, however, it is difficult to apply ARB in the form of a structural element, as the transition itself (welded connection) should be analyzed.

As deformation of welded structure stressed elements quite satisfactorily obeys the plane-section hypothesis, at each transition from one calculation model of a fragment to another one, it is the most rational to introduce ARB not in the form of a structural element, but as plane ARB — section of structural element of the next model. If certain conditions of interaction of ARB in the form of a plane section with fragment models are followed, it is believed to be possible to perform, using FEM, calculations of local stresses in welded connections of structures of any degree of complexity, adequately transferring hereditary information about SSS from one calculation model to another one, allowing for the loading fea-



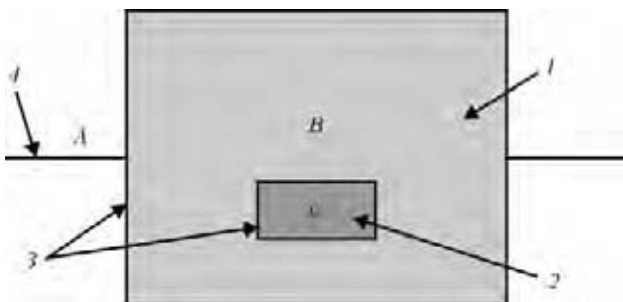
**Figure 1.** ARB schematic: 1 – master node; 2 – ARB; 3 – rigid connection between the nodes (radius-vector)

tures. When ARB in the form of a plane section is used in interconnection with plane-section hypothesis, it is important to ensure fulfillment of the two main conditions: master nodes of the previous model and slave nodes of the next model are located in one plane; interaction of master node with the slave one is taken to be such, at which the regularity of structural element behaviour is preserved. Here, displacements  $u_s$  and angles of rotation  $\theta_s$  of each slave node are connected through radius-vector  $\rho_{m-s}$  (Figure 1) with displacements  $u_m$  and angles of rotation  $\theta_m$  of master node by the following dependence:

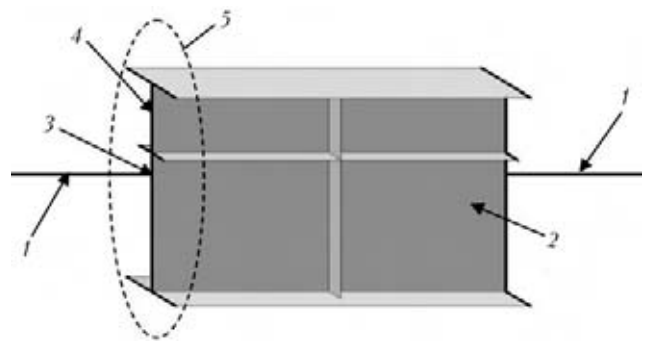
$$\begin{pmatrix} u_s \\ \theta_s \end{pmatrix} = \begin{pmatrix} u_m + \theta_m \rho_{m-s} \\ \theta_m \end{pmatrix}.$$

In this work a procedure is proposed for calculation of local stresses in the zones of welded joints of large-sized space structures using ARB. In terms of the proposed procedure such notions as structure fragment and node are introduced. A fragment is any part of the structure, including a node. Taken as the node is that part of the structure (fragment), in which the mutual influence of structural elements on its SSS is manifested. For analysis of the real work of the studied welded connection, using standard FE library, one 3D FE model of the entire structure is created with the specified accuracy of approximation of the accepted structural forms. This model, allowing for space interaction of structural elements, analyzes welded connection SSS based on successive consideration of models with different types of FE (Figure 2, A–C): rod model of a structure, shell model of a fragment, and 3D model of a node.

At the first stage the rod model is considered, in which the structure load-carrying elements are approximated by rod FE with the respective rigidity



**Figure 2.** Schematic of calculation model of structure with ARB for calculation of local stresses in welded connections by the proposed procedure: 1 – shell model of structure fragment; 2 – 3D model of welded connection; 3 – ARB; 4 – rod model of structure



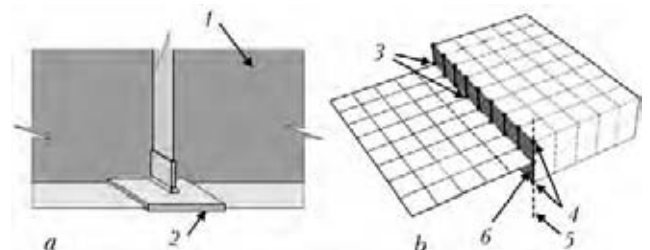
**Figure 3.** Schematic of introducing ARB between the rod and shell models: 1 – rod FE; 2 – shell model of structure fragment; 3 – center of gravity of section; 4 – ARB; 5 – section of structural element of shell model of fragment

characteristics. Forces in all the elements are determined by the results of its calculation. At the second stage rod FE in the analyzed locations of the structure are replaced by 3D model of the fragment.

For adequate transfer of membrane and bending forces through ARB from rod model A to shell model of fragment B (see Figure 2), master node is introduced by rod FE and is located in the center of gravity of the section of adjacent structural element of a fragment with shell approximation, and slave nodes are represented by shell FE (Figure 3).

At the third stage in the locations of analyzed welded connection C (see Figure 2) shell FE are replaced by connection model with 3D FE approximation (Figure 4, a). Here transfer of membrane and bending forces through ARB from shell model of fragment B to 3D model of welded connection C (see Figure 2) is ensured as a result of superposition of median surface of shell FE on the neutral line of 3D model section. Master nodes are assigned by shell FE, and slave nodes – by 3D FE. Master and slave nodes belong to FE face of the next model (Figure 4, b).

So, the constructed calculation model of a structure with ARB ensures adequate transfer of external force impacts from fragment to fragment and enables studying local stress distribution in welded joint zone, taking into account 3D work of the structure. Its application greatly simplifies analysis of the actual operation of structure welded connections, allowing for interaction of structural elements included into the connection at application of alternating load, for instance, reversed load. Thus, the procedure provides a qualitatively new tool for analysis and allowing for



**Figure 4.** Replacement of shell FE by 3D model (a) and introduction of ARB between the shell and 3D FE (b): 1 – shell model of structure fragment; 2 – 3D model of connection; 3 – master nodes; 4 – slave nodes; 5 – face with master and slave node; 6 – ARB

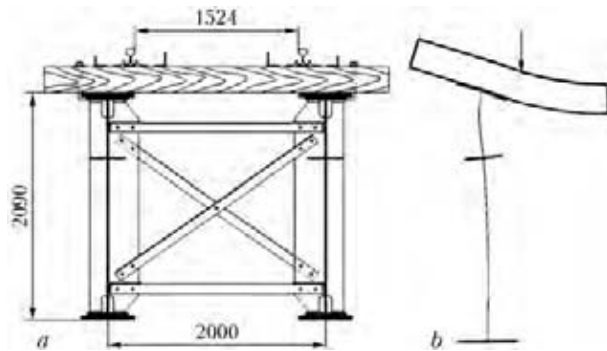


Figure 5. Cross-section of welded span structure of bridge (a) and out-of-plane deformation of its web (b)

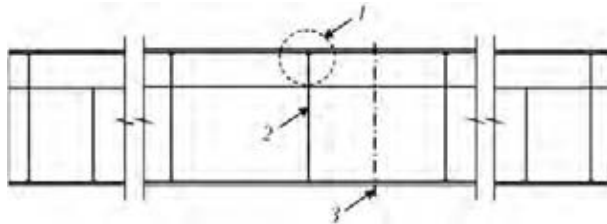


Figure 6. Location of the analyzed welded connection: 1 – analyzed welded connection; 2 – transverse stiffener; 3 – span middle

service load of welded connections at assessment of fatigue life of structures operating under the conditions of alternating impacts.

In operation of bridge span structures the most critical elements are welded connections, exposed to

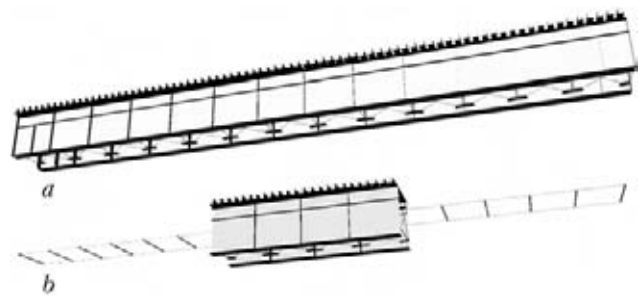


Figure 7. Calculated models of all-welded span structure (for explanations see the text)

direct impact of vehicles [4]. Their fatigue strength largely depends on the features of element interaction, allowing for application of concentrated loads. Therefore, for substantiation and evaluation of the proposed procedure effectiveness, calculation of SSS of a welded connection of a typical all-welded span structure of a railway bridge was performed.

The span structure consists of two welded girders with 27 m span, combined into space structure by a system of longitudinal and transverse braces (Figure 5, a). Height of girders is equal to 2.09 m, distance between their axes is 2 m. Girder webs are strengthened by transverse stiffeners with 2 m spacing, as well as longitudinal stiffeners along the entire span length. Bridge deck is supported by wooden sleepers.

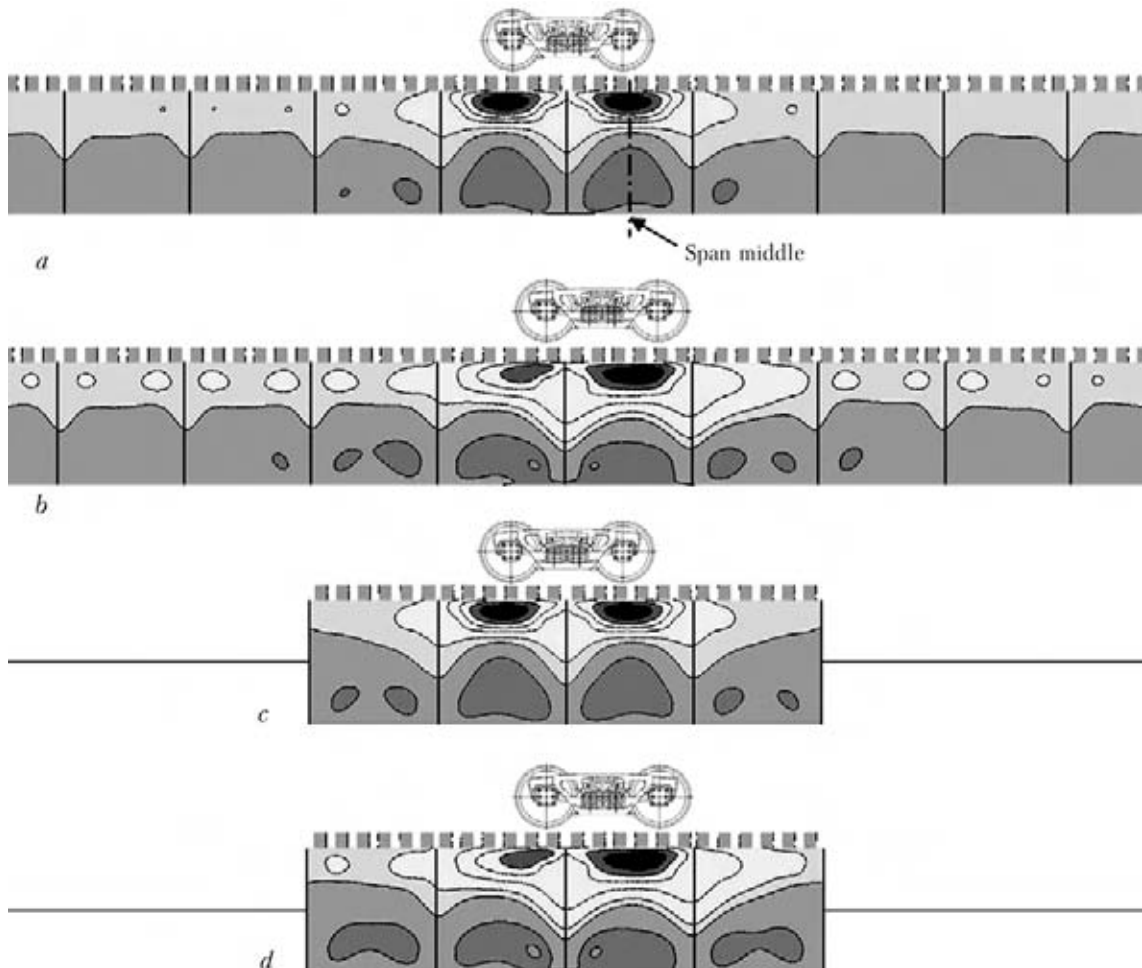


Figure 8. Isofields of transverse displacements of vertical web in the bays by the first (a, b) and second (proposed) (c, d) model



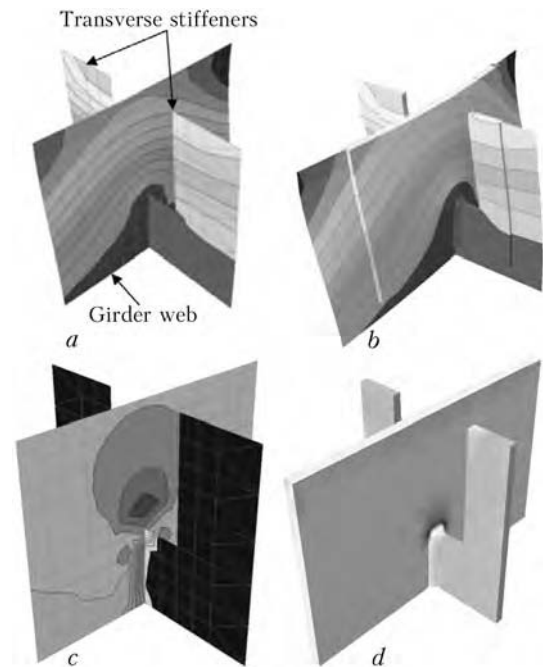
Passage of each axle of moving load has an important influence on formation of span structure SSS that, in its turn, causes a change of local interaction of elements. In addition to the main bending of the girders, it also leads to torsion of the upper girth and out-of-plane deformation of its web in the bays (Figure 5, *b*), as well as local bending of elements in the zone of transverse stiffeners. Local interaction of elements changes significantly, depending on the moving load position. Therefore, fatigue analysis of welded connections should take into account the features of the nature of change, quantity and repeatability of the applied alternating impacts.

As verification calculation for substantiation of the proposed procedure postulates, SSS of elements of a welded connection for welding transverse stiffeners in the span middle part (Figure 6) obtained from two calculation models was compared, taking into account the different position of the freight car truck. The first model approximated the structure load-carrying elements by shell FE along the entire length of the span (Figure 7, *a*), and the second model was constructed by the proposed procedure (Figure 7, *b*).

At analysis of formation of span structure SSS by the results of numerical calculation by the first model a marked dependence of the nature of structure element interaction on moving load position was noted. Truck axle passage over the adjacent bays essentially influences the redistribution of web SSS. At symmetrical position of the truck relative to the transverse stiffener, a symmetrical deformation of the web develops in the bays adjacent to the analyzed welded connection (Figure 8, *a*). Maximum transverse deformations of one sign form in the web upper parts, and those of the other sign form in the lower part. This corresponds to S-shape of transverse out-of-plane bending of the web. Here, welded connection elements have their own quite definite kind of loading. As truck axle approaches the transverse stiffener, SSS redistribution starts, leading to asymmetry of web deformation (Figure 8, *b*). Loading level of connection elements is changed. By the results of investigations of the regularities of web SSS change in the adjacent bays at load passage, it is established that in order to represent an adequate loading of welded connection, it is necessary to analyze a fragment, including four bays.

Comparison of the results of calculation by the first and second models (see Figure 8) showed that regularities of SSS formation in the considered sections practically coincide by their nature and level. SSS can slightly differ on fragment boundaries. On the other hand, it does not in any way affect the results of analysis of the studied connection. Thus, in order to determine the real work of welded connections of span structures, it is quite sufficient to perform detailed approximation of just the fragment, in which the analyzed welded connection is located.

Equivalence of evaluation of web SSS in the studied bays by both the models, allowed performing comparative analysis of SSS formation in the zone of interruption of a weld made for attachment of the trans-



**Figure 9.** SSS in the zone of interruption of weld made for attachment of transverse stiffener to the web of span structure: *a, b* – isofields of transverse displacements of elements in the shell and 3D models; *c, d* – distribution of local stresses on the outer surface of the girder web in the shell and 3D models, respectively

verse stiffener to the web. By the results of calculations it was established that the 3D model has an adequate loading through ARB in the form of a plane section, that is indicated by the similarity of displacements (Figure 9, *a, b*). On the other hand, the nature of distribution of local stresses in the models differs significantly. Local stresses in the weld zone in the 3D model give a more comprehensive representation of its actual condition (Figure 9, *d*). Therefore, in evaluation of service life of span structures analysis of the nature of the change in local SSS of welded connection by 3D model is preferable.

Thus, introduction of ARB in the form of a plane section connecting in one calculation model of the structure fragments from FE of different types, greatly simplifies analysis of the real work of welded connections, allowing for 3D interaction of structural elements included into the connection under the conditions of alternating loading. ARB in interrelation with the plane-section hypothesis ensures an adequate transfer of external force impacts from one model of the fragment to another one and enables studying the local distribution of stresses in the welded joint zone, allowing for 3D work of the entire structure. This provides a qualitatively new tool for allowing for service loading of elements in evaluation of fatigue life of various-purpose metal structures.

1. Vinokurov, V.A., Kurkin, S.A., Nikolaev, G.A. (1996) *Welded structures. Fracture mechanics and criteria of serviceability*. Ed. by B.E. Paton. Moscow: Mashinostroenie.
2. Gorodetsky, A.S., Evzerov, I.D. (2007) *Computer models of structures*. Kiev: Fakt.
3. Perelmuter, A.V., Slivker, V.I. (2007) *Computational models of buildings and possibilities of their analysis*. Moscow: DMK Press.
4. Luchko, J.J., Sulym, G.T., Kyrian, V.I. (2004) *Fracture mechanics of bridge structures and methods of prediction of their residual life*. Ed. by J.J. Luchko. Lviv: Kamenyar.



# ELECTRON BEAM WELDING OF THICK-WALL SHELLS OF ALUMINIUM AMg6 AND M40 ALLOYS

E.G. TERNOVOJ and A.A. BONDAREV

E.O. Paton Electric Welding Institute, NASU, Kiev, Ukraine

Results of investigations on EBW of 40–90 mm thick semi-finished products of aluminium alloys AMg6 and M40 are given. Optimal welding parameters were selected. Properties, microstructural peculiarities and hardness of the resulting joints were studied for horizontal and vertical welds. The EBW technology in fabrication of large-size thick-walled shells of aluminium alloys was developed and passed the industrial testing.

**Keywords:** electron beam welding, aluminium alloys, shells, longitudinal and circumferential joints, welding conditions, joint properties, hardness, microstructure, industrial testing

The comparison of technological capabilities of the known methods of fusion welding showed that the most challenging method in manufacture of large-size shells of aluminium alloys of large thicknesses is electron beam welding (EBW) [1, 2]. To obtain the required properties of joints in EBW it is necessary to preset the optimal condition parameters, sizes and geometry of fusion zone, sizes of softening zone, etc. [3–9].

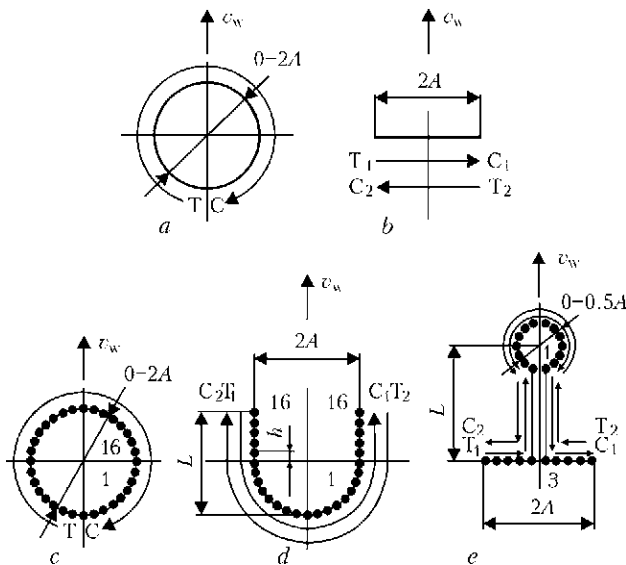
In EBW of AMg6 and M40 alloys the decrease of content of elements with high vapor pressure in weld metal is possible which results in decrease of strength characteristics, formation of porosity and cracks in weld metal and near-weld zone [10–14]. In this case the authors of works [1, 2, 5, 9] recommend horizontal arrangement of electron beam which favors the sufficient decrease of defects in weld metal.

The purpose of this work is the development and industrial testing of EBW technology for circumferential and longitudinal butts of shells of aluminium AMg6 and M40 alloys of 40–90 mm thickness, providing preset sizes of fusion zone, formation of two-side reinforcement bead and high properties of joints across the whole thickness of a butt.

During selection of condition parameters, level of deepening of focal spot and working distance for maximum penetration, welding of specimens of AMg6 and M40 alloys with partial penetration without beam scanning was performed. The length of specimens was 500 mm, thickness – 40 mm. The specimens were welded from power source ELA 60/60 in the installation UL-179 at residual pressure in the chamber of  $1.33 \cdot 10^{-3}$  Pa. The welding speed was set constant at all conditions and equal to 36 m/h. Basing on carried out experiments the working distance of 220 mm was selected at deepening of focal spot from –10 to +20 mm.

The optimization of welding conditions with through penetration was performed on the plates of AMg6 alloy of  $500 \times 200 \times 40$  mm size at the welding speed of 18–85 m/h by a beam without deflections and scanning beam of horizontal and vertical upward welds. The beam current depending on speed of welding varies in the range of 130–275 mA.






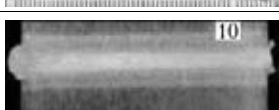




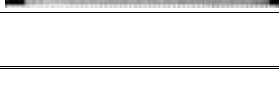
During welding of specimens of butt joints the technological circular and transverse scans, as well as discrete scans with adjustable time of delay of beam in the spots of its interruptions were applied [15, 16]. The trajectories of scanning were selected in a form of different curves of the second order (circle, semi-circle, ellipse, semi-ellipse) and their combination with longitudinal or transverse scanning (Figure 1), and shape and parameters were controlled using oscillograph S1-83. Independently of type of scanning or correlation of time of delays of beam on the trajectory of scanning, the amplitude of scanning across the butt was tried to be unchanged in welding of the same thickness in all technological variants and all spatial positions of joints (Figure 2). The conditions of welding of butt joints of AMg6 and M40 alloys and their macrosections are given in Table 1.



**Figure 1.** Shapes and trajectories of scans applied in welding of specimens of aluminium alloys: *a, b* – circular and transverse continuous scanning; *c–e* – discrete scanning; *A* – scanning amplitude; *h* – pitch of discrete movement; 1 (minimal), 16 (maximal) and 3 – areas of front and rear fronts of weld pool with corresponding heat input



**Table 1.** Conditions of welding of upwards vertical and horizontal welds on plates of AMg6 and M40 alloys by horizontal beam

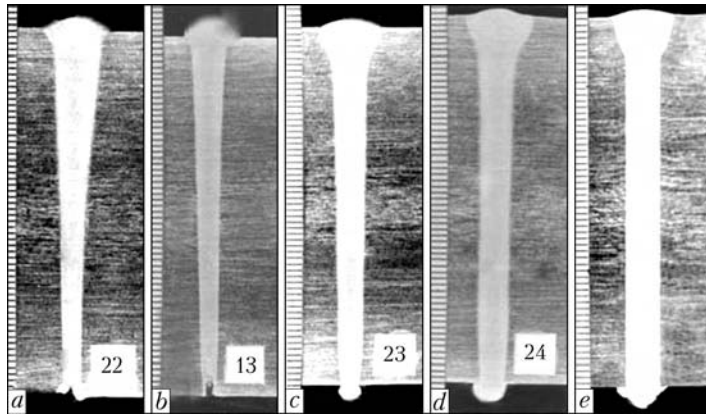
Number of experiment	Alloy	Spatial position of butt welding	Thickness of plates, mm	Beam current, mA	Focusing current, mA	Welding speed, m/h	Macrosection
1	AMg6	Horizontal	40	220	865	30	
2		Vertical upwards	60	275	895	20	
3		Same	90	330	915	12	
4*		Horizontal	90	330	915	12	
5*	M40	Vertical upwards	40	395	870	45	
8		Horizontal	40	395	870	45	
9		Vertical upwards	50	365	822	25	
10		Same	50	465	902	30	
11		»	50	365	870	36	
12		»	50	495	902	45	
13		Horizontal	65	630	915	36	

\*Welding using scanning beam with a circular scan.

The evaluation of quality of welded joints was performed applying 100 % control of density of joints using X-ray method, measuring of geometric sizes of penetration zone and HAZ on transverse sections, determining the composition of weld metal according to base alloying components using method of local spectral analysis, investigating the microstructure of different zones of welded joints and distribution of hardness, determining the strength characteristics of joints and their scattering across the thickness of billets.

The X-ray control of joints did not detect any large defects in a form of pores, cracks, lacks of penetration or voids in welds.

While producing horizontal welds on the plate of AMg6 alloy the clearly distinct structural heterogeneity across the weld section is observed, especially in its lower part (Figure 3). The presence of practically continuous chain of secondary phase precipitates across the layers of crystallization (Figure 3, c) results in considerable anisotropy of properties across the section of a butt and large discrepancy of their values in the range of one batch of specimens being tested. While producing vertical upward joints of plates of M40 alloy the defects in a form of non-fused hollows closer to root weld and also microdefects in HAZ metal in a form of low-melting intergranular layers,



**Figure 2.** Macrosections of butt joints of AMg6 alloy of 60 mm thickness produced using scanning: *a, b* – respectively, continuous circular and transverse scanning; *c* – discrete circular scanning; *d* – discrete U-shape scanning; *e* – discrete combined scanning (circle with transverse scanning); *a, d* – welding using horizontal beam on the vertical plane; *b, c, e* – welding upwards using horizontal beam

coagulated inclusions and preliminary fused eutectic phases facilitating formation of single micropores and porosity resulting in decrease of impact toughness along the fusion boundary are possible. The coefficient of strength decreases to the level of  $0.85\sigma_t$  of base metal.

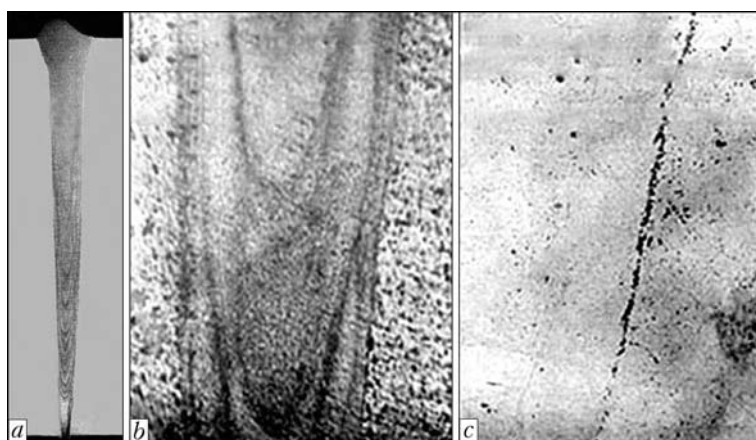
The processing and analysis of results of evaluation of joints of AMg6 and M40 alloys with parallel boundaries of penetration zone prove that in this case the stable weld formation across the whole depth independently of thickness of semi-products at welds width of 5–8 mm and double-sided formation of reinforcement beads (macrosections in Table 1) is achieved. In addition in the course of mechanical tests of joints their high properties were established and metallographic examinations of weld metal and HAZ showed that using this method the sizes of grains in upper, middle and root parts of weld metal are refined and stabilized, the content of hydrogen and thickness of precipitates in intergranular layers are reduced, HAZ sizes are decreased.

The chemical compositions of base and weld metal of produced joints of AMg6 (thickness of 40, 60 and 90 mm) and M40 (thickness of 40, 50 and 65 mm) alloys appeared to be identical for all thicknesses. Thus, AMg6 alloy contains (wt.%): 6.65–6.75 Mg;

0.55–0.59 Mn; Al – base, and alloy M40 contains 5.0 Cu; 3.60–3.70 Mg; 0.43 Mn; Al – base. The losses of magnesium for evaporation in weld metal did not exceed 0.02–0.04 %.

The results of mechanical tests of produced welded joints of AMg6 and M40 alloys for all thicknesses evidence (Tables 2 and 3) that joints are characterized by high stability of values of ultimate tensile strength and impact toughness, whereas heterogeneity of properties across the whole thickness of the butt is practically absent. The most peculiar feature is that the impact toughness of joints with Charpy notch across the middle of the weld is by 15–20 % higher than that in base metal and preserved almost at the same level when the notch along the fusion boundary was performed.

The analysis of microstructure of joints of AMg6 alloy detected by reagent of Keller showed that except the  $\alpha$ -solid solution of magnesium and manganese, there are double and more complicated phases in aluminium, arranged in the form of thin, sometimes continuous chains along the grain boundaries in the base metal and between branches of dendrites in a weld metal (Figure 4). In the lower part of joints, due to the higher rates of solidification, the central dendrites



**Figure 3.** Laminar structural heterogeneity in weld on AMg6 alloy of 90 mm thickness produced by EBW with circular scanning: *a* – macrosection of joint; *b* – macrostructure ( $\times 20$ ) of joint in the lower part of weld; *c* – microstructure ( $\times 300$ ) of weld at the area of secondary phase precipitation





**Table 2.** Mechanical properties of base metal and EB-welded joints of plates of AMg6 alloy

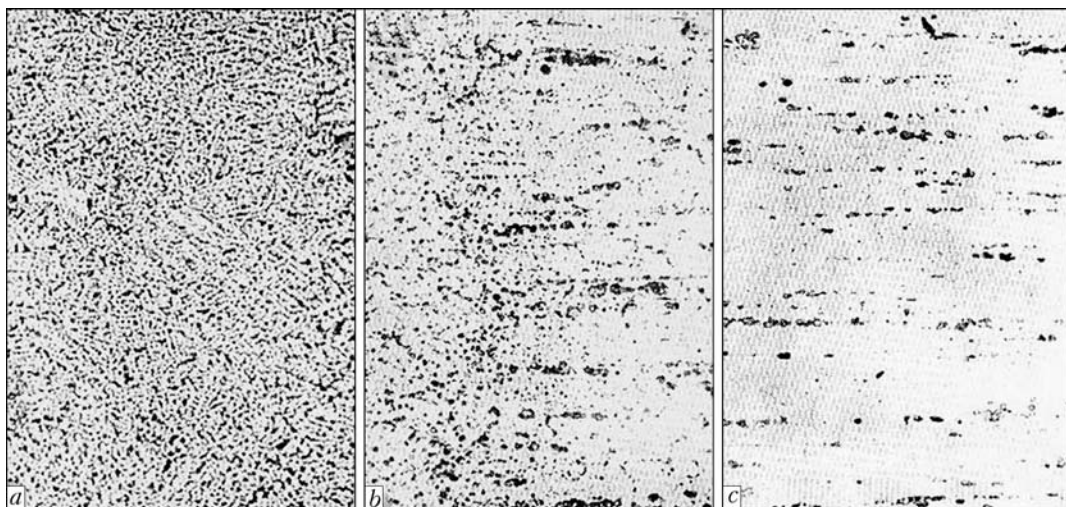
Number of specimen	Thickness of BM and butt, mm	$\sigma_t$ , MPa	KCV, J/cm <sup>2</sup>		Object of testing
			Notch across the weld middle	Notch along the weld boundary	
1	40	$\frac{350-355}{360}$	$\frac{22-25}{23}$	–	BM, upper part
2*		$\frac{262-309}{280}$	$\frac{20-21}{20}$	$\frac{12-15}{14}$	Butt joint, defects in a form of holes
3*		$\frac{313-324}{324}$	$\frac{23-26}{25}$	$\frac{15-17}{16}$	Butt joint, laminar heterogeneity
4		$\frac{345-350}{348}$	$\frac{27-29}{28}$	$\frac{18-22}{20}$	Butt joint
5	60	$\frac{346-352}{350}$	$\frac{18-19}{18}$	–	BM
6		$\frac{335-340}{340}$	$\frac{25-27}{27}$	$\frac{18-22}{21}$	Butt joint
7	90	$\frac{342-354}{350}$	$\frac{18-19}{19}$	–	BM
8		$\frac{335-338}{336}$	$\frac{22-25}{23}$	$\frac{17-19}{19}$	Butt joint

\*Welding by circular scanning beam.

**Table 3.** Mechanical properties of base metal and EB-welded joints of plates of M40 alloy

Number of specimen	Thickness of BM and butt, mm	$\sigma_t$ , MPa	KCV, J/cm <sup>2</sup>		Object of testing
			Notch across the weld middle	Notch across the weld boundary	
1	40	$\frac{400-415}{400}$	$\frac{9.7-11.0}{10.8}$	–	BM
2*		$\frac{313-322}{320}$	$\frac{3-6}{5}$	$\frac{5.0-5.6}{5.0}$	Butt joint
3		$\frac{388-392}{390}$	$\frac{5.1-6.2}{5.3}$	$\frac{6.8-7.2}{7.0}$	Same
4	50	$\frac{410-420}{415}$	$\frac{9.8-11.5}{10.5}$	–	BM
5		$\frac{365-375}{370}$	$\frac{7.6-8.5}{7.9}$	$\frac{6.9-7.8}{7.1}$	Butt joint

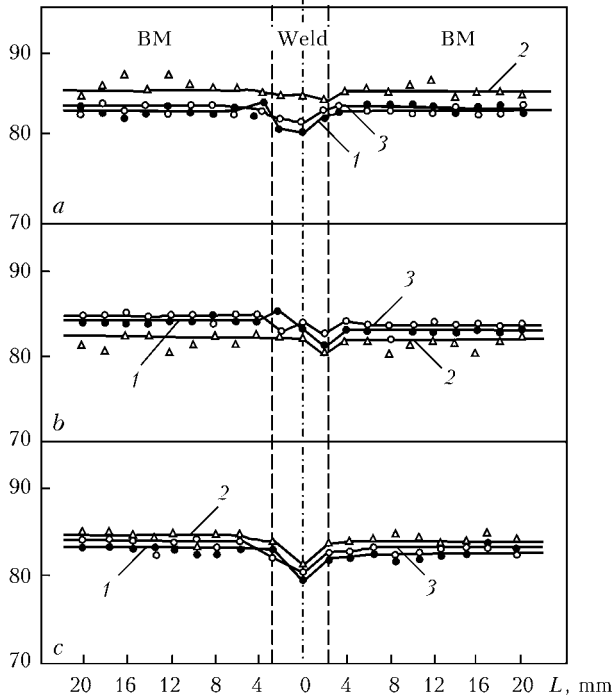
\*Welding by circular scanning beam.



**Figure 4.** Microstructure ( $\times 160$ ) of characteristic zones of welded joint of AMg6 alloy of 40 mm thickness: *a* – weld metal; *b* – fusion zone; *c* – base metal



HRB

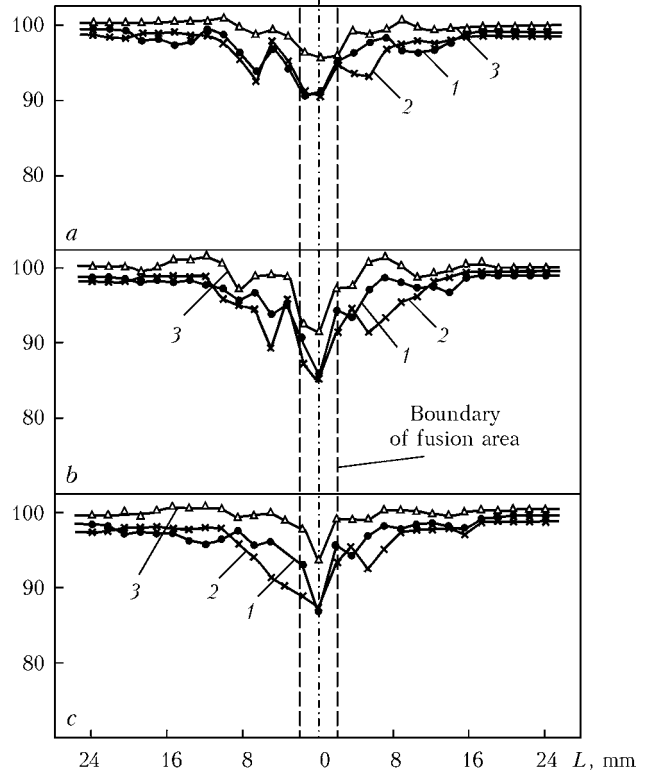


**Figure 5.** Distribution of hardness across the EB-welded joints of AMg6 alloy 90 mm thick (rolled metal): *a-c* – levels of hardness measurements at the distance from the plate surface on the side of beam input are 10, 45, 80 mm, respectively; 1 – continuous circular scanning (butt); 2, 3 – discrete scanning (2 – penetration; 3 – butt)

are formed with more branched structure as compared to the structure of upper part of a butt. There are no defects in fusion zone except of single micropores.

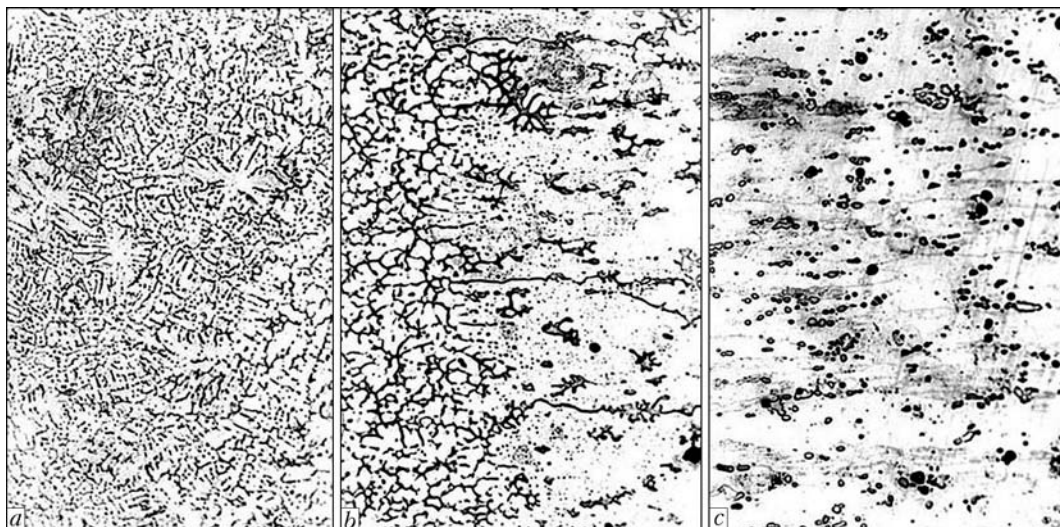
During measurement of hardness of welded joints of AMg6 alloy of 90 mm thickness using Rockwell device with a ball of 1 mm at loading of 600 N at three levels along the section of a butt, the considerable decrease in hardness of base metal (*HRB* 82–84) up to the fusion boundary was not observed. In the upper part of a butt the hardness of weld metal is *HRB* 80 and is insufficiently increased up to *HRB* 82–83 in the middle part of a weld, and closer to reverse bead the hardness is decreased to *HRB* 79–80

HRB

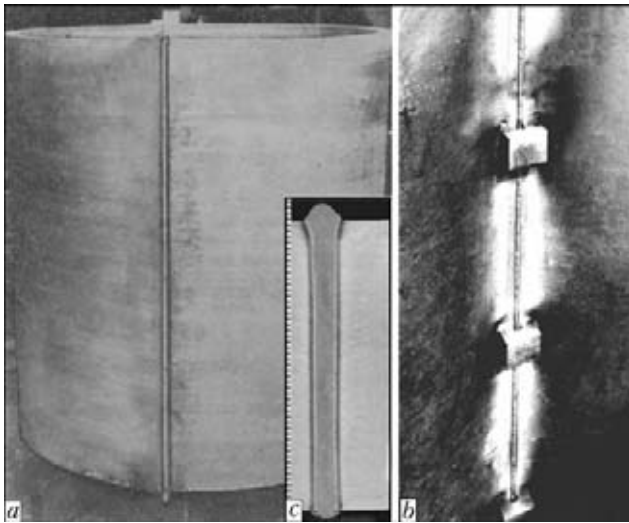


**Figure 6.** Distribution of hardness in EB-welded joints of M40 alloys 50 mm thick: 1–3 – the same as in Figure 5

(Figure 5). The selection of optimal welding conditions of butt joints for M40 alloy was performed on plates of 50 mm thickness at the speeds of 25, 30, 36 and 45 m/h (see Table 1). The measurement results of hardness are shown in Figure 6. From the Figure it is seen that decrease in welding speed from 45 to 25 m/h results in increase of HAZ (from 9 to 13 mm to one side, including a weld), but it does not almost change a hardness of weld metal at all levels of measurements. In addition using heat treatment (artificial ageing) the hardness of weld metal can be increased. The influence of welding speed on microstructure of weld and near-weld zone showed that decrease of welding speed makes weld structure and eutectic in-



**Figure 7.** Microstructures ( $\times 160$ ) of different zones of welded joint of M40 alloy 50 mm thick: *a* – weld metal; *b* – fusion zone; *c* – base metal



**Figure 8.** Appearance of welded shell of M40 alloy (a), reversed bead of longitudinal weld (b) and microsection of joint (c)

terlayers in HAZ metal coarser, though the weld structure remains rather fine-dispersed and uniaxial. The influence of welding speed on recrystallization of base metal was studied. The metallographic analysis showed that area of base metal recrystallization in welding at the speed of 25 m/h does not exceed 4 mm. The microstructure of weld and near-weld zone for butt joint of M40 alloy of 50 mm thickness produced at the speed of 45 m/h is given in Figure 7. As is seen, the decrease of welding speed to 25 m/h does not influence the change of weld metal composition. However, the softening along the fusion boundary and decrease of impact toughness by 2 times as compared to base metal are observed. The increase of welding speed to 45 m/h and artificial ageing of welded joints allowed increasing the impact toughness in HAZ to 20 % as compared to that at 25 m/h.

As a result of carried out works on EBW semi-finished products of aluminium AMg6 and M40 alloys, the industrial testing of technology of welding the shells with circumferential and longitudinal joints of 40, 50, 60, 65 and 90 mm thickness was developed and carried out at the PA «Strela» (Orenburg, RF). In Figure 8 the shell with outside diameter of 1250 mm, height of 1500 mm and wall thickness of 50 mm of sheet rolled metal of M40 alloy with longitudinal butt joint produced by EBW is shown, and in Figure 9 – shell with inner diameter of 800 mm, height of 1700 mm and thickness of walls of 40, 60 and 90 mm with circumferential butt joints, made of AMg6 alloy forgings.



**Figure 9.** Appearance of welded shell with changeable thickness of wall made of AMg6 alloy forgings (a), and macrosection of joint (b)

1. Bondarev, A.A. (1980) EBW, its advantages and main principles in development of welding technology of aluminium alloys. In: *Proc. of 1st All-Union Conf. on Welding of Light, Nonferrous and Refractory Metals and Alloys* (Kiev, 21–23 Nov., 1978). Kiev: Naukova Dumka, 106–110.
2. Bondarev, A.A. (1984) State-of-the-art and advantages of electron beam welding process of aluminium alloy structures. In: *Proc. of Soviet-American Seminar on Welding of Aluminium Alloys of Cryogenic and General Purposes* (Tashkent, 17 Oct. 1982). Kiev: Naukova Dumka, 10–19.
3. Olshansky, N.A., Khokhlovsky, A.S., Balayan, R.F. et al. (1985) Properties of welded joints of large thickness alu-

- minium and magnesium alloys made by EBW. In: *Proc. of 2nd All-Union Conf. on Welding of Light, Nonferrous and Refractory Metals and Alloys* (Tashkent, 17 Oct. 1982). Kiev: Naukova Dumka, 164–166.
4. Pisarsky, V.I. (1977) EBW of large thickness aluminium alloys. In: *Proc. of All-Union Conf. on EBW* (Kiev, 17–29 Oct. 1975). Kiev: Naukova Dumka, 168–171.
5. Bondarev, A.A., Tretyak, N.G., Kuzmenok, O.S. et al. (1978) Technology of EBW of large-sized structures of AMg6 alloy. *Avtomatich. Svarka*, **9**, 54–56.
6. Bondarev, A.A., Tretyak, N.G. (1980) Influence of parameters on sizes of penetration zone and joint properties in electron beam welding of alloy 1201 plates. In: *Proc. of 1st All-Union Conf. on Welding of Light, Nonferrous and Refractory Metals and Alloys* (Kiev, 21–23 Nov. 1978). Kiev: Naukova Dumka, 114–117.
7. Nazarenko, O.K., Kajdalov, A.A., Kovbasenko, S.N. et al. (1987) *Electron beam welding*. Kiev: Naukova Dumka.
8. Khokhlovsky, A.S., Yakhontov, S.A. (1980) Effect of hydrodynamic processes in penetration channel on EBW joints of light alloys. *Trudy MEI*, **475**, 9–21.
9. Voropaj, N.M., Bondarev, A.A., Ivanov, N.P. et al. (1972) Development of EBW technology of product bodies of AMg6 alloy. *Svarochn. Proizvodstvo*, **3**, 18–20.
10. Bondarev, A.A., Voropaj, N.M., Rabkin, D.M. et al. (1972) EBW of aluminium alloy spherical vessels. *Avtomatich. Svarka*, **5**, 44–47.
11. Zajtsev, V.I., Skorospelov, V.V. (1980) Experience in fabrication of welded vessels of heat-resistant aluminium alloy M40. In: *Proc. of 1st All-Union Conf. on Welding of Light, Non-Ferrous and Refractory Metals and Alloys* (Kiev, 21–23 Nov. 1978). Kiev: Naukova Dumka, 76–81.
12. Ishchenko, A.Ya., Ignatiev, V.G., Chayun, A.G. et al. (1979) Weldability of aluminium alloy M40. *Avtomatich. Svarka*, **10**, 15–18.
13. Bondarev, A.A., Rabkin, D.M. (1974) Evaporation of volatile elements in EBW of aluminium alloys. *Ibid.*, **3**, 13–16.
14. Detsik, N.N. (1980) Peculiarities of evaporation of weld alloyed elements in intermediate vacuum EBW. *Elektrotekhn. Promyshlennost. Series Electric Welding. Issue 4*, 1–4.
15. Bondarev, A.A., Skryabinsky, V.V. (1987) Welding of aluminium alloys with programming of electron beam density distribution by heating spot. In: *Automatic control of technological process of electron beam welding*. Kiev: PWI.
16. Lankin, Yu.N., Bondarev, A.A., Dovgodko, E.I. et al. (2009) Control system for beam scanning in electron beam welding. *The Paton Welding J.*, **9**, 13–16.



# VACUUM DIFFUSION WELDING OF $\gamma$ -TiAl INTERMETALLIC ALLOY TO 12Kh18N10T STEEL

G.K. KHARCHENKO, A.I. USTINOV, Yu.V. FALCHENKO, L.V. PETRUSHINETS, S.G. GRIGORENKO, V.A. KOSTIN and V.P. GURIENKO

E.O. Paton Electric Welding Institute, NASU, Kiev, Ukraine

A two-stage technology for vacuum diffusion welding of intermetallic alloy  $\gamma$ -TiAl to 12Kh18N10T steel using interlayers has been developed. It is shown that application of a nanolayered interlayer of Ti-Al system from the side of intermetallic and nickel interlayer from the side of steel provides a uniform distribution of microhardness in the bond.

**Keywords:** vacuum diffusion welding,  $\gamma$ -TiAl intermetallic alloy, 12Kh18N10T steel, nanolayered insert, joint zone, microstructure, microhardness

Complexity of welding intermetallics of Ti-Al system to steel is determined by low mutual solubility of titanium and iron, whereas formation of carbides, intermetallics and eutectics in the joint zone makes it impossible to perform direct welding of intermetallics to steel by any of the known fusion welding processes.

As a rule, joints of titanium and its alloys to steel, made by diffusion welding, have low impact toughness values [1–3].

In solid-phase welding of titanium to steel, interlayers, in particular niobium (or vanadium) and copper, are used to produce sound joints without formation of brittle intermetallic phases in the butt [4, 5]. These materials, however, differ from each other both by melting temperature and by strength characteristics (Table 1). Copper is used as material blocking carbon diffusion into niobium (strong carbide-forming metal). Main disadvantage of copper in this composition is its low melting temperature  $T_{\text{melt}} = 1083$  °C.

According to the data of work [2], in welding of titanium alloys to stainless steel through intermediate barrier interlayers the copper region, through which fracture propagates, has the lowest strength in the joint zone.

There are few studies on welding intermetallics of Ti-Al system to steel [6, 7]. In diffusion welding of intermetallic of Ti-Al system (at. %: Ti-48Al-2Cr-

2Nb) to steel without application of interlayers (temperature  $T_w = 950$  °C, pressure  $P_w = 25$  MPa, welding time  $t_w = 6$  min) transition  $\text{Ti}_3\text{Al} + \text{FeAl} + \text{FeAl}_2/\text{TiC}$  intermetallic layers form in the butt between  $\gamma$ -TiAl and steel, leading to welded joint embrittlement [6].

Welding of intermetallic to stainless steel with application of thin interlayers in the form of titanium, vanadium and copper foils, preventing formation of brittle intermetallics in the butt, was studied in work [7]. Intermetallic alloy (at. %: Ti-47.2Al-1.17Ni-0.56Cr-0.11Nb) was welded to steel. Welding was performed at  $T_w = 1000$  °C,  $P_w = 20$  MPa,  $t_w = 60$  min. At selection of welding temperature, the authors proceeded primarily from physical properties of copper, as at increase of welding temperature above 1083 °C melting of copper interlayer and copper pressing out of the butt take place, and welded joint strength decreases markedly [6]. At optimum welding mode, samples fail mainly through  $\text{Ti}_3\text{Al}$ -TiAl layer and partially through base metal ( $\gamma$ -TiAl).

The objective of our investigations was to develop a technology of vacuum diffusion welding (VDW) of  $\gamma$ -TiAl intermetallic alloy to 12Kh18N10T steel with a more uniform distribution of strength in the butt. The object of investigations were  $\gamma$ -TiAl intermetallic alloy (at. %: Ti-48Al-2Nb-2Cr) and 12Kh18N10T steel.

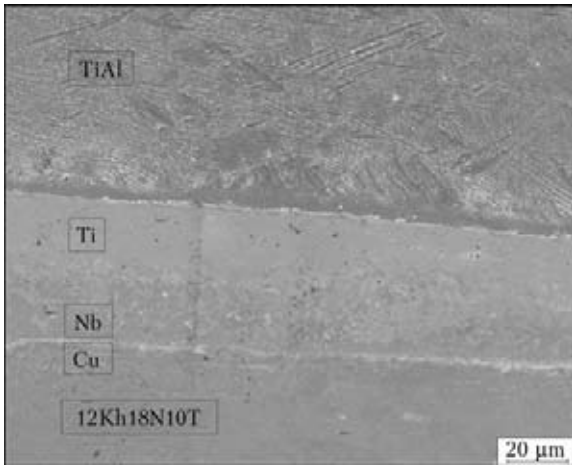
At temperature of  $\gamma$ -TiAl welding equal to 1000 °C, formation of physical contact in the butt is incomplete, because of high hardness and low ductility of the

**Table 1.** Mechanical properties of applied materials

Material	$T_{\text{melt}}$ , °C	$\delta$ , %	$\sigma_t$ , MPa	$E$ , MPa
12Kh18N10T	1455	40	510–860	198,000
Copper	1083	60	216–235	128,700
Nickel	1453	35–40	390–490	201,900
Niobium	2468	30–40	345–491	89,100
Titanium	1668	40–55	245–345	108,000
$\gamma$ -TiAl	~ 1450	1.5	550–900	180,000

**Table 2.** Composition and thickness of interlayers applied in welding

Interlayer type	Interlayer composition	Thickness, $\mu\text{m}$
Ti-Al	Ti-52 at. % Al	20
Titanium	Titanium	100
Niobium	Niobium	50
Copper	Copper	50
Nickel	Nickel	50



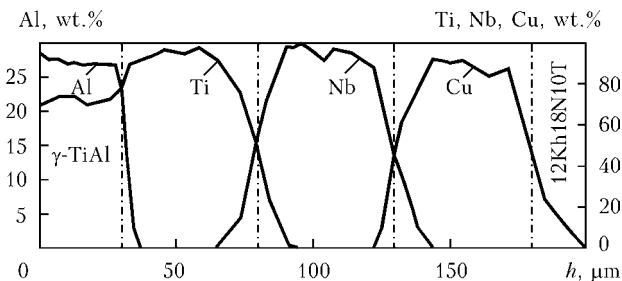
**Figure 1.** Microstructure ( $\times 600$ ) of the zone of the joint of  $\gamma$ -TiAl to 12Kh18N10T steel with application of solid interlayers (titanium, niobium, copper)

material [8]. A large number of defects were found in the joint zone. Based on our results, sound welded joints of  $\gamma$ -TiAl can be obtained at higher values of temperature (approximately, 1200 °C), that is in agreement with the data of [9].

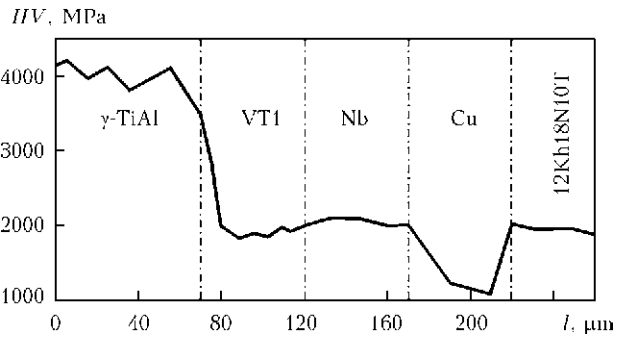
As such different materials as intermetallic alloy and copper interlayer, differing by their physico-chemical properties, are being joined, welding of  $\gamma$ -TiAl intermetallic to 12Kh18N10T steel was performed in two stages. At the first stage interlayers of titanium and niobium were welded to the intermetallic at 1200 °C, and at the second stage stainless steel was joined to the assembly through a copper interlayer at a lower temperature (1000 °C).

Samples of 15 × 15 × 5 mm size were cut out in an EDM machine. Table 2 gives the characteristics of interlayers used in welding. Samples were welded in unrestrained state.

Microstructure of the VD-welded joint, made by of  $\gamma$ -TiAl intermetallic alloy to 12Kh18N10T steel through interlayers of titanium, niobium and copper, is given in Figure 1. Metallographic investigations showed that in the zone of  $\gamma$ -TiAl/Ti/Nb+Cu/12Kh18N10T joint such defects as cracks and pores are absent. As follows from Figures 1 and 2, active diffusion processes with formation of a wide zone of bulk interaction from the  $\gamma$ -TiAl side take place in the joint zone during welding.



**Figure 2.** Element distribution in the zone of the joint of  $\gamma$ -TiAl to 12Kh18N10T steel with application of solid intermediate interlayers from titanium, niobium and copper:  $h$  – interlayer thickness



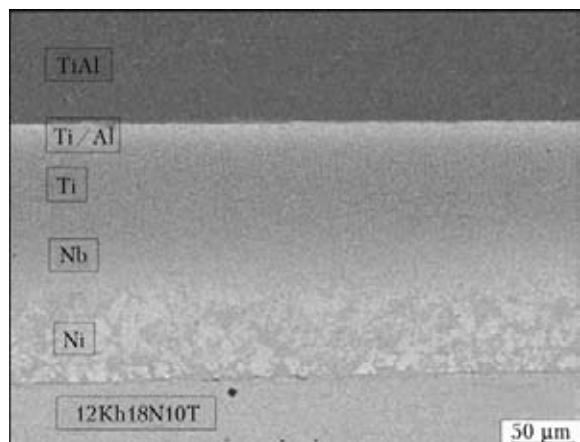
**Figure 3.** Distribution of microhardness across the zone of  $\gamma$ -TiAl + 12Kh18N10T joint made with application of interlayers from titanium, niobium and copper

At investigation of microhardness distribution in the zone of  $\gamma$ -TiAl + 12Kh18N10T joint (Figure 3) it was established that an increase of microhardness up to 4050 MPa was noted on the boundary of  $\gamma$ -TiAl intermetallic-titanium interlayer. In this region 8.95 at.% Al is found due to aluminium diffusion from the intermetallic towards titanium.

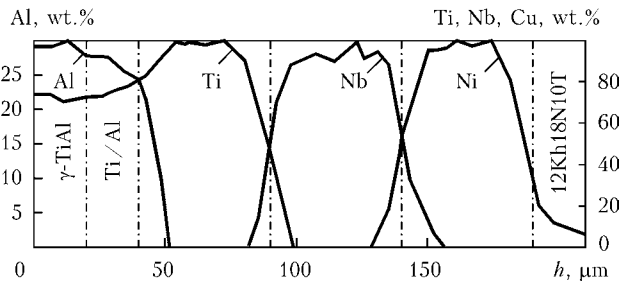
An abrupt lowering of microhardness (to 1100 MPa) was found from the side of stainless steel on the boundary with copper interlayer, which corresponds to microhardness value of copper. It is obvious that a critical point in terms of performance of  $\gamma$ -TiAl/Ti/Nb + Cu/12Kh18N10T welded joint is the region of copper location, where microhardness values are 2 times lower than in the adjacent sections.

Nanolayer of Ti-Al type of total thickness of 20  $\mu$ m and thickness of individual layers of aluminium and titanium of approximately 20 nm was used to equalize microhardness in the joint zone from the intermetallic side (see Table 2), that ensures additional activation of the surfaces being welded.

It should be also noted that at slow heating of nanolayered Ti/Al interlayers at 50 °C/min rate, characteristic for VDW, the following sequence of phase transformations was recorded:  $Al_3Ti \rightarrow Al_5Ti_2 \rightarrow Al_2Ti \rightarrow AlTi$  [10]. In nanolayered interlayers diffraction indications of  $Ti_3Al$  intermetallic formation are absent. Formation of diffusion layer of Ti/Al composition more ductile than  $Ti_3Al$ , between the inter-



**Figure 4.** Microstructure of the zone of TiAl + 12Kh18N10T joint made with application of Ti/Al-Ti-Nb-Ni interlayers



**Figure 5.** Element distribution in the zone of TiAl + 12Kh18N10T joint made with application of Ti/Al–Ti–Nb–Ni interlayers

metallic alloy and titanium interlayer during welding, can have an essential influence on improvement of welded joint quality [6].

Ti/Al type interlayer was placed between the intermetallic and titanium interlayer. Nickel interlayer was inserted between steel and niobium, as its diffusion mobility in iron and its strength characteristics are higher than those of copper (see Table 1).

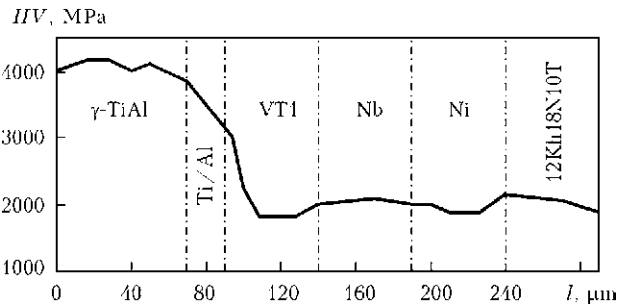
In Nb–Ni pair a latent period is in place at intermetallic formation. So, at 1000 °C time of formation of an intermetallic of approximately 1.5 μm thickness is equal to 11 min [11].

Welding was conducted in two stages: intermetallic was joined to Ti/Al–Ti–Nb interlayers at  $T_w = 1200$  °C,  $P_w = 40$  MPa,  $t_w = 20$  min with subsequent welding of an interlayer of nickel and 12Kh18N10T steel at  $T_w = 1000$  °C,  $P_w = 20$  MPa,  $t_w = 10$  min.

Metallographic examination of the joints showed that there are no welding defects in the butt. As is seen from welded joint microstructure (Figure 4) and element distribution (Figure 5), diffusion processes proceed actively in the butt during welding, leading to formation of bulk interaction zones between the intermetallic and titanium, as well as niobium and titanium. Analysis of microhardness values in the zone of  $\gamma$ -TiAl–Ti/Al–Ti–Nb–12Kh18N10T joint (Figure 6), made by VDW, showed that the nature of microhardness distribution is more uniform than in welding with Ti–Nb–Cu interlayers.

## CONCLUSIONS

1. Considering the differences in physico-chemical properties of welded materials, a two-stage schematic of welding  $\gamma$ -TiAl to 12Kh18N10T steel was proposed.



**Figure 6.** Microhardness distribution across the zone of  $\gamma$ -TiAl + 12Kh18N10T joint made with application of Ti/Al–Ti–Nb–Ni interlayers

2. In joints made by VDW of intermetallic  $\gamma$ -TiAl alloy to 12Kh18N10T steel through Ti–Nb–Cu interlayers an abrupt lowering of microhardness values on the copper interlayer is noted.

3. Application of nickel instead of the copper interlayer in welding  $\gamma$ -TiAl to 12Kh18N10T steel allows producing sound welded joints at uniform distribution of microhardness in the butt.

- Charukhina, K.E., Golovanenko, S.A., Masterov, V.A. et al. (1970) *Bimetallic joints*. Moscow: Metallurgiya.
- Gurevich, S.M., Zamkov, V.N., Blashchuk, V.E. et al. (1986) *Metallurgy and technology of welding of titanium and its alloys*. Kiev: Naukova Dumka.
- Charukhina, K.E., Kazakov, N.F. (1964) *Vacuum diffusion welding of dissimilar metals*. Leningrad: LDNTP.
- Kazakov, N.F. (1976) *Diffusion welding of materials*. Moscow: Mashinostroenie.
- Shmakov, V.M., Izmirlieva, A.N. (1967) Diffusion welding of dissimilar metals. In: *Welding of new high-strength materials*. Kujbyshev.
- He, P., Feng, J.C., Zhang, B.G. et al. (2002) Microstructure and strength of diffusion-bonded joints of TiAl base alloy to steel. *Materials Characterization*, **48**, 401–406.
- He, P., Feng, J.C., Zang, B.G. et al. (2003) A new technology for diffusion bonding of intermetallic TiAl to steel with composite barrier layers. *Ibid.*, **50**, 87–92.
- Ustinov, A.I., Falchenko, Yu.V., Ishchenko, A.Ya. et al. (2009) Producing permanent joints of  $\gamma$ -TiAl based alloys using nanolayered Ti/Al interlayer by vacuum diffusion welding. *The Paton Welding J.*, **1**, 12–15.
- Nakao, Yo., Shinozaki, K., Hamada, M. (1991) Diffusion bonding of intermetallic compound TiAl. *ISIJ Int.*, **31**(10), 1260–1266.
- Ustinov, A.I., Olikhovskaya, L.A., Melnichenko, T.V. et al. (2008) Solid-phase reactions in heating of multilayer Al/Ti foils produced by electron beam deposition method. *Advances in Electrometallurgy*, **2**, 19–26.
- Kharchenko, G.K., Shevchuk, T.V., Ignatenko, A.I. (1976) Study of niobium-nickel interlayer–steel joint made by pressure welding. *Avtomatich. Svarka*, **9**, 71–72.



# LASER WELDING OF SHEET STAINLESS STEEL BY MODULATED RADIATION

A.G. LUKASHENKO, T.V. MELNICHENKO and D.A. LUKASHENKO

E.O. Paton Electric Welding Institute, NASU, Kiev, Ukraine

The effect of power modulation frequency and shape of laser radiation pulses on formation of weld metal structure in welding of austenitic steel of 18-10 type was investigated. It is shown that pulse laser radiation can affect solidification of weld metal and formation of fine-grained structure in it. Optimal range of modulation frequency was determined.

**Keywords:** laser welding, thin sheet, stainless steel, solidification, weld, modulated radiation, laser welding parameters, microstructure

In welding production effective utilization of power and material resources can be achieved by introducing fundamentally new power-saving technologies and equipment.

Known are various methods of controlling the solidification process. Here, the objective is to modify weld structure, in particular, produce fine-grained structure that in the majority of cases essentially improves welded joint properties. Two main methods of controlling weld structure are singled out: metallurgical and technological [1]. Metallurgical method is based on weld pool modification by chemical elements using both filler materials fed into the welding zone, and preliminary preparation of metal before welding (work-hardening, cold-working, application of technological inserts) [2]. Technological method, in addition to optimization of welding modes, envisages an external impact on the weld pool (mechanical, thermal, electromagnetic).

Method of pulsed-periodic impact with application of laser radiation as the heat source became widely accepted recently [3–8]. Studying the physical processes, running in weld pool at such an impact, is extremely complicated [9]. Absence of strict mathematical models of the process, and short duration of thermal processes ensure research performance on the basis of an integrated approach by combining qualitative assessments, experiments, and local simulation with theoretical substantiation.

Achieving high technological strength and mechanical characteristics of welded joints is one of the main objectives in laser welding of thin-walled structures. Here, in order to prevent hot and cold cracks in the weld metal, the possibility of achieving fine-grained primary structure in it becomes important in thin metal welding [10–12].

In this work the influence of parameters of pulsed-periodic laser impact, shape of laser radiation pulses and their repetition rate on formation of weld struc-

ture in welding austenitic steel at constant average heat input power was studied.

According to statistical approaches of thermodynamics [13] at metal solidification the probability of formation of nuclei  $w_1$  can be presented as

$$w_1 = M_1 \exp(-\Delta G_k / (k_B T)), \quad (1)$$

where  $k_B$  is the Boltzmann constant;  $T$  is the temperature;  $\Delta G_k$  is the critical or maximum value of free energy.

Here

$$\Delta G_k = \frac{16\pi s^3 T_m^2}{3\Delta T^2 Q^2}, \quad (2)$$

where  $s$  is the surface tension;  $T_m$  is the metal melting temperature;  $Q$  is the latent heat of solidification.

However, with increase of overcooling the diffusion process is decelerated, slowing down the approach of new atoms from the liquid to the crystal. The probability of transition from the liquid phase into the solid phase at nucleus formation is

$$w_2 = M_2 \exp(-U / (k_B T)), \quad (3)$$

where  $U$  is the energy of diffusion self-activation.

Probability  $w$ , determining the number of solidification centers  $n$ , is equal to the product of probabilities of process components:

$$w = w_1 w_2 = M_3 \exp(-(\Delta G_k + U) / (k_B T)), \quad (4)$$

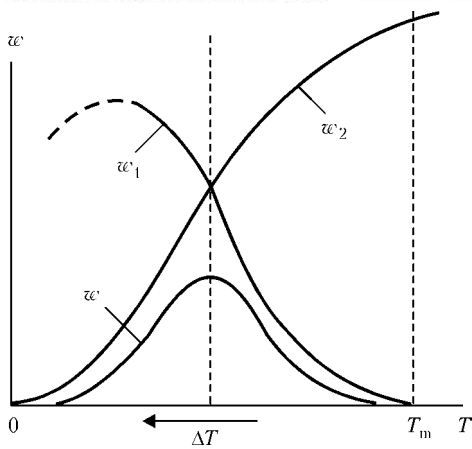
where  $M_1$ – $M_3$  are the constant coefficients, dependent on metal properties.

After substitution of expression (2) into (4), we will obtain the dependence of the number of solidification centers on temperature:

$$w = M_3 \exp\left(-\left(\frac{16\pi s^3 T_m^2}{3\Delta T^2 Q^2} + U\right) / (k_B T)\right). \quad (5)$$

Dependence of the probability of nuclei initiation on the degree of overcooling is given in Figure 1.

Thus, under the influence of two opposite tendencies there exists the overcooling value, providing optimum conditions for formation of maximum number of nuclei.



**Figure 1.** Influence of the degree of overcooling on the conditions of nucleus formation

The forming weld structure is essentially affected also by the solidification rate. Linear rate of crystal face growth is determined as

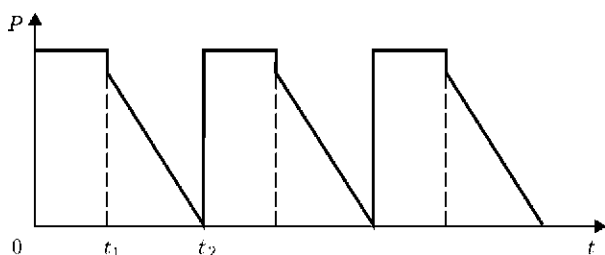
$$w = M_4 \exp \left( - \left( \frac{\pi s^3 \alpha T_m}{\Delta T Q} + U_1 \right) / (k_B T) \right). \quad (6)$$

Increase of the number of solidification centers and slowing down of crystal growth rate promotes crystallite refinement.

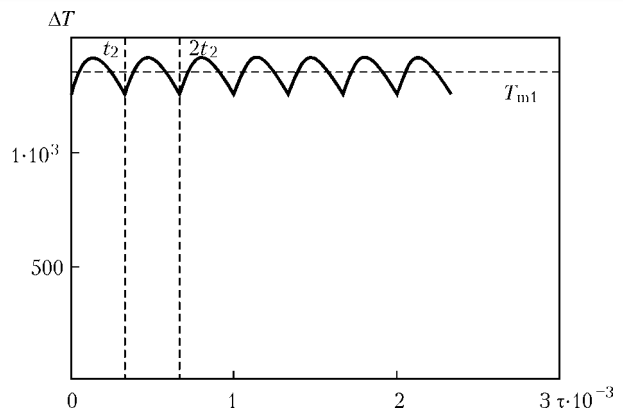
To determine the technological parameters, providing optimal conditions of producing the fine-grained structure of weld metal, laser welding was performed by complex-shaped modulated radiation (Figure 2). Pulse shape had a steep leading front and smoothly falling rear front, which contained two regions: melting and solidification. First (0;  $t_1$ ) provides material melting without intensive evaporation, and the second region ( $t_1$ ;  $t_2$ ) has a gradient, the change of angle of which allows changing the solidification rate, while the region length allows determination of the optimum degree of overcooling of the metal being welded.

Using as the model of heat transfer process the moving linear concentrated source in a plate with application of the method of sources, we will obtain a quasi-stationary temperature process (Figure 3).

The objective of modeling is selection of the shape and frequency of repetition of laser pulses, at which the change of weld pool temperature in the region of the zone of liquidus–solidus phase transition is ensured, as well as achieving the calculated values of the degree of welded metal overcooling.



**Figure 2.** Pulse-periodic law of variation of laser radiation power



**Figure 3.** Quasi-steady process of weld pool temperature variation

**Materials and equipment.** A strip 0.2 mm thick from 1.4541 steel to DIN EN 10028-7:2000, which is an analog of 0818N10T steel, was used.

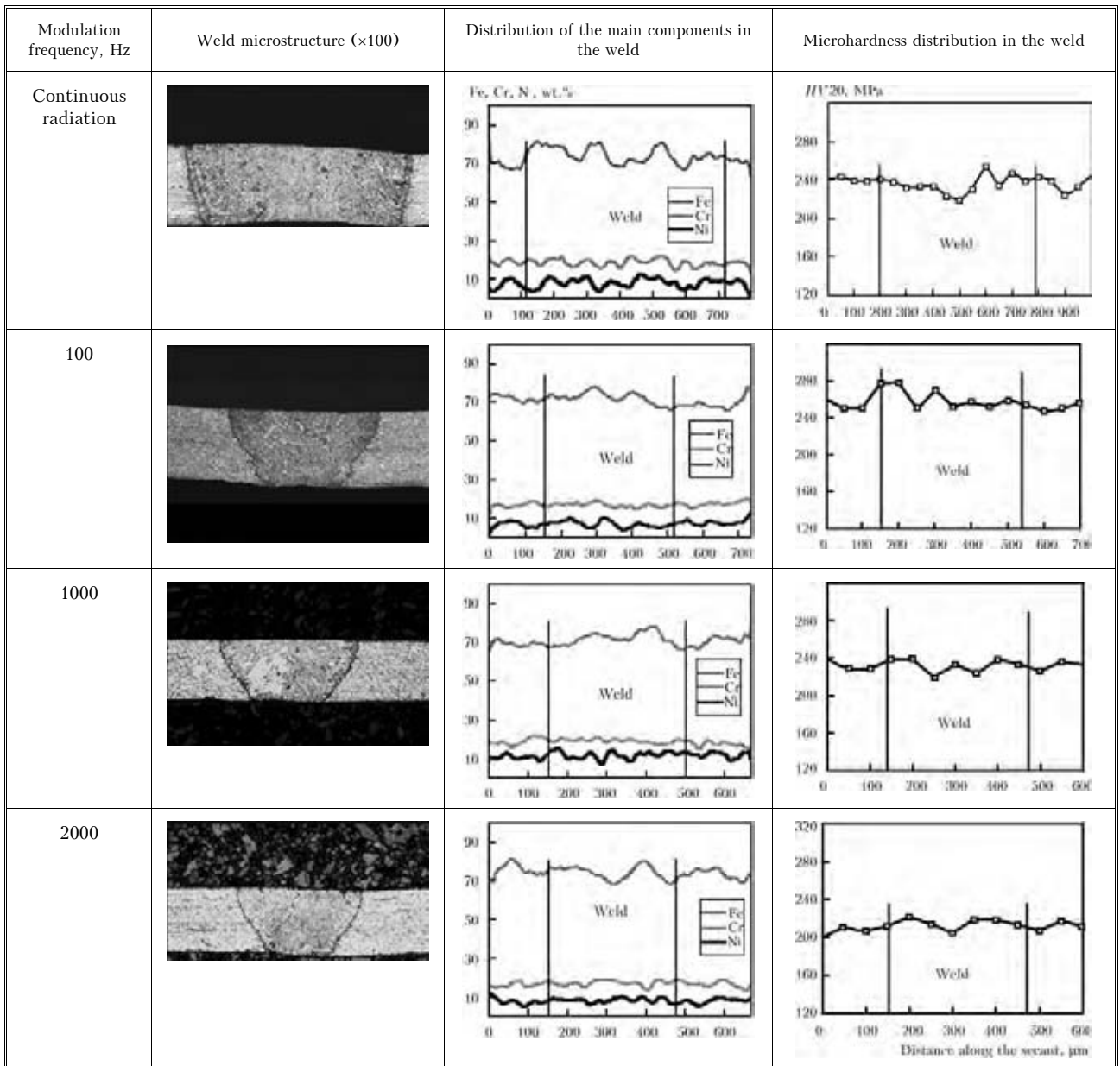
Samples were welded in a three-coordinate welding complex ARMA-100M (manufactured by PWI) fitted with ytterbium fiberoptic single-mode laser of YLR-100-AC type with radiation power of 100 W (manufacturer is IPG Laser, Germany), in which the generating core is of 10 μm diameter [14]. Laser radiation was focused onto metal in a beam of 40 μm diameter. Argon was used as shielding gas on top and below. Penetration was studied on a whole metal sheet.

**Experimental procedure.** Samples of stainless steel strip (wt. %: 0.72 Si; 0.25 Ti; 18.8 Cr; 1.68 Mn; 69.65 Fe; 8.9 Ni) were welded by continuous laser radiation of 57 W power and modulated laser radiation. Shape of modulated pulse corresponded to that given in Figure 2. Pulse amplitude was 100 W; modulation frequency was 100, 1000, 2000, 3000, 5000, 10,000 Hz, and calculated values of the degree of overcooling were 151, 143, 136, 125, 106 and 82 K. Average value of input power was 57 W, welding speed was 0.33 cm/s. Samples for metallographic analysis in the form of transverse sections of welded joints were prepared by a standard procedure using polishing-grinding machine of Struers. Microstructure and composition of base metal and welded joints were analyzed using optical microscope Reichert Polyvar Met and scanning microscope CamScan fitted with energy-dispersive system of local analysis Energy 200. Microhardness of welded joints in the weld cross-section was measured with Vickers indenter in Reichert Polyvar Met microscope at 0.2 N load with 50 μm step.

**Results and their discussion.** Macrostructure of welded joint of stainless steel samples made at different types of laser radiation, distribution of the main components in the weld zone and nature of the change of microhardness in the joint zone are given in Figure 4.

Investigations results show that the proposed method of laser welding provides weld zone composition by the main elements on base metal level both at continuous and at cyclic impact of laser radiation.





**Figure 4.** Weld macrostructure, distribution of the main components and microhardness in the transverse section of welded joints made at different frequencies of laser radiation modulation

A certain depletion of the melting zone as to manganese approximately to 1.2 wt.% should be noted. In all the welding modes cracks are absent either in the weld zone, or in the HAZ metal.

At the impact of continuous radiation, a dendritic austenitic structure forms in the weld (Figure 5), which is characteristic for the high solidification rate in laser welding. Coarse equiaxed grains of up to 10 μm size form in the zone adjacent to the fusion line.

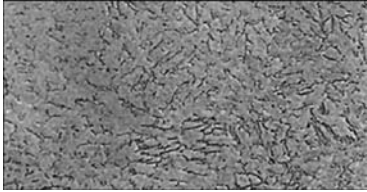
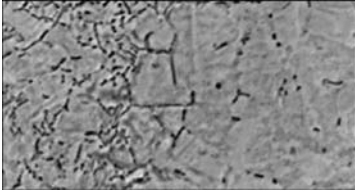
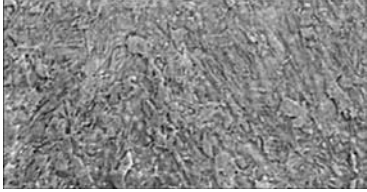
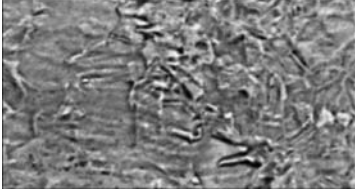
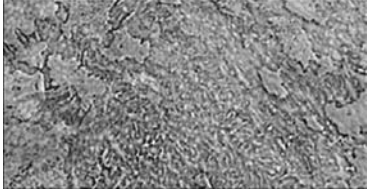
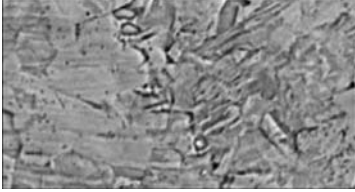
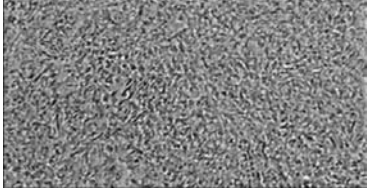
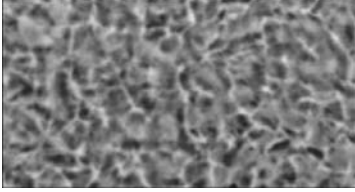
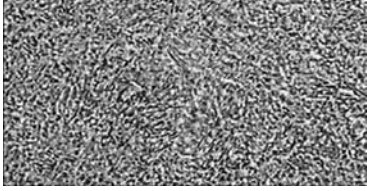
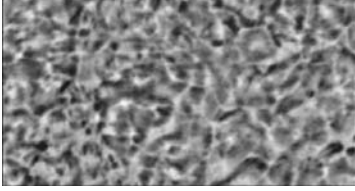
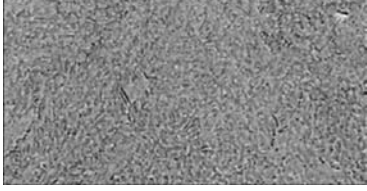
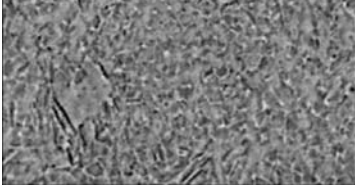
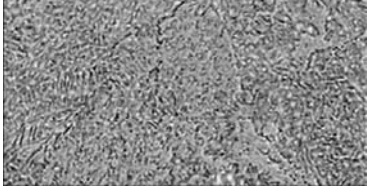
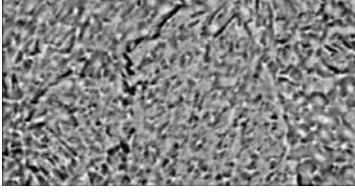
Laser processing of stainless steel by modulated radiation with modulation frequency of 100 Hz leads to formation of welding lines in the weld structure that considerably impairs its quality. Weld structure is inhomogeneous because of the mixed form of solidification that causes formation of coarse crystallites with regions of Widmanstaetten structure. Different weld regions have different microhardness, because of

structural inhomogeneity (see Figure 4) that may lead to deterioration of the mechanical properties of welded joint.

At 1000 Hz frequency of laser radiation modulation structural homogeneity was not improved, however, regions of cellular form of solidification (see Figure 5) appeared. Weld microhardness was equalized. Increase of modulation frequency of laser impact up to 2000 Hz ensures a predominantly cellular shape of solidification and formation of fine austenitic grains of about 3 μm size with ferrite precipitates along the grain boundaries. At the given welding mode a structurally homogeneous weld forms with different microhardness of the different zones.

Analogous homogeneous microstructure was also observed at modulation frequency of 3000 Hz. Characteristics of distribution of the main components and



Modulation frequency, Hz	Weld microstructure ( $\times 300$ )	Near-weld zone microstructure ( $\times 600$ )
Continuous radiation		
100		
1000		
2000		
3000		
5000		
10,000		

**Figure 5.** Microstructure of the weld and near-weld zone in welded joints made at different frequencies of laser radiation modulation

microhardness practically did not differ from the previous experiment. It should be noted that in these cases the fusion line becomes thinner, whereas the austenitic grain becomes smaller that is positive for mechanical properties of the near-weld zone.

Further increase of pulse frequency up to 5000 and 10,000 Hz leads to deterioration of the homogeneity of weld structure formation and its coarsening.

This laser welding process was applied in development of the technology for manufacturing small



series of straight-seam thin-walled welded pipes of different diameters from stainless steels, used in manufacture of bellows and bellows assemblies.

## CONCLUSIONS

1. Use of modulated laser impact in welding of stainless steel samples affects the morphological features of solidification of structural components of the welded joint.

2. Increase of modulation frequency promotes an increase of the number of solidification centers and formation of a fine-grained cellular austenitic structure.

3. Application of an inclined shape of the rear front of laser radiation pulse provides a slowing down of crystallite growth that also leads to formation of a fine-grained cellular structure of the weld.

4. Influence of modulation frequency on weld structure is of a limited nature. Modulated pulse parameters, optimum for weld metal structure, were determined. Formation of structurally-homogeneous weld with minimum size of austenite grains of about 3  $\mu\text{m}$  occurs at modulation frequency of 2–3 kHz. Here, the calculated values of optimum degree of overcooling are in the range of 125–136 K.

1. Morozov, V.P. (2010) Effect of oscillation mechanism of solidification on process of primary structure refinement of weld metal and heat-affected zone. *Nauka i Obrazovanie*, **9**, 1–18.

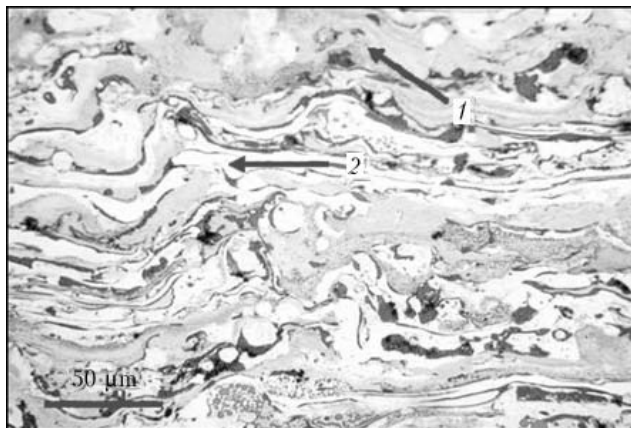
2. (1974) *Technology of fusion electric welding of metals and alloys*. Ed. by B.E. Paton. Moscow: Mashinostroyeniye.
3. Levin, Yu.Yu., Erofeev, V.A., Sudnik, V.A. (2008) Physical-technological conditions for producing defect-free joints in pulsed laser welding. *Svaroch. Proizvodstvo*, **4**, 20–24.
4. Kayukov, S.V., Gusev, A.A., Samartsev, G.V. et al. *Method of pulsed laser welding and unit for its realization*. Pat. 2120364 RF. Int. Cl. B 23 K 26/00. Fill. 27.09.96. Publ. 20.10.98.
5. Basiev, T.T., Fedin, A.V., Chashchin, E.A. et al. *Method of laser welding of metals and alloys*. Pat. 2186667 RF. Int. Cl. B 23 K 26/20. Fil. 10.01.2000. Publ. 10.08.2002.
6. Myshkovets, V.N., Maksimenko, A.V., Shalupaev, S.V. et al. *Method of laser welding of metals*. Pat. 2269401 RF. Int. Cl. B 23 K 26/20. Fil. 27.08.04. Publ. 10.02.06.
7. Bruncko, J. (2010) Laserove mikrozarvanie kovovych materialov. *Zvaranie-Svarovani*, **9/10**, 219–222.
8. Celen, S., Karadeniz, S., Ozden, H. (2008) Effect of laser welding parameters on fusion zone morphological, mechanical and microstructural characteristics of AISI 304 stainless steel. *Materialwissenschaft und Werkstofftechnik*, **39(11)**, 845–850.
9. Grigoriant, A.G., Shiganov, I.N., Misyurov, A.I. (2006) *Technological processes of laser treatment: Manual*. Ed. by A.G. Grigoriant. Moscow: MGTU im. N.E. Bauman.
10. Nazarchuk, A.T., Snisar, V.V., Demchenko, E.L. (2003) Producing welded joints equivalent in strength on quenching steels without preheating and heat treatment. *The Paton Welding J.*, **5**, 38–43.
11. Rayamyaki, P., Karkhin, V.A., Khomich, P.N. (2007) Determination of main characteristics of temperature field for evaluation of the type of weld metal solidification in fusion welding. *Svaroch. Proizvodstvo*, **2**, 3–7.
12. Sillen, R. (2005) Introduction to thermal analysis of metals. *Litio Ukrainy*, **5**, 6–8.
13. Volchenko, V.N., Yampolsky, V.M. (1988) *Theory of welding processes: Manual*. Moscow: Vysshaya Shkola.
14. (2009) *YLR-100-AC. Ytterbium fiber laser: User's guide*. IPG Laser GmbH.

## NEWS

### WEAR-RESISTANT COATINGS FOR BILLET CCM

Protective Coatings Department of the E.O. Paton Electric Welding Institute is working in the field of thermal spraying of coatings with pseudo-alloy structure, which have high wear-resistant and antifriction properties. For protection of the surface of copper

items from abrasive wear, a coating series was developed, which is applied by the method of electric arc metallization, and the structure of which consists of a mixture of copper particles with the second component, ensuring the coating resistance to abrasive wear (for instance, NiCr, Mo, Ti, etc.). One of the objects of these coatings application are plates of CCM mould. Presence of copper in the coating structure (~ 50 wt.%) ensures preservation of a high enough heat conductivity of the coating (up to 200–300 W/(m/deg)), which is an important factor under the conditions of CCM operation. Thickness of coatings, applied for this purpose, is equal to 2 mm. Hot hardness of the coating, for instance, Cu–NiCr, at 20–400 °C exceeds that of copper 3 times, its rupture strength is equal to 240 MPa. Resistance of pseudo-alloy coatings to abrasive wear at 300–350 °C is higher than that of pure copper from 5 up to 100 times, depending on coating composition. Work on testing the developed coatings under the real service conditions of CCM is being conducted.



Coating with 57 wt.% Cu–43 wt.% NiCr: 1 – Cu; 2 – NiCr



# EXPERIMENTAL REVIEW OF THE WELDING METALLURGY OF HIGH-STRENGTH ALUMINIUM ALLOY 7025-T6

M. OLABODE, P. KAH and J. MARTIKAINEN

Lappeenranta University of Technology, Lappeenranta, Finland

In this review, various aspects such as designations, definitions, applications, properties and weldability of high-strength aluminium alloys are presented. The effect of heat input on microstructure and hardness of the 7025-T6 alloy welded joints is studied. It is shown that at constant heat input the welding speed had no effect on the weld hardness. Thus, limiting heat input in welds on high-strength aluminium alloys is important to preserve their mechanical properties.

**Keywords:** *high-strength aluminium alloys, alloy 7025-T6, pulsed MIG welding, heat input, Vickers hardness, welding metallurgy*

Light welded metal structures are in high demand, and the market keeps growing along with societal needs. The diversification of aluminium structures also continues to grow. Welding is an important process in producing these structures. The fusion welding of high-strength aluminium alloys (HSA) using pulsed MIG method involves heat input and is, thus, challenging but accomplishable if proper care is taken to understand the nature and behaviour of HSA being welded. A number of studies [1–3] have shown that earlier technologies available for welding HSA present poor weldability due to the presence of copper in the alloy. However, new technologies like pulsed MIG welding, pulsed TIG welding and friction stir welding (FSW) can be effectively compared with conventional fusion methods. FSW proved to be presently the most acceptable process as it allows obtaining important metallurgical advantages, for example, no solidification and liquation cracking, compared with fusion welding [4]. Based on literature review, this paper outlines the definitions, properties, applications, weldability, welding defects of HSA and studies their weldability with a focus on the effect of heat input on welding metallurgy using the pulsed MIG process. This study adopts both a literature review of HSA and an experimental study of 7025-T6 alloy welded by robotised pulsed MIG method. In addition, the effect of heat input and welding speed as welding parameters on welding metallurgy of HSA are presented. It was found that the grains reduce in size as heat input decreases, and welding speed had no effect on the hardness across the weld if heat input was kept constant. The hardness of HSA joints lower in the HAZ than in the parent metal. This study is of significance as there are limited studies available about the welding metallurgy of the 7025-T6 alloy.

**Alloy designation.** Aluminium alloys are grouped into cast and wrought ones and are identified with a

four digit number system. Cast alloy designations are similar to those of wrought alloys but with a decimal between the third and fourth digit (123.0). The second part of the designation is the temper which accounts for the fabrication process. When the second part starts with T, e.g. T6, it means that the alloy was thermally treated. The numbers show the type of the treatment and other consequent mechanical treatment, namely T6 shows that the alloy is solution heat-treated and artificially aged [5]. In alloy designations F denotes as fabricated and O – annealed. An additional suffix indicates the specific heat treatment. H denotes strain-hardened (cold-worked) and it is always followed by at least two digits to identify the level of cold-working and other heat treatments that have been carried out to attain the required mechanical properties. W denotes solution heat-treated, it is followed by a time indicating the natural ageing period, e.g. W 1 h. T denotes thermally treated and is always followed by one or more numbers to identify the specific heat treatment [4].

The full designation therefore has two parts which specify the chemistry and the fabrication history, e.g. in 7025-T6, 7025 specifies the chemistry while T6 – the fabrication. Aluminium is classified based on the chemical composition. The classification is mainly in two categories based on the type of production which are wrought aluminium alloys (fabricated alloys) and cast aluminium alloys. Others can be categorised on the basis of strain hardening possibility or heat treatment [6]. The wrought aluminium category is large because aluminium can be formed to shapes by virtually any known process including extruding, drawing, forging, rolling etc. Wrought alloys need to be ductile to aid fabrication, whereas cast aluminium alloys need to be fluid in nature to aid castability [7]. Cast aluminium alloys are identified with four digits in their classification. A decimal point separates the third and fourth digit. The first digit indicates the alloy group which is based on the major alloying element (Table 1) [8]. The next two digits denote the aluminium alloy itself or the purity of the alloy. In lxx.x series



**Table 1.** Cast aluminium alloy classification [6–9]

Series	Alloying elements	Content, %	Tensile strength, MPa	Series average value, MPa
1xx.x	Al	Min 99.0		
2xx.x	Cu	4.0–4.6	145–476	302
3xx.x	Si	5–17	159–359	249
	With added Cu and/or Mg	5–17	159–359	249
4xx.x	Si	5–12	131–296	187
5xx.x	Mg	4–10	138–331	232
7xx.x	Zi	6.2–7.5	241	241
8xx.x	Sn	–	138–221	163
9xx.x	Others	–	–	–

alloys, these two digits denote the purity in percentages. For example, 150.0 show the minimum 99.5 % purity of the aluminium alloy. In the groups 2xx.x–9xx.x series, the two digits signify the different alloys present in the group. The last digit signifies how the product is formed. For example, 0 denotes casting, and 1 or 2 – ingot based on what chemical composition the ingot has.

Further modifications from the original cast aluminium alloy groups are identified by adding a serial letter in front of the numerical denotations. The serial letters are assigned in alphabetical order starting with A but omitting I, O, Q and X [8]. X is left out with experimental alloys.

Wrought alloys are given four digits. The first one represents the alloy group which is based on the major alloying element (Table 2). The second digit tells how the alloy has been modified or the limits of impurity. 0 in the second digit denotes an original alloy. Numbers 1–9 signify the different alloy modifications with slight variation in their compositions. In the 1xxx series the second number denotes the modifications in impurity limits: 0 implies that the alloy has a natural impurity limit, 1–9 imply that special control has been carried out on one or more impurities or alloying element. The last two numbers represent the purity of the alloy [6].

In the 1xxx series the last two numbers signify the alloy level of purity. For example, 1070 or 1170 implies that at least 99.7 % Al is present in the alloy, 1050 or 1250 – no less than 99.5 % Al, and 1100 or 1200 – at least 99.0 % Al. For all the other series of aluminium alloys (2xxx–8xxx) the last two numbers have no special significance but are used to identify alloys in the group [6, 8].

**High-strength and ultra high-strength aluminium alloys.** Aluminium alloys with at least 300 MPa yield strength are regarded to be HSA, whereas ultra high-strength aluminium alloys (UHSA) are those with yield strength of 400 MPa or more. HSA and UHSA are generally included in the 2xxx, 7xxx, and 8xxx series. There are no strict rules as to what series HSA and UHSA belong to. For example, two alloys can have significantly different yield strengths within the same series. To be exact, the HSA and UHSA can be classified only specifically to certain alloys in the series. For generality purpose, however, an average range of the series yield strength is used to identify HSA and UHSA (see Table 2).

*Properties and applications of HSA and UHSA Series.* The 2xxx series includes the Al–Cu alloys. The major characteristics of the 2xxx series are heat treatability, high strength both at room and elevated temperatures, and high tensile strength range of 68.9–520 MPa [9, 10]. The alloys can be joined mechani-

**Table 2.** Wrought aluminium alloy classification [6, 8, 9]

Series	Alloying elements	Content, %	Tensile strength, MPa	Series average value, MPa
1xxx	Al	Min 99.0	10.0–165	94.4
2xxx	Cu	1.9–6.8	68.9–520	303
3xxx	Mn	0.3–1.5	41.4–285	163
4xxx	Si	3.6–13.5	70.0–393	275
5xxx	Mg	0.5–5.5	40.0–435	194
6xxx	Mg and Si	0.4–1.5	40.0–435	241
	Si	0.2–1.7	40.0–435	241
7xxx	Zn	1.0–8.2	80.0–725	399
8xxx	Others	–	110–515	365

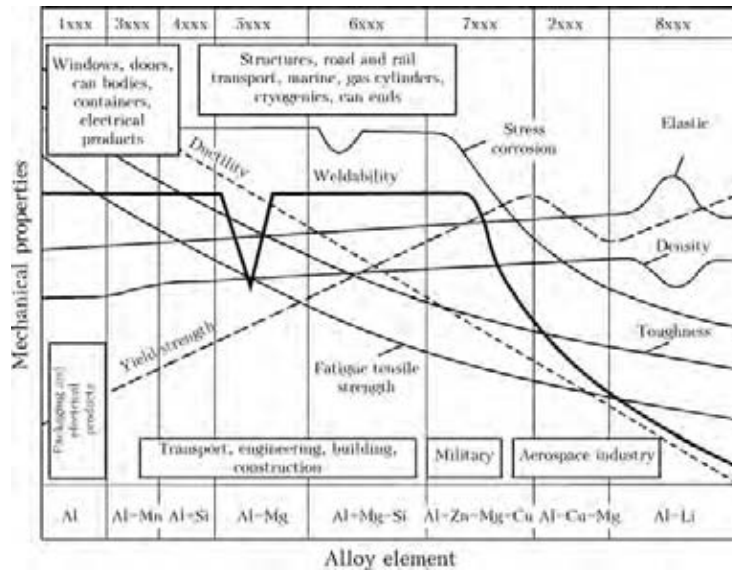


Figure 1. Mechanical properties of aluminium alloys

cally while some are weldable [11]. The chemical composition is usually copper and some other possible elements, like magnesium, manganese and silicon. They comprise high strength products that are usually typical of the aviation industry (2024 alloy). In the industry they are expected to meet high engineering standards due to high safety requirements. These requirements make the 2xxx series expensive. However, the alloys are also used in the manufacture of truck bodies (2014 alloy); 2011, 2017 and 2117 alloys are extensively used for fasteners and screw machine stock. Under naturally aged T4 condition, the 2xxx series alloys have similar mechanical properties as mild steel, with a proof strength of about 250 MPa and an ultimate tensile strength of around 400 MPa. They also have good ductility. When T6 conditioning is used, the proof strength gets up to 375 MPa and the ultimate tensile strength can get up to 450 MPa. This, in turn, lowers ductility [11]. Moreover, they are generally painted or clad to increase their corrosion resistance. Succinctly, the 2xxx series alloys are used for the construction of aircraft internal and external structures, internal railroad car structural members, structural beams of heavy dump and tank trucks and trailer trucks, and the fuel tanks and booster rockets of space shuttles [10].

The 7xxx series includes the Al-Zn alloys with magnesium to control the ageing process. The alloy group possesses very high strength in the high toughness versions. They are also heat treatable with an ultimate tensile strength range of 220–610 MPa. They can be mechanically joined and, with selected welding method like pulsed MIG process, they are weldable. Some 7xxx alloys content copper to yield the highest strength in the series. However, these alloys are not commercially weldable (Figure 1). The weldability reduces as the copper content increases [1–3]. Thus, in commercial applications they are mechanically joined, e.g. by riveting.

The 7xxx alloys are mainly used when fracture critical design concepts are important, e.g. the Foresmo Bridge in northern Norway. Al-Mg alloys are used for building the girders system. Another main application is in the aircraft industry [10]. They have poor corrosion resistance compared to, for example, the 5xxx series and are thus clad in many applications. They are used for critical aircraft wing structures of integrally stiffened aluminium extrusions and long-length drill pipes, and premium forged aircraft parts are made from 7175-T736 (T74) alloy [10].

The 8xxx series includes alloys with aluminium and other elements such as iron, nickel and lithium (not presented in Table 2). These elements provide a specific property to the alloy, e.g. nickel and iron yield strength to the alloy with almost no loss to electrical conductivity [10]. The high strength members of the series mainly consist of lithium and copper. The lithium proportion is higher than that of copper. The relatively recently developed Al-Li alloys 8090, 8091 and 8093 are also included in the series. Lithium has lower density than aluminium and relatively high solubility. Thus, it can be alloyed with aluminium in sufficient quantities. A significant reduction in density (usually about 10 % less than other aluminium alloys) is attainable. The resulting alloys have increased stiffness, and they also respond to age-hardening. Some of the series alloys are heat treatable [12]. They are therefore referred to as special alloys and have high conductivity, strength (tensile strength of 110–515 MPa [9]) and hardness. These alloys are used in the aviation industries (8090, 8091). The Al-Ni-Fe alloy 8001 is used in nuclear power generation for applications demanding resistance to aqueous corrosion at elevated temperatures and pressures. The alloy 8017 is used for electrical conduction [10].

*Weldability of high-strength aluminium alloys.* The increasing industrial need for aluminium alloys has resulted in profuse research on how to weld the



new alloys. There are more ranges of applicable welding processes available on the market. Based on studies it can be stated that:

- within the scope of manufacturing technology, 94 % of alloys can be welded and over 50 % have optimal weldability;
- industrially weldable thickness range is 0.1–450 mm (the latter, exceptional case, in a single pass by means of electron beam welding (EBW));
- high welding speeds are attainable with reduced thicknesses (0.8–3.0 mm), for example, the laser welding of butt joints, varying between 5 and 3 m/min;
- metallurgical problems caused by welding heat input are present with all fusion methods, but reduced in the concentrated energy processes, where heat input is more precise and hence the HAZ is less extensive. FSW produces a low level of metallurgical disturbance;
- with concentrated energy processes, the presence of the Al<sub>2</sub>O<sub>3</sub> film on the surfaces undergoing welding does not compromise the quality of the weld. However, pre-weld cleaning is encouraged;
- both EBW and FSW can be conducted without the use of gas to protect the weld pool from oxidation;

• traditional methods give inferior mechanical properties with respect to those of the corresponding base materials. The decrease varies from 20 to 35 % and is highly influenced by the metallurgical state of the base material. Particularly, an insignificant or even zero reduction is only found with the FSW process, which is, at the same time, the only welding process offering fatigue characteristics of butt joints that are entirely comparable to the base metal in the as-welded condition;

• generally all fusion welding methods, with the exception of FSW, give welds affected by widespread porosity;

• generally, and considering similar sized welding equipment, laser and FSW technologies involve up to 10 times higher investments than traditional technologies, but the level of productivity is decidedly superior. Currently, large scale of the aluminium alloy structural components welded by FSW have at least 10 % lower costs compared to those welded by MIG process [13].

*Work preparation.* The successful welding of HSA is very dependent on the work preparation due to the extra consideration necessary for welding aluminium compared to steel. It depends on using a suitable weld-

**Table 3.** Work preparation guide [4, 9, 14, 15]

Consideration	Precautions
Stress in weld	Avoid sudden changes in thickness as they act as stress raisers in the weld. It is better to taper a section in the joint if it is to be joined with a thinner section Ensure a good fit-up prior to welding. Aluminium is intolerant of poor fit-up and joints should have the smallest gap possible to allow the penetration of the filler into the joint. In a general fit-up, gaps of more than 1.5 mm are not acceptable. Larger gaps are easy to fill in steel but will introduce excessive stresses in aluminium due to thermal contraction. This will compromise the life of the weld Ensure a good alignment of the joint prior to welding. A misaligned weld will introduce bending stresses, which will also shorten the life of the weld Make sure that the joint preparation is suitable for the thickness of the material and complies with the drawing
Conditions for good quality welds	Make sure that the ambient conditions are suitable for welding. Aluminium is very sensitive to hydrogen contamination, so that any moisture will result in defective welds due to porosity. Welding outdoors is particularly risky as condensation can form on the joint during cold weather or the component may be left out in the rain. If welding is to be carried out during humid periods, moderate preheating may be usefully applied to prevent hydrogen porosity. Even if the joint is dry, the risk of draughts destroying the gas shield must be considered. Welding of aluminium is best carried out in a dedicated warm, dry, draught-free area indoors
Pre-weld cleaning of joint	Aluminium is very intolerant of contamination in the joint. Cleaning should start with a wipe by a clean cloth soaked in a solvent such as acetone to remove oil and grease from the joint area and 25 mm over both sides of the joint. All aluminium products have a very thin layer of oxide on the surface. This melts at about 2060 °C [4, 14] compared with 660 °C [9] for pure aluminium. This oxide must be removed after degreasing and before welding by mechanical cleaning with a stainless steel wire brush, which is reserved for aluminium use only. A grinding disk must not be used as these are made from corundum (aluminium oxide) and will deposit particles in the surface. This is precisely the material that cleaning intends to remove. The weld should preferably be made immediately after cleaning, but welding within 3 h of cleaning is acceptable
Suitability of welding consumables	Welding is normally carried out using argon or mixture of argon and helium, and the purity of these gases is important. A minimum purity of 99.995 % is required. Wire for MIG welding is normally supplied clean enough and it is sufficient to always ensure that the spool is preferably removed from the welding machine and placed in a clean plastic bag overnight or at least covered to keep it clean



**Table 4.** Shielding gases for MIG welding of aluminium [16]

Metal transfer mode	Shielding gas	Characteristics
Spray	100 % Ar	Best metal transfer and arc stability, least spatter, good cleaning action
	Ar + 65 % He	Higher heat input than in 100 % Ar, improved fusion characteristics on thicker material, minimised porosity
	Ar + 75 % He	Highest heat input, minimised porosity, least cleaning action
Short circuiting	Ar or Ar + He	Ar satisfactory on sheet metal, Ar + He preferred for thicker base materials

ing process, storage, handling and workpiece preparation as well as applying a practically acceptable joint design [1].

The workpiece to be joined with the pulsed MIG process involves joint preparation which is imperative to ensure quality welds. Based on the thickness of the workpiece, the joints need to be bevelled and in some cases a root back-up must be applied. It is important to clean the joint surface to remove the thin oxide layer (Al<sub>2</sub>O<sub>3</sub>). The removal can be done by mechanical abrasion processes like brushing with stainless steel brushes or by chemical etching. The Al<sub>2</sub>O<sub>3</sub> layer regenerates itself when scratched. It is responsible for the corrosion resistance in aluminium alloys [14] and also for the arc instability problem because it is electrically non-conductive. Al<sub>2</sub>O<sub>3</sub> is hygroscopic and it is usually found hydrated. The melting temperature is 2060 °C [4, 14] which is high when compared to the melting temperature range of 476–657 °C of the 7xxx series alloys [9]. A work preparation guide is presented in Table 3.

**Shielding gas.** The primary function of shielding gas is to protect the weld metal from the atmosphere because heated metal (around the melting point) usually exhibits a tendency to react with the atmosphere to form oxides and nitrides. For aluminium it easily reacts with oxygen at room temperatures. In selecting the shielding gas, the criteria that should be met are as follows [4, 16–18]:

- gas must be able to generate plasma and stable arc mechanism and characteristics;
- it should provide smooth detachment of molten metal from the wire and fulfil the desired mode of metal transfer;
- it should protect the welding head (in the arc immediate vicinity), molten pool and wire tip from oxidation;
- it should help to attain good penetration and good bead profile;
- it should not be detrimental to the welding speed of the process;
- it should prevent undercutting tendencies;
- it should limit post-weld cleaning;
- it should not be detrimental to the weld metal mechanical properties.

The recommended shielding gas for pulsed MIG welding of 7xxx aluminium is argon [1, 17] at flow

rate of about 20 l/min. A mixture of argon and helium can also be used and even helium alone. Helium increases weld penetration, offers higher arc energy and, thus, an increased deposition rate [1, 19]. When the section is lower than 50 mm, helium should be used [4]. More details can be seen in Table 4.

**Welding defects in HSA and UHSA.** The welding of aluminium is rather critical despite the fact that it has a lower melting point compared to steel. The welding of aluminium is critical because of the following considerations [6, 18]:

- stable surface oxide needs to be eliminated before welding;
- presence of residual stresses causes weld cracking due to the high thermal expansion coefficient of aluminium;
- high heat conductivity of aluminium implies that great heat is required to achieve welds, whereas high heat input increases the possibility of distortion and cracking;
- high shrinkage rates on solidification enhance cracking;
- high solubility of hydrogen in molten aluminium causes porosity;
- general susceptibility of the 2xxx, 7xxx and 8xxx series to weld cracking.

Applicable major welding defects in HSA series include hot cracking, porosity, joint softening, not recoverable on post-weld ageing, poor weld zone ductility (HAZ degradation) and the susceptibility of the joint to stress corrosion cracking (Table 5).

**Experimental set-up.** The experiment was carried out using a robotised pulsed MIG welding machine. The schematics of the MIG welding process are presented in Figure 2.

The robot movement was programmed and some test sample welds were made, after which alloy 7025-T6 was welded. Many different welds were made, and the weld parameters were varied to study the effect of heat input on properties of the weld metal. Furthermore, the effect of the welding speed was studied.

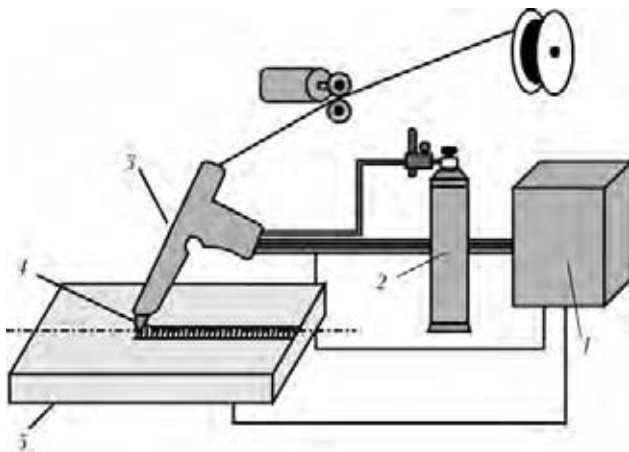
The MIG torch used was Fronius Robacta 5000 360 (max 500 A). The torch was connected to the Motorman (EA1900N) robot. The robot has 6 axes and can attain an accuracy of up to ±0.06 mm. A torch angle of 10° pushing weld direction was used to allow for the purging of the weld area ahead of the arc. The





**Table 5.** Defects in aluminium welds and their prevention [11, 15, 18, 20]

Defect	Cause	Remedy
Oxide inclusions	Insufficient cleaning of the joint Oxide layer on welding wire or filler rods Sharp edges on the joint groove	Thoroughly wire brush before welding and after each pass, then wipe clean Clean wire and rods by abrading with stainless steel wool or «Scotchbrite» Use fresh spool of wire Break sharp edges in weld preparation
Porosity in weld	Inadequate shielding Dye penetrants, lubricants Welding current too high Contaminated shielding gas Incorrect torch angle Travel speed too high Contaminated wire or rods Moisture	Increase gas flow Eliminate draughts Reduce electrode extension Remove any defects fully Clean surfaces with a solvent Keep lubricants away from the weld area Reduce current and refer to the weld procedure Check gas hoses for loose connections or damage Check torch coolant to ensure no leaks Replace gas cylinders Use correct angle and refer to the weld procedure Apply correct speed and refer to the weld procedure Clean wire or rods with solvent Preheat and clean the surface
Porosity in fusion zone	Hydrogen in the base metal	Improve the degassing practice Reduce sodium additions Apply 100 % He shielding
Cold cracking	High joint restraint	Slacken holding clamps Preheating
Hot cracking	Excessive dilution by parent Interpass temperature too high	Reduce welding current Add more filler wire Reduce welding current Cool between passes and sequence welds
Undercutting	Welding current too high Travel speed too high and insufficient filler metal Arc length too long	Reduce current Reduce speed and refer to the weld procedure, add more filler metal Reduce arc length
Lacks of fusion	Welding current too low Travel speed too high Poor joint preparation Incorrect torch angle	Increase current and refer to the weld procedure Reduce travel speed, and refer to the weld procedure Improve joint preparation Apply correct torch angle, and refer to the weld procedure
Crater cracking	Improper breaking of arc	Reduce arc current gradually Use «Crater fill» control if available. «Back weld» over last 25 mm of the bead
Overlap	Slow travel speed Welding current too low Too much filler metal Incorrect torch angle	Increase speed and refer to the weld procedure Increase current Reduce filler metal addition Change torch angle
Drop through	Slow travel speed Welding current too high Joint gap too wide Too much heat built up in part	Increase travel speed Decrease welding current Reduce gap and improve the fit-up Reduce interpass temperature



**Figure 2.** Schematics of MIG welding process: 1 – power source; 2 – shielding gas; 3 – MIG torch; 4 – filler wire; 5 – aluminium workpiece

filler wire extension was 2 mm, and the nozzle-to-workpiece distance (stick-out length) was 18 mm. The shielding gas used was 99.995 % argon and the filler wire was 4043 aluminium. The workpiece was a 5 mm thick plate with an area of 100 × 250 mm. The samples were bead-on-plate welds, so there was no bevelling. However, the joints were cleaned mechanically by using a stainless steel bristle brush reserved for aluminium only.

Many experimental trials were performed, for which 6 different samples of 7025-T6 alloy were selected. The first three samples (A, B and C) had the same feed rate so as to investigate the effect of the welding speed (10, 20 and 30 mm/s). The other three samples (D, E and F) had approximately the same heat input to investigate the effect of constant heat input on the weld. The pulse current frequency was approximately 250 Hz in each weld.

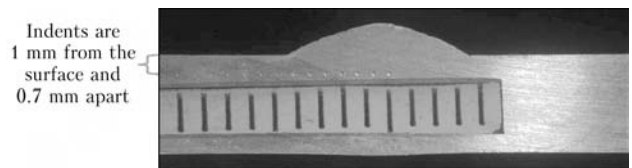
For samples A–C, the feed rate was constant at 10 m/min, and the heat input varied. Heat input  $Q$  for all samples was calculated as [21]

$$Q = \frac{VI-60}{1000S} \cdot 0.8, \quad (1)$$

where  $Q$  is the heat input, kJ/mm;  $V$  is the voltage, V;  $I$  is the current, A;  $S$  is the welding speed, mm/min; 0.8 is the efficiency of the pulsed MIG process.

For samples D–F, heat input was approximately constant and the feed rates were selected as 10, 12 and 14 m/min, respectively.

The base material was a 5 mm thick 7025-T6 plate, and the welding wire was ER 4043 (Table 6). The typical mechanical properties of the wire include the



**Figure 3.** Hardness testing on a weld sample

yield stress of 55 MPa, tensile strength of 165 MPa and an elongation of 18 %. The shielding gas was 99.995 % argon and it was supplied through the MIG torch to protect the weld pool from the atmosphere, because heated metal (around the melting point) usually exhibits a tendency to react with the atmosphere to form oxides and nitrides. For aluminium it easily reacts with oxygen at room temperatures. The recommended shielding gas for pulsed MIG welding 7xxx series aluminium is argon [17].

The hardness testing experiment of the welds was done on a Vickers hardness machine. The test method involved the indentation of the test workpiece with a diamond indenter in the form of right pyramid with a square base and angle of 136° between opposite faces; subjected to a weight of 1–100 kg. The full load was normally applied for 10–15 s. The two diagonals of the indentation made on the surface of the material after the removal of the load were measured using a microscope and their averages calculated [22].

This test was carried out by a 3 kg weight indentation of the diamond tool tip on the prepared weld cross-section. The weight can be varied for different materials, but 3 kg was sufficient because aluminium is relatively soft and 3 kg is enough to create an indentation. Moreover, it is important that the weight is low enough for the aluminium test piece to resist it. The indentations were done at about 1 mm from the weld surface in a row (Figure 3).

The distance between each indentation was 0.7 mm. The shape of the indentation resembled a rhombus. The depth of the indents depended on the material hardness. The dimension of the diagonals of an indentation was measured and the average value from the diagonals was looked up from the hardness table of  $HV3$  to determine the hardness value. The values were then plotted against the distance of each indentation from the weld centreline.

**Results and discussions.** *Effect of heat input on HSA.* Micro- and macrostructure, as well as weld appearance on samples A–C, are presented in Figures 4–6. The picture of each sample shows the microstructure using an ×8 magnification lens for analysing the unmixed zone (UZ), partially melted zone (PMZ),

**Table 6.** Chemical composition of base metal and filler wire used, wt. %

Metal	Al	Be	Cr	Cu	Fe	Mg	Mn	Si	Ti	Zn	Other each	Total
7025	91.5	–	0.30	0.10	0.40	1.50	0.60	0.30	0.10	5.0	0.05	0.15
ER 4043	–	0.0001	–	0.01	0.20	0.01	0.01	4.80	0.02	0.01	–	–

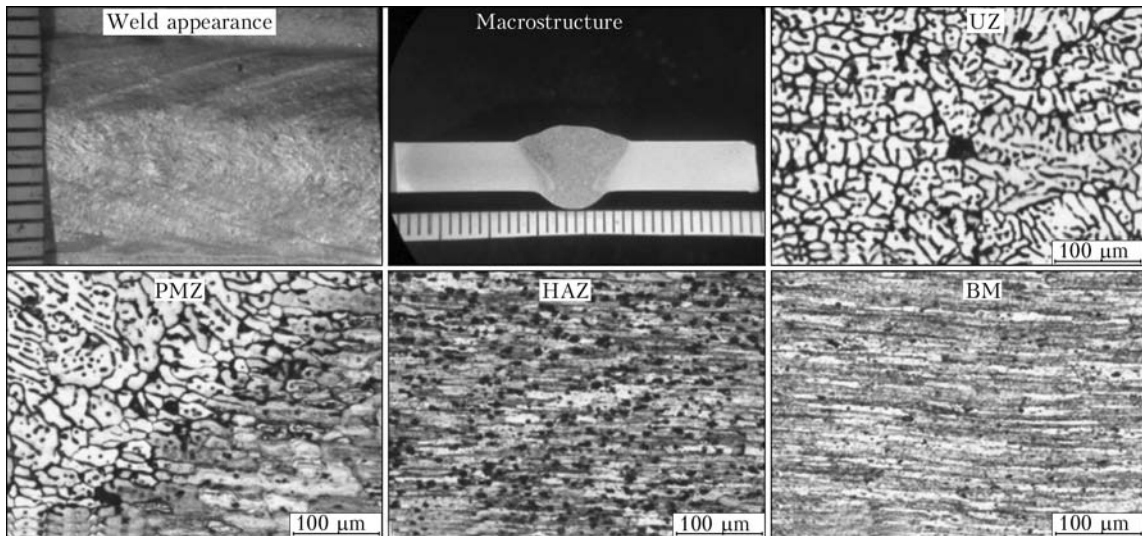


Figure 4. Experimental results for sample A welded at  $v_{w,f} = 10$  m/min,  $v_w = 10$  mm/s,  $Q = 0.318$  J/mm,  $U = 20.1$  V and  $I = 198$  A

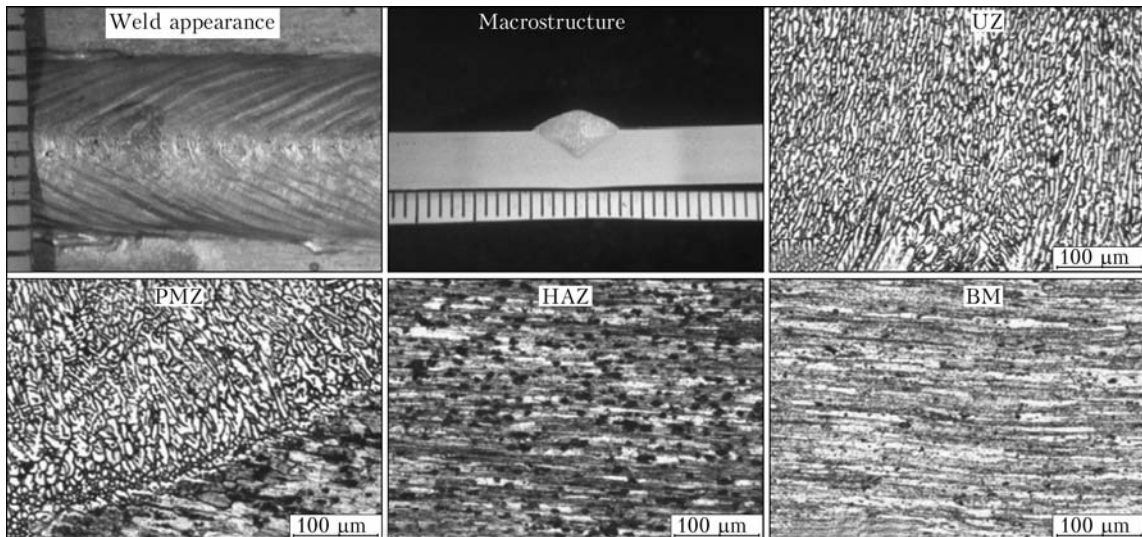


Figure 5. Experimental results for sample B at  $v_{w,f} = 10$  m/min,  $v_w = 25$  mm/s,  $Q = 0.127$  J/mm,  $U = 19.4$  V and  $I = 205$  A

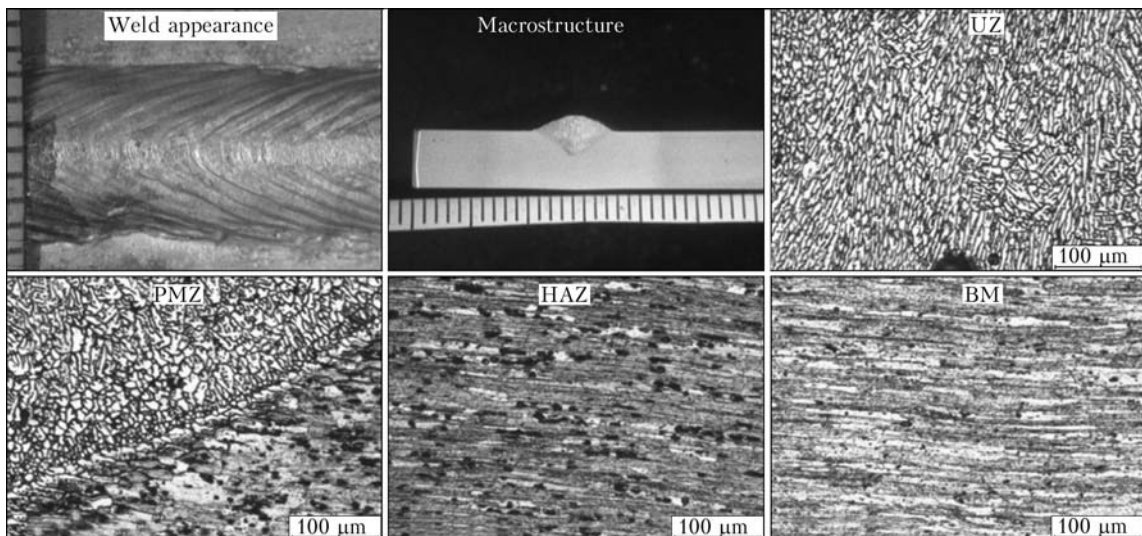


Figure 6. Experimental results for sample C at  $v_{w,f} = 10$  m/min,  $v_w = 30$  mm/s,  $Q = 0.106$  J/mm,  $U = 19.4$  V and  $I = 205$  A

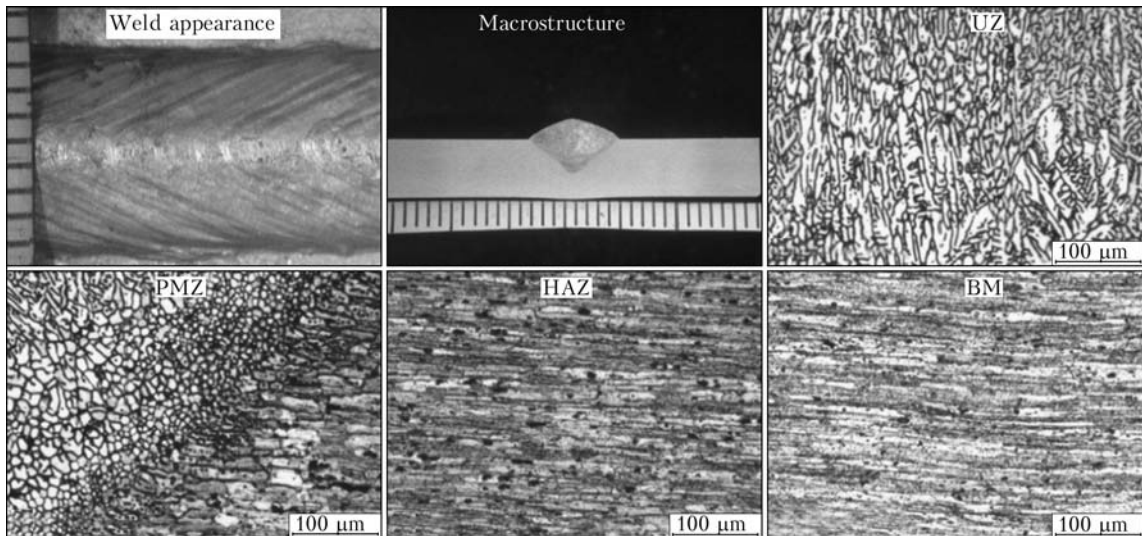


Figure 7. Experimental results for sample D at  $v_{w,f} = 10$  m/min,  $v_w = 20$  mm/s,  $Q = 0.16$  J/mm,  $U = 19.8$  V and  $I = 202$  A

heat-affected zone (HAZ) and base metal (BM). The transition around the weld interface is of great significance. The picture shows how the grains have been transformed, from which inferences can be made as to the mechanical properties of the weld samples.

Comparing samples A, B and C (see Figures 4–6), it can be seen that the grain sizes around the weld interface are small when heat input is low, and vice versa. Furthermore, the transition flow of cells at the interface as it moves from the UZ to the HAZ is smoother with higher heat input where the grain sizes are bigger. With lower heat input as in sample C (see Figure 6) the transition is not as smooth, so the interface is distinct. Heat input is inversely related to the welding speed. When the welding speed increases, heat input reduces. The higher the heat input, the higher the cooling rate. A high cooling rate allows epitaxial growth to occur and also for the cells to grow large, as seen by comparing sample A to samples B and C. In sample A, the HAZ is about 17 mm from the weld centreline, which is the greatest distance of

the three samples (see Figure 4). Thus, it can be said that the higher the heat input, the wider the HAZ.

The grains of UZ in sample C compared to B and A are very fine, which shows that low heat input in A and B is insufficient to melt the pool and penetrate the weld. The high heat input and high welding speed caused high heat energy on the weld in sample C, which makes the weld bead large with a wider root.

Sample C has fine grains compared to B and A, which shows that with high heat input and welding speed there is higher nucleation. In sample C, the grain growth is low compared to A and B because aluminium dissipates heat relatively fast through heat sinks; low heat input means that the high conductivity of aluminium strongly affects the weld microstructure (sample C cools fast).

By comparing the results from samples D, E and F presented in Figures 7–9 it can be noted that keeping the heat input relatively constant but varying the welding speed causes changes in the microstructure. As the welding speed and the wire feed rate increase,

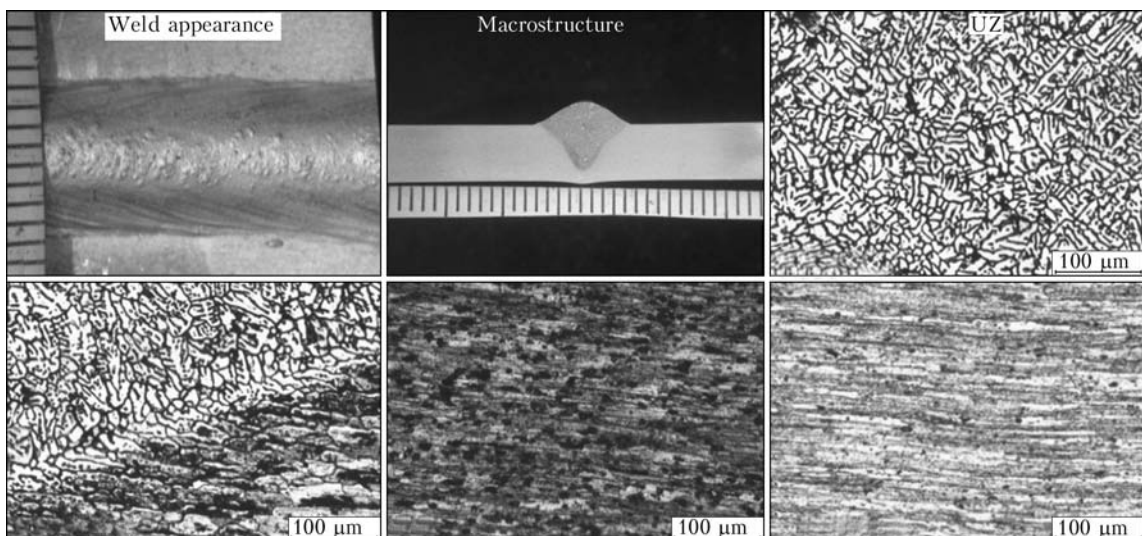


Figure 8. Experimental results for sample E at  $v_{w,f} = 12$  m/min,  $v_w = 24$  mm/s,  $Q = 0.163$  J/mm,  $U = 20.3$  V and  $I = 241$  A

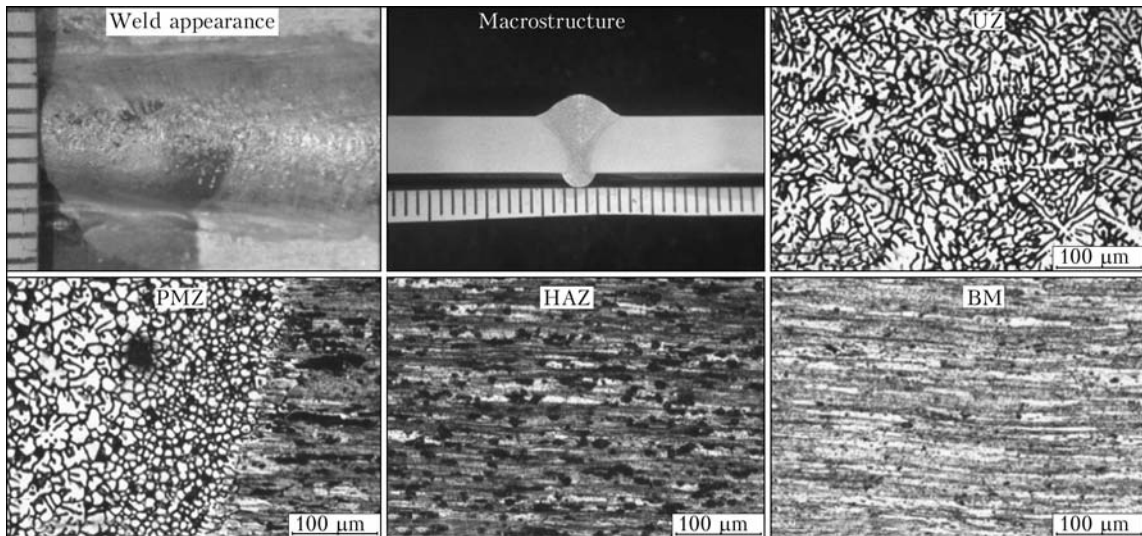


Figure 9. Experimental results for sample F at  $v_{w,t} = 14$  m/min,  $v_w = 28.8$  mm/s,  $Q = 0.158$  J/mm,  $U = 20.5$  V and  $I = 278$  A

also the grain sizes increase. Furthermore, the increased welding speed gives lower nucleation and coarser transitions of grains around the weld interface, which is similar to the effect of heat input in 7025-T6 aluminium welds.

Samples D, E and F indicate that the higher the wire feed rate, the deeper the penetration. Sample C has a constant feed rate with A and B but the grain transition at the weld interface between the UZ and the HAZ is very sharp. This may be a possible failure point as the cells are not as interlocked as in sample B. Sample A shows that the longer the solidification time, the bigger the size of the dendrite [23].

The grains are equiaxed with dendrites within the grains. Fine grain sizes appear when heat input is low, and coarse grain sizes when heat input is high. For example, the UZ in Figure 8 has fine grains due to the low heat input of 0.163 kJ/mm, whereas the UZ in Figure 4 has coarse grains due to high heat input of 0.318 kJ/mm. The grain size variations in the UZ in Figures 4–9 are mainly due to the amount of heat input, since high heat input means a high cooling rate.

A faster welding speed allows narrow welds even with lower heat input (comparing samples A–F). Sample F seems to be the best weld with a narrow bead, narrow HAZ and complete penetration. On the other hand, oxidation occurred on the surface. At a constant welding speed, high heat input increases the weld bead size and HAZ size. The PMZ shows epitaxial growth, which indicates that new grains had nucleated on the heterogeneous sites at the weld interface. There is a random orientation between the base metal grains and weld grains.

As can be seen from samples A–F, since the ratio of 7025-T6 alloy temperature gradient  $G$  to the growth rate  $R$  decreases from the weld interface towards the centre line, the solidification modes have changed from planar to cellular, to columnar dendrite and equiaxed dendrite across the weld interface. The ratio  $G/R$  determines the solidification modes found in the

microstructure. Sample C has the smallest grain size in the UZ. Thus, it can be concluded that it has the highest strength and toughness as the Hall–Petch effect predicts that both strength and toughness increase as the grain sizes reduce [24, 25]. Sample F shows that complete weld penetration can be achieved with minimal heat input if other weld data are set correctly.

Weld defects such as porosity and oxidation were found on the welds. Porosity could be due to gas entrapment during welding, whereas oxidation could be due to poor shielding gas covering (the weld pool has contact with atmospheric air).

**Hardness of HSA welded joints (7025-T6).** The hardness tests of samples A–C are presented in Figure 10, where the plots for samples A, B and C are combined on the same graph. The vertical line, labelled WI, denotes the weld interface. The points on the graph curve indicate the distance of each indentation point from the weld centreline on the horizontal axis and the hardness value when traced on the vertical axis. The graph also shows the weld zones, HAZ and BM. Sample C has the lowest heat input of 0.106 kJ/mm resulting in a high hardness profile, sample B – relatively higher heat input of 0.127 kJ/mm resulting in a lower hardness profile than sample C, and sample A – the highest heat input of 0.318 kJ/mm resulting in the lowest hardness profile.

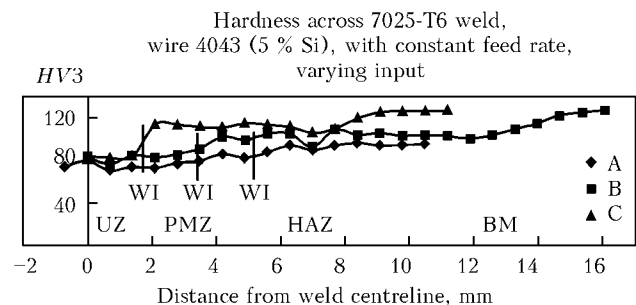
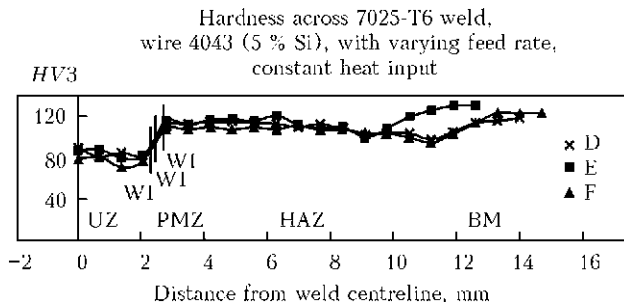


Figure 10. Hardness distribution for samples welded with varying heat input: 0.106 (C), 0.127 (B), 0.318 (A) kJ/mm



**Figure 11.** Hardness distribution for samples welded with relatively constant heat input of about 0.16 kJ/mm

Sample C also has the highest hardness at the WI, thus, implying that high heat input allows for high hardness of the WI, due to solution hardening during welding. High heat input causes solubility and thereby higher hardening through the solidification process. It can also be said that the higher the heat input, the wider the weld bead and the further away from the weld centreline is the WI. The hardness test also shows this with relatively constant heat input. The hardness pattern of samples D, E and F are similar, but E exhibits small variation. The hardness around 3 mm away from the weld centreline shows a rapid increase in the value from the previous point (around 2 mm from the weld centreline). This is due to the closeness of the WI. From samples D, E and F it can be seen that for 7025-T6 weld, hardness reduces in the weld zone and increases towards the base material. The hardness graph presents half of the symmetric welds. At the WI it can be said that the hardness values of D, E and F samples are relatively identical. This implies that at constant heat input, the hardness profile of 7025-T6 aluminium alloy remains the same.

The hardness tests of samples D, E and F, presented in Figure 11, show that the hardness profiles for the three samples are relatively similar. The WI range is within 0.5 mm as a result of a relatively constant heat input. The labelling and description of the graph is the same as for samples A-C.

## CONCLUSIONS

1. The study showed that in 7025-T6 aluminium alloys the grain size reduces as the heat input reduces. The transition of cells from the UZ to HAZ is smoother with higher heat input. At constant heat input the grain size increases when wire feed rate, welding speed and current increase simultaneously but the hardness remains relatively constant. When heat input is high, the HAZ is wider, nucleation is lower, and the grains around the weld interface are coarser.

2. In 7025-T6 aluminium alloy, high heat input results in a low hardness profile but the hardness of the UZ is the same in all the selected samples. The higher the heat input, the wider the weld bead, the further away is the weld interface and the deeper the weld penetration. The longer the solidification time, the larger the dendrites and a high cooling rate allows for epitaxial cell formation. The 7025-T6 alloy, like other high-strength aluminium alloys, experiences HAZ softening but can be restored by postweld heat treatment.

- Yeomans, S.R. (1990) Successful welding of aluminium and its alloys. *Australian Welding J.*, 35(4), 20-24.
- Graeve, I.D., Hirsch, J. (2010) 7xxx series alloys. <http://aluminium.matter.org.uk/content/html/eng/default.asp?catid=214&pageid=2144417086>
- Dickerson, P.B., Irving, B. (1992) Welding aluminium: It's not as difficult as it sounds. *Welding J.*, 71(4), 45-50.
- Mathers, G. (2002) *The welding of aluminium and its alloys*. Boca Raton: CRC Press; Woodhead Publ.
- Maurice, S. (1997) *Aluminum structures: Handbook of structural engineering*. 2nd ed. CRC Press.
- Campbell, F.C. (2006) *Manufacturing technology for aerospace structural materials*. Amsterdam; San Diego: Elsevier.
- (2008) *ASM Handbook*. Vol. 15: Casting. Materials Park: ASM Int.
- Kopeliovich, D. (2009) Classification of aluminum alloys. In: *Substances and technology*.
- (2010) *MatWeb - The Online Materials Information Resource*.
- Kaufman, G.J. (2000) *Applications for aluminum alloys and tempers*. ASM Int.
- John, D. (1999) Heat-treatable alloys. In: *Aluminium design and construction*. New York: Taylor & Francis, 301.
- Aluminum alloys and temper designations 101*. Dayco Ind., 1-5.
- Volpone, L.M., Mueller, S. (2008) Joints in light alloys today: the boundaries of possibility. *Welding Int.*, 22(9), 597-609.
- George, E.T., MacKenzie, D.S. (2003) *Handbook of aluminum: Physical metallurgy and processes*. New York: Marcel Dekker.
- Renshaw, M. (2004) The welding of aluminium castings. In: *Aluminium - light strong and beautiful*. A.F.o.S. Africa, 11-13.
- (2008) Choosing shielding gases for gas metal-arc welding. *Welding J.*, 87(4), 32-34.
- Boughton, P., Matani, T.M. (1967) Two years of pulsed arc welding. *Welding and Metal Fabr.*, Oct., 410-420.
- Olson, D.L. (1993) *Welding, brazing, and soldering: ASM handbook*. Metals Park: ASM Int.
- Blewett, R.V. (1991) Welding aluminium and its alloys. *Welding and Metal Fabr.*, Oct., 5.
- Ba Ruizhang, G.S. (2004) Welding of aluminum-lithium alloy with a high power continuous wave Nd:YAG laser. *IIV Doc. IV-866-04*.
- Hirata, Y. (2003) Pulsed arc welding. *Welding Int.*, 17(2), 98-115.
- Chandler, H. (1999) *Hardness testing*. Materials Park: ASM Int.
- Kou, S. (2003) *Welding metallurgy*. Hoboken: Wiley-Intersci.
- Sato, Y.S., Urata, M., Kokawa, H. et al. (2003) Hall-Petch relationship in friction stir welds of equal channel angular-pressed aluminium alloys. *Materials Sci. and Eng. A*, 354(1/2), 298-305.
- Vander Voort, G.F., (2004) *Metallography and microstructures*. Materials Park: ASM Int.



# HEAT-PROTECTING PROPERTIES OF THERMAL SPRAY COATINGS CONTAINING QUASI-CRYSTALLINE ALLOY OF THE Al–Cu–Fe SYSTEM

A.L. BORISOVA, Yu.S. BORISOV, E.A. ASTAKHOV, A.P. MURASHOV,  
A.N. BURLACHENKO and T.V. TSYMBALISTAYA  
E.O. Paton Electric Welding Institute, NASU, Kiev, Ukraine

Given are the investigation results on heat-protecting properties of plasma and detonation coatings (two-layer and graded), in which  $ZrO_2$  stabilised by  $Y_2O_3$  is used as a ceramic component, and alloy Al–Cu–Fe containing the quasi-crystalline  $\psi$ -phase is used as a metallic component.

**Keywords:** *plasma spraying, detonation spraying, zirconia, Al–Cu–Fe system quasi-crystalline alloy, thermal barrier coatings, internal combustion engine components*

One of the current ways of increasing the operating efficiency of gas turbine and diesel engines and extending service life of their components is to use thermal barrier coatings (TBC) [1–4], which found practical application in gas turbine engines (GTE). In this case a conventional structure of TBC consists of three layers: NiCrAlY used as a bond coat and providing adhesion of TBC to a component surface and its oxidation protection at working temperatures of 900–1100 °C,  $Al_2O_3$  used as an interlayer acting as a barrier for diffusion of oxygen to the bond coat and providing adhesion of ceramics to the heat-resistant bond coat, and external layer  $ZrO_2$ – $Y_2O_3$  characterised by heat-insulating properties. Such coatings are deposited by using the atmospheric plasma spraying, decreased-pressure plasma spraying and electron beam evaporation methods [1, 5]. Heat-resistant nickel and iron alloys are employed as materials of the GTE components.

Diesel engines are another application field for TBCs. Service conditions and goals of these coatings in diesel engines differ from those in GTE. For instance, the temperature of heating of the combustion chamber components in diesels is 350–400 °C. Application of the TBCs the gas temperature in the combustion chamber to be increased to 850–900 °C, this providing a complete combustion of fuel, decrease in its consumption (by 15–20 %) and increase in the engine power (by 8 %) [3, 6].

The most important problem whose solution is related to application of TBCs in diesel engines is to increase the ecological efficiency of their operation by reducing emissions into atmosphere. As proved by the investigation results, the emissions can be reduced by 10–11 % [7]. At present the urgency of this problem grows because of toughening of the requirements to reduction of the emissions, this being attributed to a

change to the new, Euro VI index [8]. A difference of TBCs in diesel engines also lies in a composition of structural materials of the diesels, where aluminium and titanium alloys are used to an increasing extent.

The main method for deposition of TBCs on the surfaces of the combustion chambers of diesels is plasma spraying. Conditions for formation of TBCs and their operation on the surface of such materials differ from those on heat-resistant alloys of the GTE components. The said differences in service conditions of TBCs for GTE and diesel engines make its necessary to use for the latter the top heat-insulating layers of a larger thickness (up to 1 mm or thicker) and change requirements to the bond coat material, which does not have to resist high-temperature oxidation and creep, as is the case of coatings of the Me–Cr–Al–Y system [1, 2, 6].

Therefore, development of the new compositions of TBCs for application under conditions of operation of diesel engines and the technology for their deposition on the surface of aluminium and titanium alloys is a pressing problem for this engineering area.

Alloys with a quasi-crystalline structure, and first of all alloys of the Al–Cu–Fe system, are of high recent interest to researchers and production engineers [9–11]. For example, alloy  $Al_{63}Cu_{25}Fe_{12}$ , which corresponds in chemical composition to the region of existence of the quasi-crystalline  $\psi$ -phase, has such characteristics as low thermal conductivity ( $1\text{--}2\text{ W}\cdot\text{m}^{-1}\cdot\text{K}^{-1}$ ), high values of linear thermal expansion coefficient (LTEC) ( $1\cdot 10^{-5}\text{ K}^{-1}$ ) [12] and hardness (up to 10 GPa) [13], elastic recovery ability ( $H/E < 0.02$ ), corrosion resistance in many aggressive environments [14–17], heat resistance to a temperature of 500 °C [18–21] and wear resistance [22–25]. All this allows an assumption that coatings of the Al–Cu–Fe system alloy can be applied as a binder interlayer in TBCs with  $ZrO_2$ , including for aluminium alloys. This quasi-crystalline alloy is close to  $ZrO_2$  in thermal conductivity, this decreasing the level of internal stresses between



**Table 1.** Parameters of plasma spraying of TBCs

Coating composition	Current, A	Voltage, V	Argon flow rate, l/min	Spraying distance, mm
AlCuFe	500	30	25	130–140
NiCrAlY	500	30	25	130–140
50 % AlCuFe + 50 % ZrO <sub>2</sub>	500	50	25	110–120
50 % NiCrAlY + 50 % ZrO <sub>2</sub>	500	60	25	110–120
ZrO <sub>2</sub>	500	60	25	110–120

the layers of a bond coat and ceramic coating, while in LTEC equal to  $(14-18) \cdot 10^{-6} \text{ K}^{-1}$  it is compatible with the protected components of aluminium alloys (their LTEC is  $(20-24) \cdot 10^{-6} \text{ K}^{-1}$ ), which should lead to decrease in residual stresses at an interface with the substrate and increase in adhesion strength.

Parameters of thermal spraying of coatings of the Al–Cu–Fe system alloy on different metals, including aluminium, and properties of such coatings have been much studied recently [11].

The key characteristics of the coatings (hardness, thermal conductivity, corrosion and wear resistance, etc.) have been found to depend on the phase composition of a sprayed layer, and first of all on the content of the quasi-crystalline  $\psi$ -phase.

Dependence of quasi-crystallinity of the sprayed coatings on the temperature conditions of their formation is related to the fact that size of a region of existence of the quasi-crystalline  $\psi$ -phase on the phase equilibrium diagram depends on the temperature. As the temperature decreases, the region of the  $\psi$ -phase becomes narrower, this being accompanied by widening of the neighbouring region of the approximant crystalline phase as a result of slight displacements of atoms. At the same time, the approximant phases located near the boundaries of existence of the quasi-crystalline phase can have the same properties (including thermal-physical ones) as quasi-crystals [26].

This study presents results of investigations of heat-protecting properties of plasma and detonation coatings with different structures (two- and multi-layer, graded), in which partially stabilised zirconia (ZrO<sub>2</sub> + 7 % Y<sub>2</sub>O<sub>3</sub>) is used as a material of the protecting ceramic layer, and also such materials as alloys AlCuFe containing the quasi-crystalline  $\psi$ -phase and AlCuFeTiCrSi containing the approximant  $\alpha$ -phase

are used as a bond coat material, along with traditional heat-resistant alloy NiCrAlY.

Heat-protecting properties of the coatings were investigated on a rig with specimens directly heated by the flame jet of gas torch GN-2. The C<sub>3</sub>H<sub>8</sub> and O<sub>2</sub> mixture was used as a combustible. The torch was placed at a distance of 50–60 mm from the surface of a specimen. The specimens were heated for 5 s and then cooled for 30 s by compressed air.

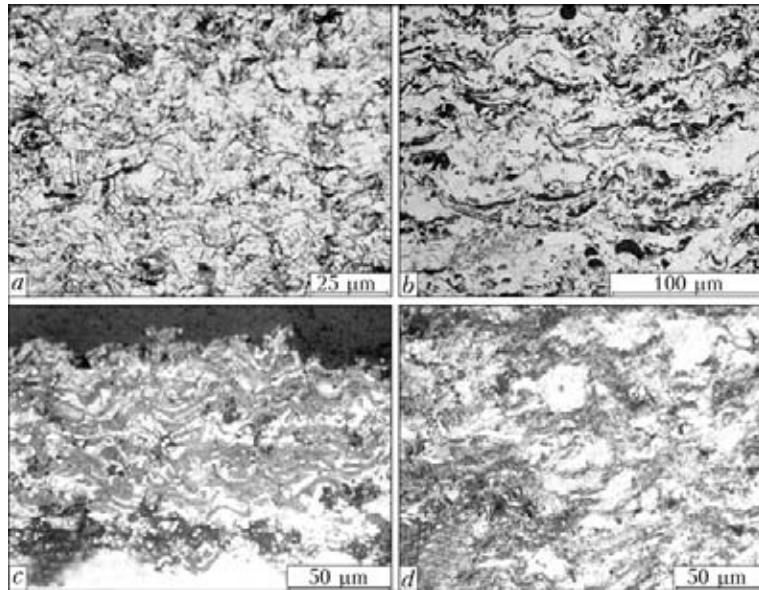
A thermocouple was calked to a depth of 2 mm in a 30 mm diameter and 3 mm thick specimen with an aluminium alloy coating on the opposite side to the coating to measure the heating-cooling process dynamics. The temperature was measured with digital multimeter UT70B. The measurement range of the instrument was 40–1000 °C, resolution was 1 °C, and error depending on the measurement range was 1–3 %. Up to 10 heating-cooling cycles were conducted for each type of the coatings. The maximal temperature of an uncoated specimen regulated by the distance to it and by the thermal power of the torch was approximately 400 °C. That corresponded to the working temperature of components of a piston group of internal combustion engines (ICE) manufactured from aluminium alloys [3].

Heat-protecting properties of the coatings sprayed by the detonation and plasma methods using AlCuFe powders containing the quasi-crystalline  $\psi$ -phase and 75 % AlCuFe + 25 % TiCrSi powder mixture containing the approximant  $\alpha$ -phase, as well as of the two-layer coatings with the ceramic thermal barrier layer of ZrO<sub>2</sub> and metallic bond coat of NiCrAlY or AlCuFe, and of the three- and five-layer (graded) coatings of the above components were investigated. In this case the task was to establish dependence of the efficiency of heat-protecting properties of the thermal spray coatings on such factors as a spraying method, structure

**Table 2.** Parameters of detonation spraying of TBCs

Coating composition	Flow rate of working gases, m <sup>3</sup> /h			Layer thickness per shot, $\mu\text{m}$	Spraying distance, mm
	C <sub>3</sub> H <sub>8</sub>	O <sub>2</sub>	N <sub>2</sub>		
AlCuFe	1.15	0.5	0.4	10–12	110
NiCrAlY	1.15	0.5	0.4	10–12	110
50 % AlCuFe + 50 % ZrO <sub>2</sub>	0.50	2.0	–	6–8	110
50 % NiCrAlY + 50 % ZrO <sub>2</sub>	0.50	2.0	–	6–8	110





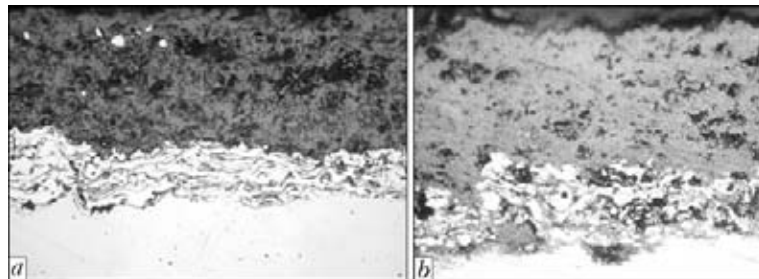
**Figure 1.** Microstructures of one-layer plasma (*a, c*) and detonation (*b, d*) coatings sprayed from  $Al_{63}Cu_{25}Fe_{12}$  (*a, b*) and 75 %  $Al_{63}Cu_{25}Fe_{12}$  + 25 %  $Ti_{60}Cr_{32}Si_8$  (*c, d*) powders

and phase composition of a coating, and thickness of a sprayed layer.

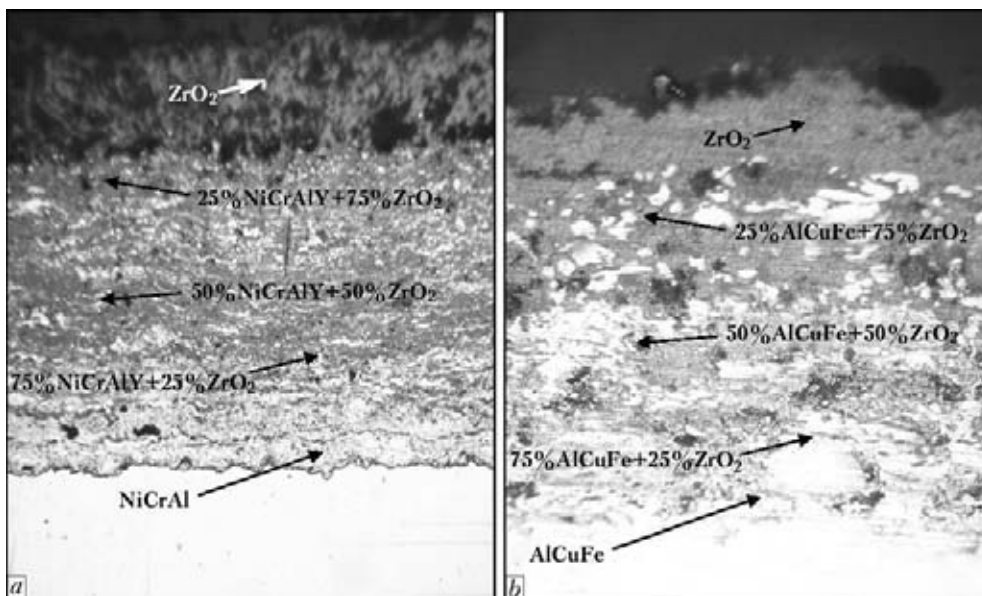
The coatings were deposited by using process parameters identified from the results of studies [27–29] dedicated to investigation of structure and phase com-

position of thermal spray AlCuFe coatings containing the quasi-crystalline phase (Tables 1 and 2).

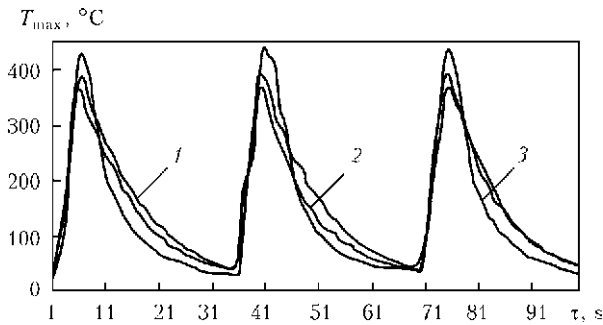
Figures 1–3 show typical structures of some of the investigated coatings, and Figure 4 shows heating–cooling cyclograms for uncoated specimens 1 and for



**Figure 2.** Microstructures ( $\times 200$ ) of two-layer coatings: *a* – plasma coating NiCrAlY– $ZrO_2$ ; *b* – detonation coating AlCuFe– $ZrO_2$



**Figure 3.** Microstructures ( $\times 100$ ) of graded thermal spray coatings: *a* – detonation coating NiCrAlY–(75 % NiCrAlY + 25 %  $ZrO_2$ )–(50 % NiCrAlY + 50 %  $ZrO_2$ )–(25 % NiCrAlY + 75 %  $ZrO_2$ )– $ZrO_2$ ; *b* – plasma coating AlCuFe–(75 % AlCuFe + 25 %  $ZrO_2$ )–(50 % AlCuFe + 50 %  $ZrO_2$ )–(25 % AlCuFe + 75 %  $ZrO_2$ )– $ZrO_2$

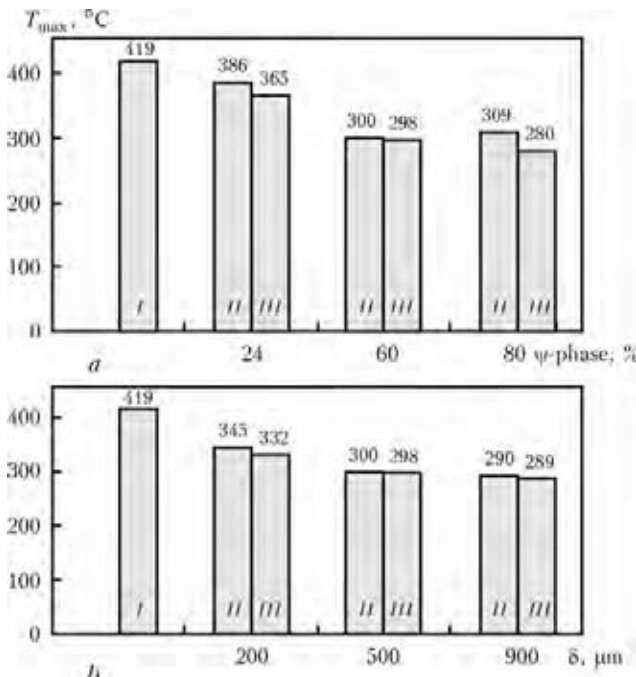


**Figure 4.** Cyclogram of heating and cooling of aluminium alloy specimens without coating (1) and with AlCuFe coating deposited by plasma (2) and detonation (3) methods (coating thickness – 400  $\mu\text{m}$ , content of the quasi-crystalline  $\psi$ -phase – 60 %)

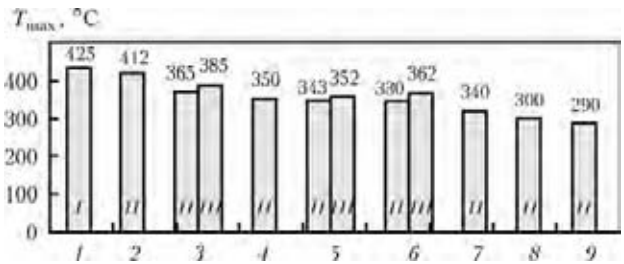
specimens with the Al–Cu–Fe system alloy coatings produced by the plasma 2 and detonation 3 methods. Analysis of the cyclograms allowed evaluating the effect of such parameters as a spraying method, thickness of the sprayed layer and content of the quasi-crystalline  $\psi$ -phase in a coating (Figure 5) on the efficiency of heat protection provided by coatings of identical compositions.

Allowing for the level of  $T_{\text{max}}$ , the content of the  $\psi$ -phase in initial AlCuFe powders exerts the most substantial effect on the efficiency of heat protection, the value of the above indicator being up to 60 wt.% (see Figure 5). Transition to application of AlCuFe powders containing 80 % of the  $\psi$ -phase (at thickness of the AlCuFe coating equal to  $(800 \pm 100) \mu\text{m}$ ) has almost no influence on the level of  $T_{\text{max}}$ .

At the same time, evaluation of the effect of thickness of the AlCuFe coating on its heat-protecting prop-



**Figure 5.** Efficiency of heat protection by the thermal spray ( $800 \pm 100 \mu\text{m}$  thick coating sprayed from the  $\text{Al}_{63}\text{Cu}_{25}\text{Fe}_{12}$  powder depending on the content of the  $\psi$ -phase in the initial powder (a) and thickness of the sprayed layer at a  $\psi$ -phase content of 60 % in the initial powder (b): I – without coating; II – detonation coating; III – plasma coating



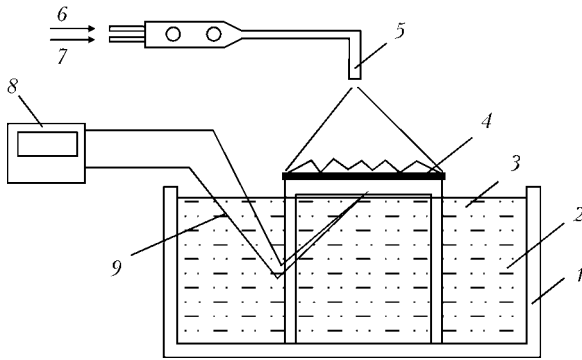
**Figure 6.** Efficiency of heat protection by plasma and detonation coatings: 1 – without coating; 2 – NiCrAlY; 3 – AlCuFe; 4 – NiCrAlY +  $\text{ZrO}_2$ ; 5 – NiCrAlY + (50 % NiCrAlY + 50 %  $\text{ZrO}_2$ ); 6 – AlCuFe + (50 % AlCuFe + 50 %  $\text{ZrO}_2$ ); 7 – NiCrAlY + (75 % NiCrAlY + 25 %  $\text{ZrO}_2$ ) + (50 % NiCrAlY + 50 %  $\text{ZrO}_2$ ) + (25 % NiCrAlY + 75 %  $\text{ZrO}_2$ ) +  $\text{ZrO}_2$ ; 8 – AlCuFe + (75 % AlCuFe + 25 %  $\text{ZrO}_2$ ) + (50 % AlCuFe + 50 %  $\text{ZrO}_2$ ) + (25 % AlCuFe + 75 %  $\text{ZrO}_2$ ) +  $\text{ZrO}_2$ ; 9 – AlCuFeTiCrSi + (75 % AlCuFeTiCrSi + 25 %  $\text{ZrO}_2$ ) + (50 % AlCuFeTiCrSi + 50 %  $\text{ZrO}_2$ ) + (25 % AlCuFeTiCrSi + 75 %  $\text{ZrO}_2$ ) +  $\text{ZrO}_2$  (see designations I–III in Figure 5)

erties (Figure 6) showed that this effect decreases with increase in thickness from 200 to 900  $\mu\text{m}$ . Decrease in the  $T_{\text{max}}$  level compared to that of the uncoated specimens per 100  $\mu\text{m}$  of the coating thickness is 37.0–43.5  $^{\circ}\text{C}$  at a coating thickness of 200  $\mu\text{m}$ , 23.8–24.0  $^{\circ}\text{C}$  at a coating thickness of 500  $\mu\text{m}$ , and 14.3  $^{\circ}\text{C}$  at a coating thickness of 900  $\mu\text{m}$ . It was established that the AlCuFe plasma coatings compared to the detonation ones provide a more efficient protection of the substrate from heat flows, this most likely being associated with a lower content of the  $\psi$ -phase in the latter. This is caused by a more intensive oxidation of material of the spraying particles, the size of which in detonation spraying is 1.5–2 times smaller than in plasma spraying.

The efficiency of heat protection by the thermal spray coatings depending on the composition and internal structure (two- and multilayer) was compared on specimens with the identical total thickness of the protective layer equal to 500–600  $\mu\text{m}$  (Figure 6). Analysis of the results showed that decrease in temperature of the protected substrate, showing the effi-



**Figure 7.** Piston of aluminium alloy with thermal barrier coating



**Figure 8.** Schematic of the rig for testing heat-protecting properties of quasi-crystalline coatings: 1 – bath; 2 – water; 3 – piston; 4 – coating; 5 – gas flame torch; 6 – oxygen; 7 – propane; 8 – instrument UT70B; 9 – thermocouple

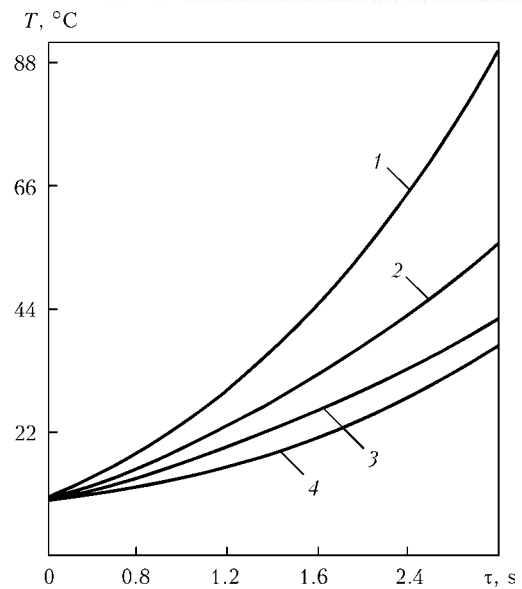
ciency of heat protection provided by the coatings, depends on the following factors:

- coating composition. The AlCuFe coatings as a metallic component are superior to the NiCrAlY coatings (the value of  $T_{\max}$  is 24–47 °C lower);
- coating structure. The highest effect is achieved with the five-layer (graded) coatings, which are superior to the traditional two-layer ones (decrease in  $T_{\max}$  is 125–135 °C, compared to 95 °C);
- deposition method. For all the coatings investigated, the plasma method is advantageous over the detonation one (difference in decrease in  $T_{\max}$  is 20–30 °C).

The efficiency of protection grows with increase in thickness of the protective layer. However, in this case the level of internal stresses leading to separation of a coating from the substrate because of differences in LTEC also grows. From this standpoint, the AlCuFe coatings are advantageous over the NiCrAlY ones when they are deposited on aluminium alloys, which is attributable to closeness of their LTEC. The data shown in Figure 6 are indicative of the presence of an optimal value of the coating thickness, which is related to its diminishing effect on the efficiency of heat protection.

As the given results proved a high potential of the AlCuFe coatings containing the quasi-crystalline  $\psi$ -phase in use as thermal barrier ones for components of ICEs made from aluminium alloys, it is of interest to study their behaviour under the conditions close to service ones for the ICEs.

The AlCuFe plasma coating produced by spraying a powder with 45 % of the quasi-crystalline  $\psi$ -phase, the detonation coating of the AlCuFeTiCrSi powder containing 50 % of the approximant  $\alpha$ -phase and, for comparison, the ZrO<sub>2</sub> plasma coating with a bond coat of alloy NiCrAlY were tested. The coatings were applied to an ICE piston with a diameter of 78 mm and 76 mm high, made from the aluminium alloy (Figure 7). Thickness of the coatings was (450 ± 50) μm. The tests were carried out on a rig (Figure 8) by heating the piston surface with a torch located at a distance of (55 ± 5) cm from the piston surface. Heat-



**Figure 9.** Dynamics of heating of a piston with the gas torch: 1 – without coating; 2 – ZrO<sub>2</sub> with NiCrAlY bond coat; 3 – AlCuFe; 4 – AlCuFeTiCrSi

ing was performed for 3 s, and cooling – for 30 s. The dynamics of heating of the piston bottom was averaged over the results of 10 thermal cycles (Figure 9).

It was established that the ultimate temperature of the piston bottom heated for 3 s by the flame of the gas torch at the absence of a coating was 102 °C, and that for the ZrO<sub>2</sub> coatings with the NiCrAlY, AlCuFe and AlCuFeTiCrSi bond coats was 71, 60 and 56 °C, respectively.

The experimental data obtained on behaviour of materials of the Al–Cu–Fe system alloy containing the quasi-crystalline  $\psi$ -phase, and of the Al–Cu–Fe–Ti–Cr–Si system alloy with an approximant structure ( $\alpha$ -phase) used as thermal barrier coatings on the surfaces of aluminium alloy components are indicative of their high efficiency. Under conditions of cyclic heating with a propane-oxygen jet of the torch, they are superior in the indicator of a maximum achievable temperature of the substrate to the traditional two-layer thermal barrier coating, i.e. NiCrAlY/ZrO<sub>2</sub>. Such thermal-physical properties of the investigated coatings, along with the LTEC values close to those of aluminium alloys, make them promising for development of TBCs for diesel engines manufactured from light alloys. In operation of ICE with a TBC the losses of heat in the cooling system will be reduced, the working temperature in the combustion chamber will be increased, and the technical and economic indices of operation of a diesel engine will be improved. Decrease in temperature of the engine components will allow intensity of their wear to be reduced.

1. Iliushchenko, A.F., Ivashko, V.S., Okovity, V.A. et al. (1998) *Thermal barrier coatings based on ZrO<sub>2</sub>*. Minsk: NII PM.
2. Kolomytsev, P.T. (1991) *High-temperature protective coatings for nickel alloys*. Moscow: Metallurgiya.



3. Nikitin, M.D., Kulik, A.Ya., Zakharov, N.I. (1977) *Thermal barrier and wear-resistant coatings for diesel components*. Leningrad: Mashinostroenie.
4. Zhu, D., Miller, R.A. (1999) Thermal barrier coatings for advanced gas turbine and diesel engines. In: *NASA/TM 209453*.
5. Moskal, G. (2009) Thermal barrier coatings: characteristics of microstructure and properties. Generation and directions of development of bond. *J. Achiev. in Mat. and Manufac. Eng.*, **37**(2), 323–331.
6. Soltani, R., Samadi, H., Garcia, E. et al. (2005) Development of alternative thermal barrier coatings for diesel engines. In: *Proc. of SAE Int.* (Toronto, 2005), **1**.
7. Buyukkaya, E., Engine, T., Cerit, M. (2006) Effects of thermal barrier coating on gas emissions and performance of a LNR engine with different injection timings and valve adjustments. *Energy Conversion and Management*, **47**, 1298–1310.
8. Bailey, N., Mill, B., Whyman, P. (2011) New, low cost thermal barrier coating developed specifically for diesel engine applications to solve heat issues associated with 2013 Euro VI emissions introduction. *Automotive Industry Today*, **2**.
9. Huttunen-Saarivirta, E. (2004) Microstructure, fabrication and properties of quasicrystalline Al–Cu–Fe alloys: a review. *J. Alloys and Compounds*, **363**, 150–174.
10. Adeeva, L.I., Borysova, A.L. (2002) Quasi-crystalline alloys as a new advanced material for protective coatings. *Fizyka i Khimiya Tv. Tila*, **3**(3), 454–464.
11. Borysova, A.L., Borysov, Yu.S., Adeeva, L.I. et al. (2005) Thermal spray coatings containing quasi-crystalline phase, properties and applications (Review). *Ibid.*, **6**(1), 124–136.
12. Haberkern, R., Lindqvist, P., Fritsch, G. (1993) Transport properties of quasicrystalline AlCuFe. *J. Non-Crystalline Solids*, **153/154**, 303–307.
13. Edagawa, K., Kajiyama, K., Takeuchi, S. (1999) Thermal expansion and Gruneisen parameters of quasicrystals. *Mat. Res. Soc. Symp. Proc.*, **553**, 403–408.
14. Borisov, Yu.S., Borisova, A.L., Golnik, V.F. et al. (2007) Corrosion resistance of thermal spray coatings of quasi-crystalline phase-containing AlCuFe base alloys. *The Paton Welding J.*, **2**, 27–31.
15. Rudiger, A., Koster, U. (2000) Corrosion behavior of Al–Cu–Fe quasicrystals. *Mat. Sci. and Eng.*, **294/296**, 890–893.
16. Chungen Zhou, Rui Cai, Shengkai Gong et al. (2006) Hot corrosion of AlCuFeCr quasicrystalline coating on titanium alloys with NaCl deposit. *Surface and Coatings Techn.*, **201**, 1718–1723.
17. Massiani, Y., Ait Yaazza, S., Dubois, J.M. (1995) Electrochemical corrosion behaviour of quasicrystalline coatings in dilute acetic acid. In: *Proc. of 5th Int. Conf. on Quasicrystals*, 790–793.
18. Srinival, V., Barua, P., Chosh, T.B. et al. (2004) Oxidation behavior of Al–Cu–Fe nanoquasicrystal powders. *J. Non-Crystalline Solids*, **334/335**, 540–543.
19. Yamasaki Michiaki, Tsai An Pang (2002) Oxidation behavior of quasicrystalline Al<sub>63</sub>Cu<sub>25</sub>Fe<sub>12</sub> alloys with additional elements. *J. Alloys and Compounds*, **342**, 473–476.
20. Sanchez, A., Garcia de Blas, F.J., Algaba, J.M. et al. (1999) Application of quasicrystalline materials as thermal barriers in aeronautics and future perspectives of use for these materials. *Mat. Res. Soc. Symp. Proc.*, **553**, 447–457.
21. Haugeneder, A., Eisenhammer, T., Mahr, A. et al. (1997) Oxidation of quasicrystalline and crystalline AlCuFe thin film in air. *Thin Solid Films*, **307**, 120–125.
22. Dubois, J.M., Kang, S.S., Von Stebut, J. (1991) Quasicrystalline low-friction coatings. *J. Mat. Sci. Lett.*, **10**, 537–541.
23. Solderet, D.J., Krotz, P.D., Daniel, R.L. et al. (1995) Microstructure and wear behavior of quasicrystalline thermal sprayed coatings. In: *Proc. of 8th Nat. Thermal Spray Conf.* (Houston, Sept. 11–15, 1995), 627–632.
24. De Palo, S., Usmani, S., Sampath, S. et al. (1997) Friction and wear behavior of thermally sprayed Al–Cu–Fe quasicrystal coatings. *Ibid.*, 135–139.
25. Galano, M., Audebert, F., Garcia Escorial, A. et al. (2009) Nanoquasicrystalline Al–Cu–Fe-based alloys. Pt 2: Mechanical properties. *Acta Mater.*, **57**, 5120–5130.
26. Goldman, A.I., Kelton, R.F. (1993) Quasicrystals and crystalline approximants. *Amer. Phys. Soc. Rev. of Modern Physics*, **65**(1), 213–230.
27. Borisova, A.L., Tunik, A.Yu., Adeeva, L.I. et al. (2010) Thermal barrier multilayer plasma coatings ZrO<sub>2</sub>–NiCrAlY. *The Paton Welding J.*, **10**, 22–28.
28. Borisova, A.L., Adeeva, L.I., Tunik, A.Yu. et al. (2010) Plasma ZrO<sub>2</sub> coatings with metallic bond coat of alloy Al–CuFe. *Ibid.*, **4**, 25–29.
29. Astakhov, E.A., Kaplina, G.S., Kokorina, N.N. et al. (2009) Study of structure and phase composition of detonation thermal-barrier coatings from quasi-crystalline alloys. In: *Proc. of Int. Conf. on Materials for Service in Extreme Conditions* (Kiev, 29–30 Sept. 2009), 101–105.



# CAPACITOR-DISCHARGE STUD WELDING IN VACUUM

B.E. PATON, D.M. KALEKO, A.R. BULATSEV and V.F. SHULYM  
E.O. Paton Electric Welding Institute, NASU, Kiev, Ukraine

Given are the results of investigations into capacitor-discharge welding of studs of aluminium-magnesium alloy AMg3 and stainless steel 10Kh18N9T under conditions of medium and high vacuum. It is shown that a high-current short-time pulsed discharge, at which the major part of evaporated metal remains in the gap between the mating surfaces, can be used for vacuum butt welding of compact-section parts to a sheet material. It is experimentally proved that up to M6 diameter studs can be welded at pressure of 1.33 Pa with a static tensile strength value of the joints being equal to that of the stud material.

**Keywords:** capacitor-discharge welding in vacuum, arc discharge, stud welding, aluminium alloy, stainless steel, volt-ampere characteristics, macrostructure, mechanical properties

Futurological research conducted by many scientists unambiguously shows that survival of the mankind at an accelerated consumption of different kinds of earth resources is possible only on a condition of exit into outer space. Minerals have already been found on the Moon with the help of space vehicles. Moreover, the absence there of atmospheric screening of solar radiation makes it possible to use the inexhaustible (within the historical time limits) energy of the Sun to meet the human demands which grow in geometric progression.

Discussions have been resumed in recent years on the expediency of construction of research laboratories on the Moon and planets of the solar systems. In 2004, the President of the United States presented a new space program, in which much consideration was given to exploration of interplanetary space. According to the Administration plans, American astronauts should create a station on the surface of the Earth satellite for «sustainable course of long-term exploration».

Therefore, it is timely to state [1] that «space vehicles and stations, as well as infrastructure of lunar outposts designed for long-term operation in space, should be fitted with welding hardware systems, allowing performance of mounting and repair operations in construction and operation of facilities, and the vehicle and mission crews should master the basic welding technologies and should have practical skills of performance of the above operations».

The E.O. Paton Electric Welding Institute of the NAS of Ukraine has accumulated a wide experience [2] in welding of metals under vacuum and zero gravity conditions. Also, the Institute initiated experiments on welding of metals in outer space using the hardware and technology it had developed. As established in the course of work on a sheet material [3], compared to electron beam welding all the rest of the welding methods have drawbacks that hamper their use in space.

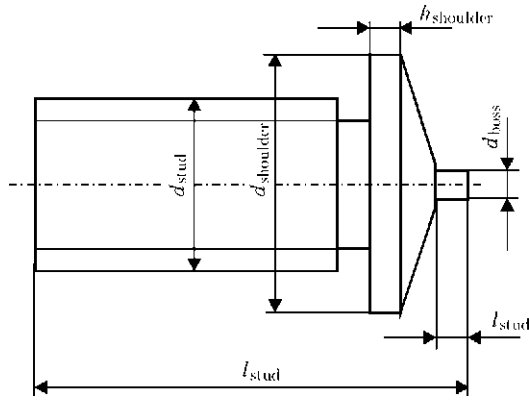
However, conditions of mounting operations on space facilities and their repair in space require wider ranges of the parts welded by using fastening elements, among which the most extensively used ones are studs of different types and designs.

All the above-said determine interest in verification of the possibility of providing an arc discharge of a millisecond time range in vacuum, as welding of studs with the arc burning at a discharge of capacitors takes place exactly in this time interval.

The authors are aware of only one study [4] on welding of studs under conditions simulating the space environment. The experiments were carried out with M5 diameter studs of aluminium alloys Al5000 (Al-Mg) and Al2319 (Al-Cu), as well as of stainless steel SUS 305 (12Kh18N12). Vacuum conditions were limited by capabilities of the laboratory equipment, i.e. to  $10^{-4}$  torr (13.3 Pa). Substantial differences between welding in low and high ( $10^{-5}$  torr) vacuum are shown below. Therefore, the previous experience does not allow reliably estimating the possibility of using capacitor-discharge stud welding in outer space. Moreover, study [4] gives no electrical characteristics of the process or numerical indicators of strength, nor does it describe metallographic examinations of welded specimens.

In our experiments we used unit K747MV developed by the E.O. Paton Electric Welding Institute as an energy source [5]. Instead of a conventional welding gun we employed a welding head mounted on a rack. The head was placed inside a vacuum chamber and was controlled by using a remote control panel, and it performed the same operations as the welding gun.

The experiments were carried out with M4 and M6 diameter studs of the RT type, made from AMg3 and 10Kh18N9T in compliance with ISO 13918 (Figure 1). The choice of the materials corresponded to the space application conditions [6]. According to the standard, sizes of a stud do not depend on the material used to make it. The M4 and M6 diameter studs had the following sizes:  $l_{\text{stud}} = 20$  mm,  $h_{\text{shoulder}} = 1.2$  mm,  $d_{\text{shoulder}} = 5.5$  and 7.5 mm (for M6),  $d_{\text{boss}} = 0.65$  (for



**Figure 1.** Design sizes of stud RT for capacitor-discharge welding (M4) and 0.75 mm (for M6), and  $l_{boss} = 0.55$  (for M4) and 0.80 mm (for M6).

Welding in forevacuum ( $10^{-2}$  torr) and in high vacuum was performed at the parameters providing a strong joint under atmospheric conditions. According to ISO 14555:2006, the joint is considered strong when it withstands bending of a stud to  $60^\circ$ . If standard tests confirmed the preservation of strength of the joint, the welding parameters were regarded as satisfactory, the process was subjected to oscillography (Textronic TDS2000B), and photoregistration of the bend test results was carried out.

Two main methods for capacitor-discharge stud welding are available: with preliminary gap and with preliminary contact [7]. Both methods can be used for welding of stainless steel, but aluminium alloys can be well welded only with the preliminary gap. However, even the first experiments in the vacuum chamber showed that the method with the preliminary contact even in forevacuum failed to provide the consistently strong joints on the M4 studs made from steel 10Kh18N9T. Analysis of oscillograms (Figure 2) indicated that in welding with the preliminary contact the time of the arc discharge phase was more than twice as long as burning of the arc in welding with the preliminary gap. Moreover, the discharge current with the first method was also higher than with the second method. As a result, metal intensively evaporated from the welding zone in welding with the preliminary contact, and the remaining amount of metal

Parameters of welding of alloy AMg3 and steel 10Kh18N9T

Material	Stud diameter	Charging voltage, V	Length of initial gap, mm	Compression force, N
AMg3	M4	100	2.5	104.6
	M6	180	3.0	104.3
10Kh18N9T	M4	120	2.2	104.9
	M6	140	2.0	105.0

*Note.* Capacitance of capacitor bank was 96 mF in all experiments.

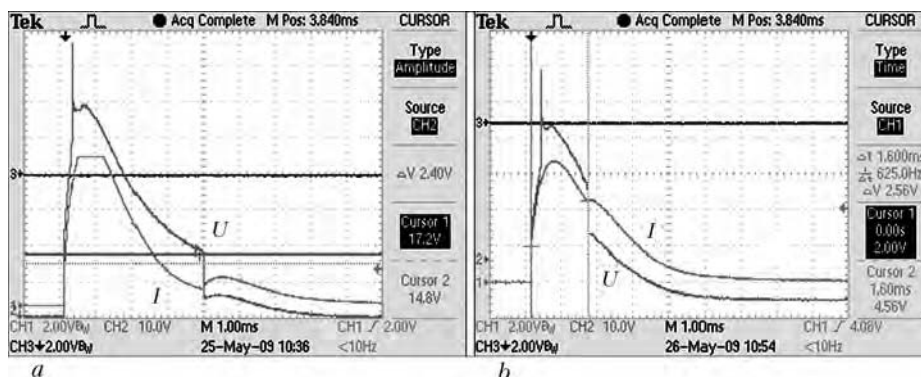
was insufficient to provide a strong joint. Undercuts along the perimeter of the joint also indicated to this character of the process.

Proceeding from this fact, all further experiments were carried out by the method of capacitor-discharge stud welding with the preliminary gap.

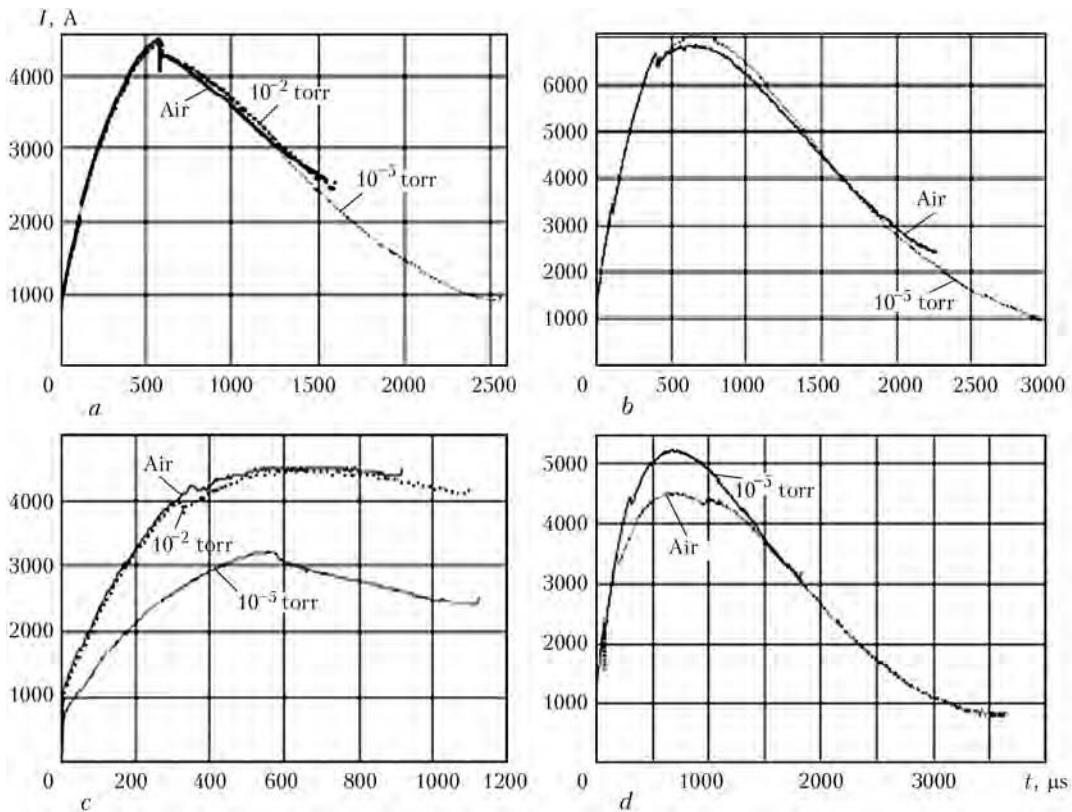
Parameters of welding of the investigated joints are given in the Table. They were kept constant for welding under atmospheric and low pressures in order to further compare characteristics of the arc and welded joints.

In welding of the aluminium alloy studs the values of current (Figure 3) and voltage (Figure 4) hardly depend on the air pressure. In welding of the steel studs in high vacuum there is an increase in the «incubation» time between the initial contact of the pieces welded and «explosion» of a thin boss made at the stud end and designed for ignition of the arc (the time moment of the «explosion» is marked by a decrease of the current). As the capacitor-discharge loop is closed even at a slight touch of the mating surfaces, the initial contact causes explosion of the microrelief and excitation of the arc between the tip of a thin boss and surface of a sheet which the stud should be welded to. The presence of the arc is evidenced by increase in voltage above 10 V, this being characteristic of the arc discharge.

Then the thin boss is heated by two sources, i.e. by the arc at the tip and by the flowing current. Dispersion of the initial microarc vapours in vacuum leads to decrease in the effective power of the arc. As



**Figure 2.** Oscillograms of current and arc voltage at discharge of capacitors in low ( $10^{-2}$  torr) vacuum in welding of M4 diameter studs of steel 10Kh18N9T with preliminary contact (a) and preliminary gap (b) (capacitor charging voltage – 120 V, capacitance – 96 mF)

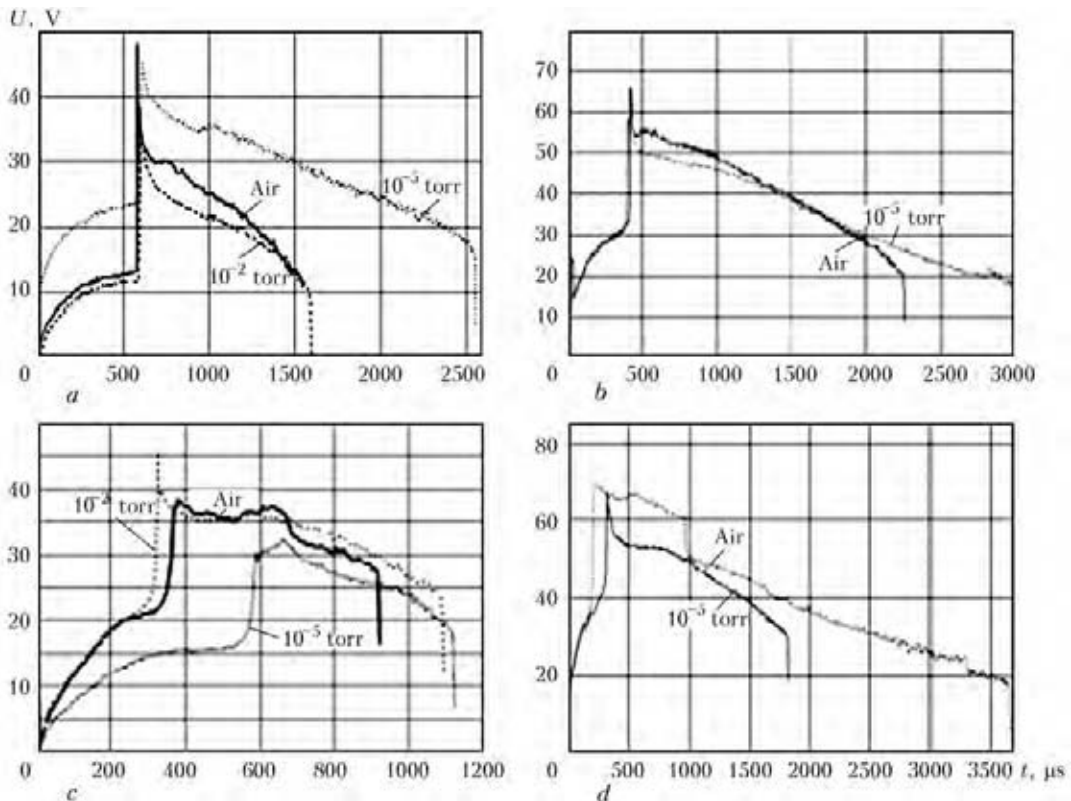


**Figure 3.** Current in capacitor-discharge stud welding under different air pressures: *a, b* – alloy AMg3; *c, d* – steel 10Kh18N9T; *a, c* – M4; *b, d* – M6

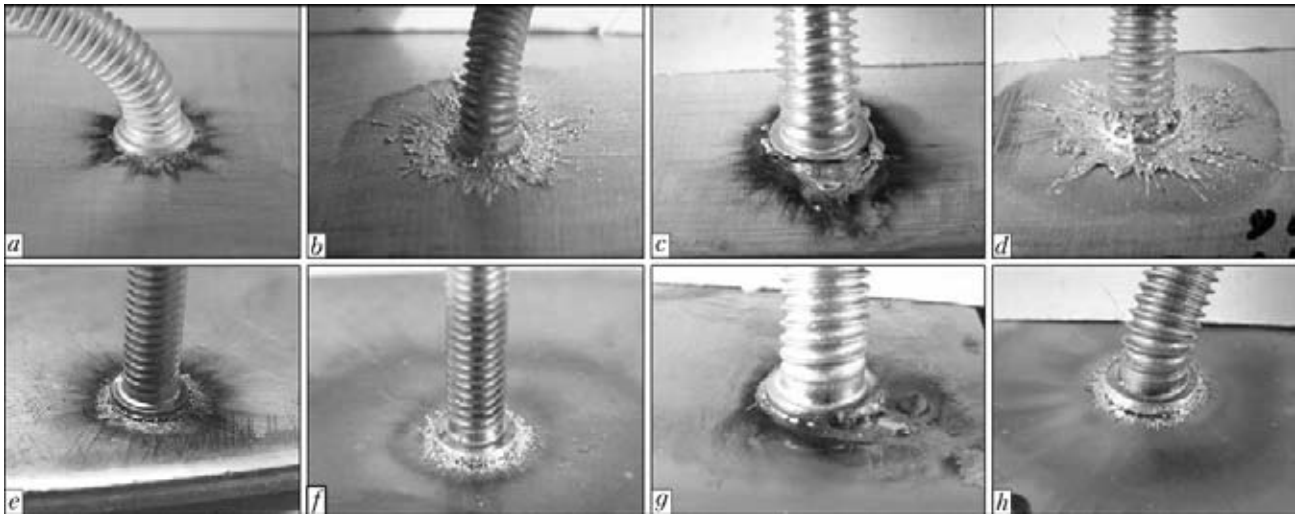
proved by the calculations based on the oscillography data, despite extension of the «incubation» time in welding in vacuum compared to welding under atmospheric pressure (M4 stud – 588 and 366  $\mu\text{s}$ , respectively), the energies released on the pieces welded

become approximately identical by the moment when the discharge transforms from the microarc to arc one (49.2 and 50.9 J, respectively).

In welding of the M6 diameter stud, because of a 1.5 times increase in length of the boss compared to



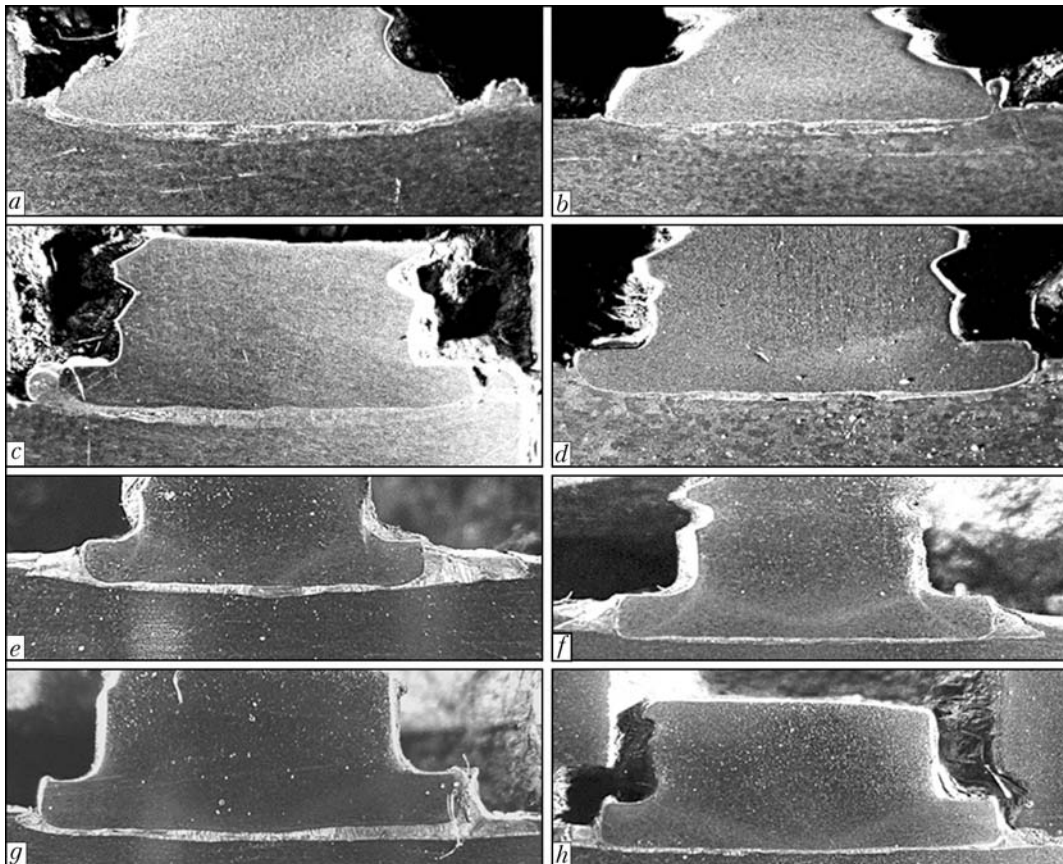
**Figure 4.** Voltage at pieces welded (*a-d* – same as in Figure 3)



**Figure 5.** Appearances of the welded joints on M4 (*a, b*) and M6 (*c, d*) studs of alloy AMg3, and M4 (*e, f*) and M6 (*g, h*) studs of steel 10Kh18N9T made under atmospheric pressure (*a, c, e, g*) and in vacuum of  $10^{-5}$  torr (*b, d, f, h*)

the M4 diameter stud (see Figure 1), an insignificant increase in diameter causes a substantial growth of the role of the internal source of heating by the flowing current. To add to it, there is a decrease in heat removal from the boss into the bulk of the stud, which leads to shortening of the time of heating of the boss to evaporation, compared to the M4 diameter stud (316  $\mu$ s in vacuum and 192  $\mu$ s under atmospheric pressure).

However, the ratios of the «incubation» time in welding of the M4 and M6 diameter studs in air and in vacuum being approximately the same, the energy released during this time on the pieces welded is much lower in welding of the M6 diameter studs in air (15.2 J) than in welding in vacuum (35.3 J), at which decrease in the effective power of the microarc is compensated for by extension of the time during which the current flows through the thin boss.



**Figure 6.** Macrostructures of the welded joints produced under atmospheric pressure (*a, c, e, g*) and in high vacuum (*b, d, f, h*) on M4 (*a, b*) and M6 (*c, d*) diameter studs of alloy AMg3, and M4 (*e, f*) and M6 (*g, h*) diameter studs of steel 10Kh18N9T joined to sheets of aluminium and stainless steel, respectively





Resistance of the arc under all the conditions investigated, except for welding of the M6 diameter steel studs, grows with decrease in the air pressure, this corresponding to the classical concepts of the arc discharge burning in gas environment [8]. In welding of the M6 diameter steel studs intensive evaporation of the boss causes a short-time local growth of pressure and dispersion of the vapours at a high initial rate, this leading to a shorter time of arcing determined by the time of levelling of the pressures in the arc gap and of a spring of upsetting of the welding head (when they are equal, the stud is lowered onto the sheet).

In the rest of the variants investigated the duration of the welding process in vacuum is longer than in air. This is related to the fact that evacuation in welding of the aluminium studs causes increase in the arc voltage, which at a constant current leads to intensification of evaporation. Extension of the process duration (Figure 4) in the experiment with the M4 diameter steel studs was caused by a lag of the main arc excitation phase due to a drop of the initial arc current (see Figure 3).

According to ISO 14555:2006, the joints with the studs welded are visually examined to check the absence of undercuts, breaks in the weld beads and other types of discontinuities. All the joints met requirements of the standard. As seen from Figure 5, the main difference between the joints produced under atmospheric pressure and in vacuum lies in increase in the area of splashing of molten metal from the welding zone taking place in vacuum. This can be explained by the fact that the counteraction of metal vapours that damp the impact of a stud onto the molten metal pool on the sheet surface under the effect of the welding head spring decreases under the vacuum conditions. Also, this is evidenced by a halo of the metal vapours in the form of a dense oxide layer on the surface of a joint welded under atmospheric pressure,

and in the form of a transparent but large-diameter layer of soot in welding in vacuum.

As noted above, all the joints welded at the optimal parameters withstood bending to an angle of not less than 60°. Static tensile tests of the welded joints showed that they all fractured in the base metal of a stud, far from the joining zone.

It can be seen from photos of the sections (Figure 6) that thickness of the molten metal solidified in the joint decreased with transition from the atmospheric pressure to the high vacuum, despite an increased duration of the discharge, which takes place in the majority of cases, at an almost unchanged current. This confirms the conclusions made from analysis of specimen appearances.

Therefore, the experiments proved the possibility of welding the up to M6 diameter studs from aluminium alloy AMg3 and stainless steel 10Kh18N9T by the capacitor-discharge method in vacuum, the resulting welded joints having strength equal to that of the stud material.

1. Paton, B.E. (2009) 25 years of welding in open space. *The Paton Welding J.*, **7**, 2–6.
2. (2003) *Space: Technology, Materials, Structures*. Ed. by B.E. Paton. London: Taylor & Francis.
3. Shulym, V.F., Lapchinsky, V.F., Demidov, D.L. et al. (2003) Peculiarities and further development of welding in space. In: *Ibid.*, 42–49.
4. Masubuchi, K., Imakita, A., Miyake, M. (1988) An initial study of remotely manipulated stud welding for space applications. *Welding J.*, **4**, 25–34.
5. Kaleko, D.M., Kononets, B.I., Oseledko, N.N. et al. (1991) Unit K747MV for capacitor-discharge stud welding. *Svarochn. Proizvodstvo*, **6**, 25–27.
6. Paton, B.E., Kubasov, V.N. (1970) Experiment on welding of metals in space. *Avtomatich. Svarka*, **5**, 7–12.
7. Kaleko, D.M., Lebedev, V.K., Chvertko, N.A. (1999) Processes of welding using the arc discharge of the capacitors. *Welding and Surf. Rev.*, Vol. 13. Amsterdam: Harwood Acad. Publ., 1–148.
8. Kaptsov, N.A. (1950) *Electric phenomena in gases and in vacuum*. Moscow; Leningrad: Gostekhteorizdat.

# FIELDS OF APPLICATION OF MAGNETIC-PULSE WELDING (REVIEW)

M.A. POLESHCHUK, I.V. MATVEEV and V.A. BOVKUN  
E.O. Paton Electric Welding Institute, NASU, Kiev, Ukraine

The review considers the main directions of investigation of magnetic-pulse welding. Weldability of the combined welded joints is evaluated, and fields of application of this process are given.

**Keywords:** magnetic-pulse welding, directions of investigations, tubular products, equipment, weldability, fields of application of magnetic-pulse welding

Magnetic-pulse welding (MPW) is used in industry in a course of several decades and its place in modern industrial production and tendencies of realization are to be determined and evaluated.

Monitoring of dynamics of publications (electronic documents in preference) with fetching by years and filtration on key word combination in a text was carried out for quality evaluation of tendencies (trend) of scientific-and-practical activity of the investigations and MPW application at present stage. Such current search systems as PdfQueen, FreePatentsOnline, Google-Scholar (Google Academy), Scirus, 2dix, PdfSearch, etc. (Figure 1) were used at that.

Google Scholar system having functions of fetching by years and filtration on exact word combination was applied as a main search system. It should be noted that many companies are not tend to put data on manufacturing peculiarities of release of their products, including MPW application, in open publishers. In this connection searching in this direction is complicated and indirect methods are to be used for analysis and opinion of experts should be relied on.

Number of educational centers in developed countries (University of Waterloo, Technische Universitat Dortmund, Fraunhofer Institute for Materials and Beam Technology IWS, Ohio State University, Wuhan University of Technology, Osaka University, Tokyo Metropolitan College of Technology, Belgian Welding Institute, etc.) [1–6] deal with the theoretical issues of MPW, and research groups of many leading automakers and airspace companies (PST, DANA, PULSAR, MAXWELL MAGNEFORM, etc.) work in the field of industrial development and implementation.

Investigations of theory and practical application of MPW have been carried out during decades in CIS countries immediately after its development in the USSR [7–9]. Number of publications on this theme against a background of increase is relatively small and number of publications on practical application of MPW is still smaller. Obviously, this is concerned with general condition of economy in these countries.

E.O. Paton Electric Welding Institute, Kharkov Polytechnic Institute, M.V. Khrunichev State Research-and-Production Space Center, Don Polytechnic Institute, Samara State Aerospace University with Samara Center of MPTM and etc. are the main centers of scientific-and-practical activity in the field of magnetic-pulse treatment of metals and MPW in CIS countries.

MPW is mainly used for joining of tubular products in the world practice. Welding of sheet products is yet mainly at the stage of research workup.

The main obstacle for MPW implementation is, apparently, a relative high cost of equipment, i.e. initial price of the unit makes from 100 thou USD, regardless all safety of modern equipment for MPW (inductors can carry up to 2 mln of pulses) and its high efficiency (minimum 6 welding pulses per minute; limitation is a time of process of loading/unloading of parts).

Another restriction is a necessity of application of advanced safety measures (high voltage, strong magnetic fields, danger of inductor breakdown) which require significant investments in addition. However, this problem can be brought to absolute minimum [10] in process of robotization and automation.

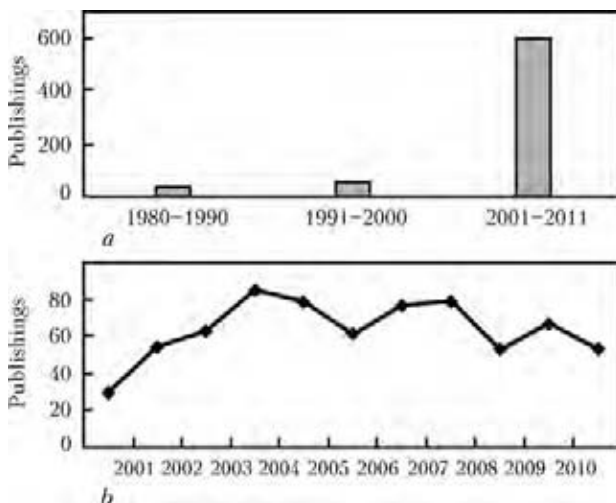


Figure 1. Dynamics of publishing in 1980–2011 (a) and 2000–2011 (b)

Table of weldability of tubular parts using MPW method

Outside pipe	Inside pipe												
	Al series 1000	Al series 3000	Al series 5000	Al series 6000	Al series 7000	Cast aluminum	Copper	Bronze	Carbon steel	Stainless steel	Nickel	Magnesium	Titanium
Al series 1000	+	+	+	+	+	+	+	+	+	+	-	+	-
Al series 3000	+	+	+	+	+	+	+	+	+	+	-	-	-
Al series 5000	+	+	+	+	+	+	+	+	+	+	-	+	-
Al series 6000	+	+	+	+	+	+	+	+	+	+	-	+	-
Al series 7000	-	+	+	+	+	+	+	+	+	+	-	-	-
Cast aluminum	-	-	-	-	-	-	-	-	-	-	-	-	-
Copper	-	-	-	-	-	+	+	+	+	+	-	-	-
Bronze	-	-	-	-	-	+	-	-	+	-	-	-	-
Carbon steel	-	-	-	-	-	-	-	-	+	+	-	-	-
Stainless steel	-	-	-	-	-	-	-	-	-	+	-	-	-
Nickel	-	-	-	-	-	-	-	-	+	-	+	-	+

Note. «+» means weldability of combination of materials, «-» absence of weldability.

Probably, MPW will become more available in the foreseeable future as the progress in the field of pulse energy storages continue (in this case special high-voltage pulse capacitor) and their production cost reduces (the price makes more than half of the cost of all MPW equipment). This is highly possible since significant scientific-and-practical and financial resources are concentrated in the field of applied physics and military-industrial complex at present time. These resources are directed on development of mobile systems of electromagnetic damaging, mobile electromagnetic guns (railotrons) and lasers in which high-voltage capacitor energy storage is one of the main energy components. Therefore, more effective capacitor systems can appear soon in civil fields of industry that allows developing available stationary or even mobile systems of MPW.

Such joints as aluminum-aluminum, aluminum-copper, aluminum-magnesium, aluminum-titanium, copper-copper, copper-steel, copper-bronze, nickel-titanium, nickel-nickel, steel-steel are made at present time in industry using MPW. Table of weldability, given in study [11], is recommended to use for tubular parts.

First of all for automakers are interested in practical application of MPW. Therefore, independent companies on development and implementation of magnetic-pulse techniques and technologies (DANA, PULSAR, PST, MAGNEFORM, etc.) direct the majority of their developments toward this sector. Respectively, manufacturers of MPW equipment get significant part of their profit exactly from automaker sector of industry.

Possibility of welding of dissimilar metals as well as simplicity of the process, high level of automation, absence of thermal deformations, good quality of welding and reproducibility of results, elimination of cleaning and usage of consumables (welding wire, gases), absence of necessity in local exhaust ventilation due to lack of harmful emissions, extremely low percent of rejects and etc. [12] attract the manufacturers in this case first of all.

Application of MPW in the motor car construction is relatively small in comparison with other technologies, but has stable tendency to growth. Experts claim that MPW has significant potential and real mass expansion [13] is foreseen in the nearest years.

Technology and equipment for MPW created by DANA (Dana Holding Group) Corporation, being the largest manufacturer and supplier of assemblies and parts for automobile market, are developed mainly for own needs of the company in contrast to «pure» companies-developers (PULSAR, PST, etc.). One of the six subdivisions of the company (Spicer Driveshaft) specializes on manufacture of main shafts including by MPW (Figure 2). Wide implementation of MPW according to assessment of DANA specialists allows creating the lightweight frames and other elements of automobile structures from dissimilar metals that result in 70 % weight decrease and 10 % reduction of fuel consumption. This, in turn, cut down harmful emissions in atmosphere including during manufacture of automobiles («green technology») [14].

Schweisstec Exhibition taken place in Stuttgart became a prominent event for motor car construction in whole and MPW, in particular. First in the world

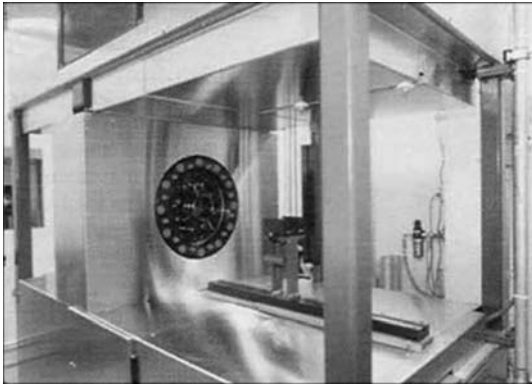


Figure 2. MPW unit at «Spicer Driveshaft» plant

lightweight frame of body of passenger car consisting of high-strength aluminum, steel and copper elements, wholly welded using MPW (Figure 3) [15], was presented by PST company (PST Products GmbH) on the Exhibition.



Figure 3. First in the world lightweight frame of car body from dissimilar metals, wholly manufactured using MPW

Developers outline the following advantages of the technology at that:

- complete absence of thermal deformations;
- welding of dissimilar metals (aluminum–steel, aluminum–copper);
- 35  $\mu$ s duration of welding pulse;
- possibility of performance of straight-line welded joints of up to 3 m length.

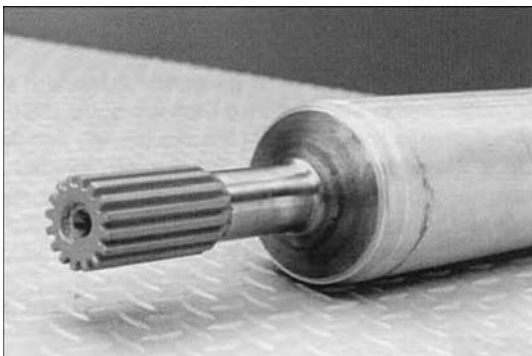


Figure 4. MP-welded steel–aluminum shaft

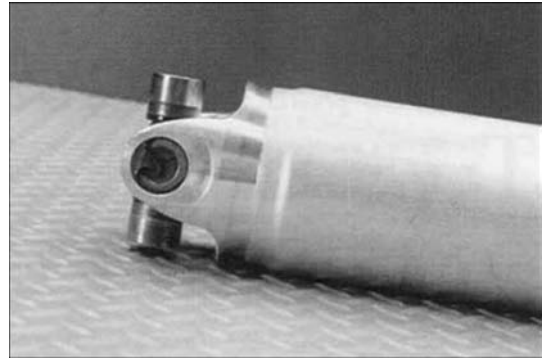


Figure 5. Aluminum (Al–Al) shaft

Vector of development of assembly technology lying in maximum possible replacement of all methods of fusion welding by MPW process as well as vector of investments in the nearest future are determined here as a matter of fact. In turn, this can indicate a direction for investigations and developments.

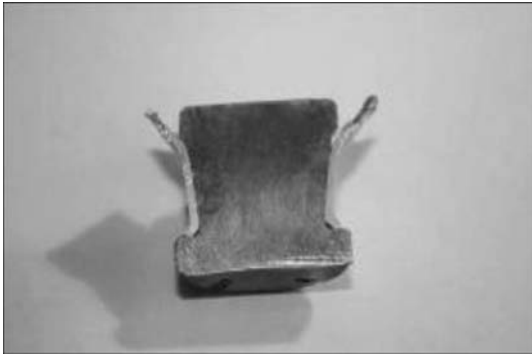
A list of some automobile assemblies and parts being manufactured using MPW (Figures 4–11) is given below [13, 16–18], i.e. shock-absorbers (aluminum or steel); elements of suspension (dissimilar metals); components of chassis; block elements; safety crash-boxes; elements of automobile air-conditioners; high-pressure gas vessels; oil filters; elements of main shaft; elements of lightweight seats; elements of fuel pipes, joints of frame elements; elements of exhaust systems [15].

Manufacture of aluminum–steel main shafts with the help of MPW allows significantly reducing their weight. At that noticeable increase of efficiency, improvement of ecology, reduction of wastes and rejects virtually to zero are observed [12].

PULSAR (Pulsar Ltd.) claims that they have invested more than 100 man-years in the development and industrial finishing of MPW. Now the company starts impetuous implementation of this technology all over the world. Thus, recent implementation of Pulsar MPW 25 unit on an assembly line of receiver-dryers of automobile air conditioners at the plant of famous manufacturer of car components (TI Auto-



Figure 6. Receiver of car air-conditioner



**Figure 7.** Fragment of cross-section of copper-aluminum joint 25 mm in diameter

itive Company) allows replacing nonconsumable electrode welding and reaching efficiency of 1000 assemblies per shift as well as increasing quality of parts and reducing percent of reject (Figures 7 and 8) [19].

Application of MPW method in assembly of bodies



**Figure 8.** Aluminum ring MP-welded to steel bolt

of fuel elements (fuel slugs) for the needs of nuclear power engineering is still under investigation. Undoubtedly, it will find wide application (Figure 11). This technology is more preferable in series of cases than others [20]. High quality and reproducibility of results, simplicity, absence of direct contact with clad surface of body appearance of new materials for bodies (from list of clad ferrite-martensitic and oxide dispersion-strengthened steels) accompany this process [21, 22].

Constantly increasing demand in permanent joints of parts from dissimilar materials exists in the aerospace field. MPW is an ideal method for joining of such dissimilar metals as titanium-nickel. Brazing or non-



**Figure 9.** Fuel filter manufactured using MPW



**Figure 10.** Sample of MP-welded main shaft (aluminum-steel) after successful strength tests in torsion

consumable electrode welding [10] is used at present time in manufacture of the fuel pipes for aerospace designation. Boeing Company, in particular, applies MPW for manufacture of high-pressure pipeline accessories (hydraulics) [23].

Process of MPW of tubular structures with preforming (joint development with Dneprodzerzhinsk



**Figure 11.** Fragment of sample of MP-welded fuel slug

State Technical University) [24] is implemented at M.V. Khrunichev SRPSC. A new method of obtaining of stamped-welded closed structures from thin sheet materials (lightweight bodies of electric couplers) using magnetic-pulse technology was developed and implemented at the same place. Developers named it as resistant MPW with simultaneous heating of joint by induced currents and effect of pulse magnetic pressure, i.e. combination of MPW and resistance welding [25].

Impact-pulse method of welding was recognized the best for development of superconductor key with



**Figure 12.** Magnetic-pulse cutting (punching) of parts of automobile designation using elements of PST equipment in Fraunhofer IWU [28]

heat control in a form of Cu–Al–Cu sandwich for the needs of cryogenic technologies. Such a key characterizes by low heat contact resistance that makes MPW application highly perspective [26]. Positive practical results in welding of films on the basis of amorphous nickel («metallic glass») useful for the needs of manufacture of micro instrument with unique properties [27] were obtained with this method.

New process of magnetic-pulse punching (Figure 12) related to MPW and developed by the specialists of Fraunhofer Institute for Machine Tools and Forming Technology (Germany) is at the stage of finishing and pre-industrial implementation. Its difference lies in absence of wear-out of mechanical tool and extremely high speed of punching, i.e. 0.2 s (this operation is performed for 1.4 s with the help of laser technologies). This project is financed by Volkswagen Company [28].

Obtaining of joints by means of magnetic-pulse crimping and some other magnetic-pulse technologies can be referred to MPW related technologies.

## CONCLUSIONS

1. MPW and related technologies are efficient and constantly developing technologies with high research and practical potential requiring further research and design efforts.

2. Field of MPW application will grow in appearance of new materials.

3. Rise of technical and economic indices of equipment in particular due to reduction of its cost and increase of life time of elements will promote interest to MPW.

4. Technological aspects of MPW (improvement of weldability of existing materials, reduction of power-consumption of the process) as well as engineering developments for improvement of tools (for example, special types of inductors, etc.) become the object of investigation and development.

5. Some fields of industry are ready for mass implementation of MPW expecting in the next years.

1. Lenen, T., Siewert, T., Babu, S. et al. (2011) *Welding fundamentals and processes*: ASM handbook 6A. ASM Int.
2. Berlin, A. (2011) *Magnetic pulse welding of Mg sheet: A thesis for degree master of applied science in mechanical engineering* (Waterloo, Ontario, Canada, 2011), 10–11.
3. Hahn, R. (2004) *Werkzeuge zum impuls-magnetischen Warmfuegen von Profilen aus Aluminium und Magnesiumlegierungen*: Diss. Berlin.
4. Groche, P., Elsen, A. (2010) Fundamentals of EMPT-welding. Technische Universitat Darmstadt. In: *Proc. of 4th Int. Conf. on High Speed Forming* (Columbus, Ohio, USA, March 9/10, 2010), 40.
5. Zhang, Y., Babu, S., Daehn, G.S. (2010) *Impact welding in a variety of geometric configurations*. Ohio: State University.
6. Desai, S.V. (2010) Scaling relationships for input energy in electromagnetic. *J. Electromagnetic Analysis & Applications*, 2, 563–570.
7. Pismenny, A.S., Pentegov, I.V., Stemkovsky, E.P. et al. (2004) Calculation of modes of magnetic-pulse welding. *The Paton Welding J.*, 11, 13–16.
8. Pismenny, A.S., Pentegov, I.V., Stemkovsky, E.P. et al. (2009) Improved method for calculating magnetic-pulse welding conditions. *Ibid.*, 1, 18–21.
9. Filimonov, A.S., Bayanova, Ya.M., Metelin, I.V. et al. (2010) *Application of magnetic-pulse welding for producing of thin-wall small-sized parts of aircrafts*. Moscow: MGТУ im. N.E. Bauman.
10. Weber, A. (2002) The cold welding process is being used for more and more high-volume applications. *Assembly Magazine*, Aug., 3–6.
11. (2011) L'assemblage par impulsion magnetique – MPT magnetic pulse technology. Technopole. *dev.swi.heig-vd.ch/fr-ch/Micro/Documents/3-Magnetic-Pulse-Technology.pdf*
12. (1982) The next wave in manufacturing solid state cold welding. *www.ai-online.com/Adv/Previous/showissue.php?id=1982*
13. Magnetic pulse welding is Dana original. *www.mtiwelding.com/files/Automotive Engineering Intl Aug. 1998 MAGNETIC PULSE WELDING.pdf*
14. Information documents of Society Dana Corp. *www.atp.nist.gov/eao/sp950-3/danacorp.pdf*
15. PST products presents the world's first EMPT welded lightweight space frame at the Schweisstec fair. *etcna.metrics.ch/public/pstproducts\_press\_release\_spaceframe\_including\_photos.pdf*
16. Kallee, S.W. (2010) Industrialisation of electromagnetic pulse technology (EMPT) in India. *www.msm.cam.ac.uk/phase-trans/2010/IPM.pdf*
17. Schafer, R., Pasquale, P., Kallee, S. (2010) The electromagnetic pulse technology (EMPT): Forming, welding, crimping and cutting. *ing.dk/modules/fsArticle/download-ad.php?fileid=740*
18. Shribman, V. (2008) Magnetic pulse welding for dissimilar and similar materials. In: *Proc. of 3rd Int. Conf. on High Speed Forming* (Dortmund, 2008). *eldorado.tu-dortmund.de/bitstream/2003/27107/29.pdf*
19. TI automotive adopts pulsar magnetic pulse welding systems for automotive air-conditioning components leading global manufacturer of automotive HVAC systems to use pulsar MPW 25 to weld automotive dryers. *Auto spectator. www.autospectacor.com/cars/automotive-manufacturing/0023205-ti-automotive-adopts-pulsar-magnetic-pulse-welding-systems-automoti*
20. Hamilton, M.L., Gelles, D.S., Lobsinger, L.J. et al. (2000) Fabrication technological development of the oxide dispersion strengthened alloy MA957 for fast reactor applications. Richland: Pacific Northwest National Laboratory. *www.pnl.gov/main/publications/external/technical\_reports/PNNL-13168.pdf*
21. McGinley, J. (2009) Electromagnetic pulse technology as a means of joining generation IV cladding materials. European Commission JRC-ITU. In: *Proc. of 17th Int. Conf. on Nuclear Engineering ICONE 17* (July 12–16, 2009, Brussels, Belgium). *www.english.pstproducts.com/index\_html\_files/icone%2017\_FINAL%20version.pdf*
22. Shri, S.C. (2011) Chetal sodium cooled fast reactors. Kalpakam: Indira Gandhi centre for atomic research. *www.igcar.gov.in/gap\_web/1.htm?stl\_4\_2\_4*
23. Fischer, A., Bolser, D.R. (2006) *Electromagnetic pulse welding of fluid joints*. Pat. Appl. 20060208481 USA. Int. Cl. F16L47/00, F16L4700. Publ. 21.09.2006.
24. Batsemakin, M.Yu. (2007) *Technology of magnetic pulse welding of thin-wall tubular parts*: Syn. of Thesis for Cand. of Techn. Sci. Degree. Rostov-na-Donu.
25. Plotnikov, V.V. (2007) *Development of process and equipment for magnetic pulse welding of light-weight electric connector shells*: Syn. of Thesis for Cand. of Techn. Sci. Degree. Rostov-na-Donu.
26. Willekers, R.W., Bosch, W.A., Mathu, F. et al. (1989) Impact welding: a superior method of producing joints with high thermal conductivity between petals at very low temperatures. Vol. 29, Issue 9, 904–906. *www.sciencedirect.com/science/article/pii/0011227589902038*
27. Minev, R.M., Dimov, S.S., Koev, S.R. et al. Explosive welding of Ni-base amorphous foils for micro-tooling applications. *www.4m-net.org/files/papers4M2008/05-13/05-13.pdf*
28. (2010) It's a knockout. Engineers find a new way to punch holes through steel. *The Economist*, Jan. 14.

# EQUIPMENT FOR HEAT TREATMENT OF WELDED JOINTS ON PIPELINES

E.A. PANTELEJMONOV

E.O. Paton Electric Welding Institute, NASU, Kiev, Ukraine

Mobile system MKT 1420 of the equipment for heat treatment of welded joints on pipelines is described. Its capabilities are shown for optimization of the preset modes of heating using flexible electrical resistance heaters. Peculiarities of design are considered, and comparative characteristics of sectional resistance heaters intended for heat treatment of welded joints and local heating of pipelines are presented.

**Keywords:** heat treatment, welded pipelines, mobile system of equipment, resistance heaters

Heat treatment (HT) of welded joints on pipelines is sufficiently complex and labor-consuming technological process. Severe requirements on power, safety, transportability and service simplicity are made to the equipment and heating devices used for HT performance.

Special attention is made to issues of meeting and maintaining of accuracy of HT modes since the latter affect stress relaxation in the welded joints and their properties. Besides, nonuniform distribution of the temperature fields along the pipe length character for local heating of the pipeline can result in appearance of stresses higher than residual ones in a near weld zone [1]. A uniform heating of the welded joint is to be provided along the perimeter of pipe at minimum temperature difference on thickness of wall, especially, at its large thickness, for elimination of such an effect. This can be provided by means of maintaining or changing of the main parameters of HT, i.e. speed of heating, duration of holding at heating temperature and speed of cooling on specific program.

The mobile systems of the equipment, which should consist of power supply with start-up equipment, systems for measurement, control and regulation of technological parameters of HT, staff protection facilities and heating devices, can provide realization of regulated modes of HT of the welded joints. Self-contained operation and relatively small dimensions allows using mobile systems in a workshop at supply from stationary electric mains or under conditions of construction site at supply from mobile power stations.

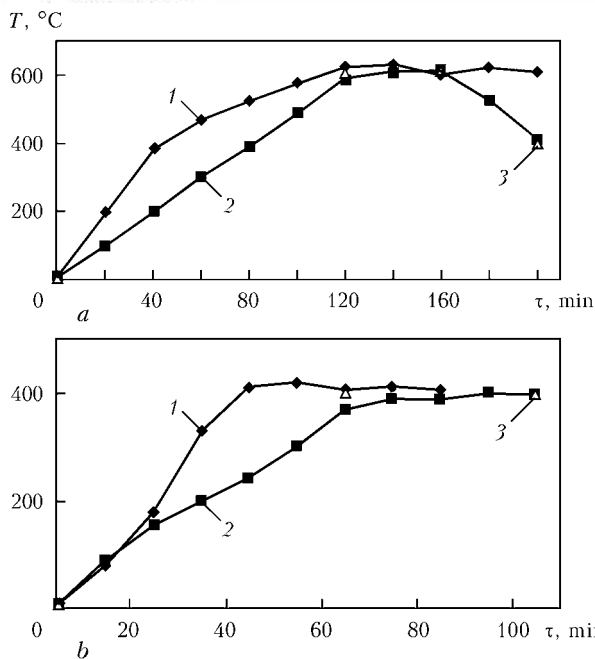
Mobile system MKT 1420 of the equipment (Figure 1) designed for performance of HT of horizontal and vertical welded joints on the pipelines of up to 1420 mm diameter, heating of joints on pipes before welding and accompanying heating in welding [2] was developed at the E.O. Paton Electric Welding Institute. Method of radiation heating is used at that. Works can be performed simultaneously by three chan-

nels on stand-alone program. Maximum distance of system removal from the heating devices makes 20 m. Rebuilt transformers TDFZh-2002 (heating channels 1 and 2) and TDFZh-1002 (heating channel 3) are used as heaters' power supply. Control of the system is performed from a single control panel by operator (heat-treater) in manual and automatic modes. Digital device TRTsO2P makes basis of a system for regulation of heating channels. There are 12 channels for connection of the thermoelectric converters for temperature measurement. Visual control of temperature on device indices and recording on data carrier are provided for. Indicators of failure of elements of the equipment, and devices for continuous and remote control of insulation resistance of the electric mains are imbedded in a scheme of the system. Equipment of the system including power cables for connection of the heating devices are mounted at open vehicle with rigid hitch haulage attachment. Control panel, heat-ventilation unit and working place of the operator are located in a warm block. Storage facility is organized for storing of heating devices. Engineering tools provide secure servicing of the system at supply from stationary electric mains or mobile electric station.

Peculiarities of operation of MKT 1420 system can be observed at local heating of pipes of  $\varnothing 1420 \times 18$  mm (steel 17G1S) and  $\varnothing 325 \times 9$  mm (steel 10). Flexible

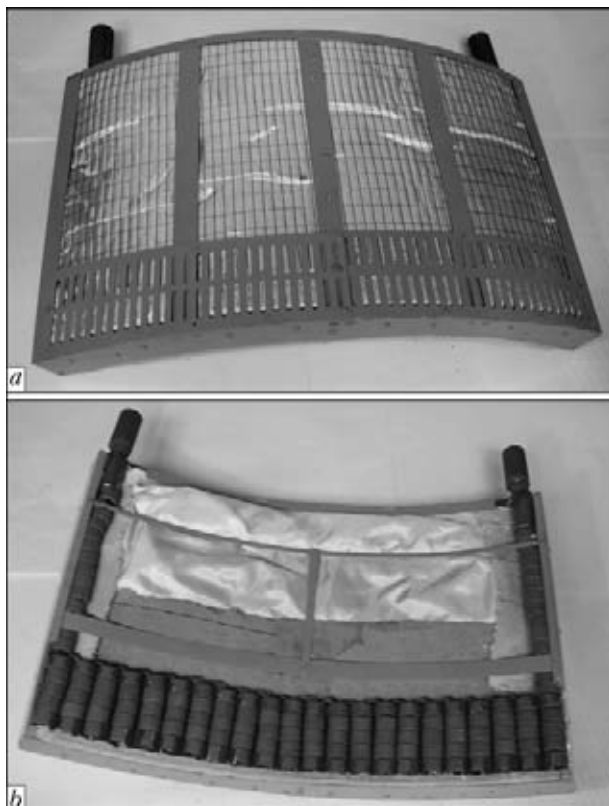


Figure 1. Mobile system MKT 1420 of the equipment



**Figure 2.** Dynamics of local heating  $T$  of pipes of  $\varnothing 1420 \times 18$  (a) and  $\varnothing 325 \times 9$  (b) mm at operation of MKT 1420 system in manual (1) and automatic (2) mode of control relative to preset mode (3)

electrical resistance heaters (FERH) were used as heating devices. Each FERH section is made in a form of flat spiral from two wires of 3.6 mm diameter. Amount of winds in the spiral equals 34 pcs [3], maximum current of the section is 120 A. Eight FERH sections were joined in two belts by four sections in heating of pipe of  $1420 \times 18$  mm. Two FERH sections



**Figure 3.** General view of SRH (a), and location of heating element (b)

were used for heating of  $325 \times 9$  mm pipe. Heat insulation of heating place consisted of TK-1 grade cardboard and MTPB sewing heat-insulated mats with cover from silica fabric and filling from kaolin wool.

Figure 2 shows the dependencies reflecting dynamics of pipe heating. The following parameters, i.e. speed 300 and 400 °C/h, temperature 600 and 400 °C, holding time 40 min, controlled cooling up to 420 °C during 20 min (for  $1420 \times 18$  mm pipe) and allowable temperature deviation  $\pm 20$  °C set the modes of heating of pipes of  $1420 \times 18$  and  $325 \times 9$  mm. Heating of pipe of  $1420 \times 18$  mm in manual mode was carried out up to the temperature of high tempering 620–650 °C (Figure 2, a) at total capacity of heating devices 59.5 kV·A. Average speed of heating was equal 300–320 °C/h. Average speed of heating made 180 °C/h in 400–650 °C range, 200 °C temperature value was achieved in pipe heating for not more than 20 min. This corresponds to the requirements of normative documents on modes of heating at high tempering of welded joints on pipelines [4] and technology of heating of pipe joints before welding.

Accuracy of adjustment of specified mode of heating in manual mode depends on qualification of operator. In this case temperature deviation for pipe of  $1420 \times 18$  mm made 200 °C in the specified interval 10–400 °C (Figure 2, a) and for  $325 \times 9$  mm pipe it was 170 °C (Figure 2, b). Temperature of pipe exceeded the specified value by 20–50 °C at stage of holding. Temperature deviation for pipe of  $1420 \times 18$  mm reduced up to  $\pm(5-8)$  °C including the stage of controlled cooling at transfer of the system in automatic control mode. Temperature deviation for pipe of  $325 \times 9$  mm lied at the level  $\pm 25$  °C for 10–400 °C range. Pipe temperature was 5–10 °C lower than the specified one at holding stage.

Special attention is made to fixation of sections of heaters and their outputs over the pipe at preparation of FERH or combined electrical resistance heaters to performance of HT. Sectional resistance heaters (SRH) were developed at the E.O. Paton Electric Welding Institute for the purpose of reduction of labouriousness of preparatory works and increase of safety of heating devices. Heating elements, heat-insulated cardboard and few layers of kaolin wool are located in a metal body with vent holes (Figure 3, a) in SRH basic design. The heating element (wire from nichrome) is realized based on FERH type. Ceramic insulators of IKN-302 type (Figure 3, b) protect the wire and outputs. Removable bushings manufactured from metal strip, with shoulders, limiting the displacement of insulators along the winding are used in the SRH design in contrast to FERH. The limiters are hold by spiral coupling belt. The outputs of heating element are rigidly fastened inside the body and equipped with reducing ceramic bushings for connec-



## Technical characteristics of the heaters

Parameter	FERH	SRH-1	SRH-2	SRH-3	SRH-4	SRH-5
Length of spiral of heating element, m	0.72	0.72	0.72	0.72	0.72	0.72
Width of spiral of heating element, m	0.08	0.10	0.10	0.10	0.10	0.10
Number of winds of spiral of heating element, pcs	22	22	22	22	22	22
Number of wires in spiral, pcs	2	2	3	3	3	3
Diameter of wires of spiral of welding element, mm	3.6	3.6	3.6	3.6	3.6	3.6
Area of heating, cm <sup>2</sup>	580	720	720	720	720	720
Thickness of pipe wall, mm	18	16	16	16	16	16
Insulation:						
cardboard + mats + mats	+	-	-	-	-	-
cardboard	-	+	+	+	+	+
cardboard + wool + cardboard	-	-	-	+	+	+
Arc voltage, V	44.3	38	36	36	43	46
Current, A	149	134	190	190	225	240
Capacity, V·A	6200	5090	6840	6840	9670	11000
Specific capacity, V·A/cm <sup>2</sup>	10.7	7.07	9.5	9.5	13.4	15.3
Volume capacity, V·A/cm <sup>3</sup>	5.94	4.42	5.94	5.94	8.39	9.58
Speed of heating in 100–400 °C range, °C/h	780	690	740	800	1200	1370

Note. Here, «+» means presence of insulation, «-» means its absence.

tion to current conducting cables. Setting of the interlocking devices over the SRH body for mutual joining in the belt and fixing around the pipe perimeter is provided for.

The Table shows the characteristics of SRH (version 1–5) and FERH. SRH designs differ in number of wires in the spiral of the heating element and heat-insulation of the device. SRH characteristics were studied at local heating of pipe from 17G1S steel of 1420 × 16 mm. The plugs were set at pipe ends. Temperature of heating was measured at points in outside and inside surfaces of the pipe at the center of heating element spiral. Difference of the temperature did not exceed 20 °C along the pipe thickness at all speeds of heating. FERH design (cardboard insulation and two layers of heat-insulated mats) provided higher speed of heating than SRH-1 (cardboard insulation) and SRH-2 (spiral from three wires, cardboard insulation). Introduction of additional insulation from cardboard and heat-insulated wool in the structure resulted in increase of speed of heating (SRH-3) at 5.94 V·A/cm<sup>3</sup> volume capacity of FERH, SRH-2 and SRH-3 heaters. Further rise of heating speed was achieved at increase of capacity of heaters (SRH-4, SRH-5).

$K = \Delta V / \Delta Q$  relationship, where  $\Delta V$  is the heating speed increment, and  $\Delta Q$  being the volume capacity increment (Figure 4), can be used for evaluation of efficiency of SRH structure. Increment of volume capacity by 1.52 V·A/cm<sup>3</sup> resulted in heating speed increment by 90 using FERH, 50 for SRH-2 and

110 °C/h for SRH-3. Current of heating element of FERH, SRH-2 and SRH-3 made not more than 70 A per wire. Some current overload (75 A per wire) is character for SRH-4. Increment of heating speed equaled 510 °C/h at increase of volume capacity of SRH-4 by 3.97 V·A/cm<sup>3</sup> and made 680 °C/h for SRH-5 at 5.16 V·A/cm<sup>3</sup>. However, service time of heating element can be reduced due to high load of SRH-5 by current (80 A on wire). SRH-3 has optimum characteristics since spiral of heating element from three wires and combination of heat insulation from cardboard and kaolin wool are used in its structure. The heater provides high speed of heating and possibility of its increment at insignificant current overload.

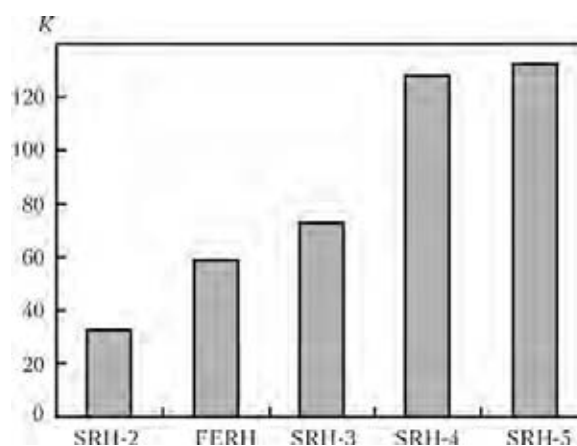


Figure 4. Index of efficiency of various heaters

Number of winds of the heating element, size and amount of SRH sections depend on pipe diameter. 12 sections of SRH-3 joined in two belts by six sections are to be used for local heating of 1420 mm diameter pipes using MKT 1420 system. Four sections should be connected in parallel to each heating channel of the system. Voltage of SRH-3 is lower than the nominal operating voltage of TDFZh transformers, common capacity of four SRH-3 does not exceed 30 kV·A and total consumed power of the system makes not less than 130 kV·A at that. Such a connection of the heating devices allows smooth adjusting of heating temperature along the pipe perimeter and providing equal current loading of all three phases of supply mains of MKT 1420 system.

**CONCLUSIONS**

1. It is shown that mobile system MKT 1420 of the equipment in assembly with FERH provides performance of HT of welded joint on pipelines of 1420 mm

diameter in accordance with the requirements of technical normative documents and high accuracy of adjustment of preset modes of local heating of pipes of Ø325 × 9 and Ø1420 × 18 mm at system operation in mode of automatic control.

2. SRH for local heating of pipelines was developed. It differs in higher efficiency of heating in comparison with FERH and simplifies the process of preparation of heating equipment for running.

1. Rojtenberg, S.Sh. (1982) *Heat treatment of welded joints of pipelines*. Moscow: Energoizdat.
2. Pismenny, A.S., Pantelejmonov, E.A. (2003) Complex of equipment for heat treatment of pipe butts in field environment. In: *Abstr. of Int. Conf. of Current Problems in Welding and Life of Structures* (24–27 Nov. 2003, Kiev, Ukraine). Kiev: PWI, 54–56.
3. Khromchenko, F.A., Korolkov, P.M. (1987) *Technology and equipment for heat treatment of welded joints*. Moscow: Energoatomizdat.
4. OST 36-50-86: Technological steel pipelines. Heat treatment of welded joints. Typical technological process. Introd. 01.01.87.

**NEWS**

**HIGH-FREQUENCY WELDING ELECTROCOAGULATOR**

E.O. Paton Electric Welding Institute developed a new generation PATON-MED™ EKV3-300 apparatus, intended for performance of various surgical procedures in medicine and veterinary practice. It provides a state-of-the-art solution of problems faced by surgery and enables practical implementation of the technology of high-frequency welding of soft live tissues.

Due to novel engineering decisions, performance of surgery with application of PATONMED™ EKV3-300 apparatus ensures:

- reliability of joining tissues without resorting to sutures, staples, medical adhesives, etc.;
- absence of tissue necrosis or foreign bodies in the wound;
- leak-proofness of the joints;
- decrease of blood losses, as well as shortening of surgery duration (speed of surgery performance increases by 30–40 %);
- absence of suppurations;
- accuracy and precision of tissue dissections;
- reliable hemostasis;
- shortening of patients rehabilitation duration in postoperative period;
- fast, convenient and reliable performance of surgical interventions;
- simplification of surgical procedures;
- absence of smoke during surgical interventions, as well as other factors adversely affecting surgeon’s health.

PATONMED™ EKV3-300 apparatus can be applied to perform operations in many surgical fields,

including general abdominal surgery, traumatology, pulmonology, proctology, urology, mammalogy, otolaryngology, gynecology, vascular surgery, operations on parenchymatous organs, ophthalmology, etc.

PATONMED™ EKV3-300 has four main operation modes: cutting, coagulation, manual and automatic welding. Each of the modes provides a broad possibility of selection of operation algorithms and working parameters of the process, depending on specific tasks.



Power source control is performed by microcontroller by special programs, which can be modified by the user preference, and a possibility of entering additional programs as required by the surgeons is also envisaged.

The apparatus is supplied with the basic kit of electric surgical tools (forceps and surgical clips). It can be also fitted with additional tools for open and laparoscopic surgery, which are made to Customer specification.

## Memorable Dates

# THEORY AND TECHNOLOGY OF SUBMERGED-ARC WELDING

*65 years ago the E.O. Paton Electric Welding Institute hosted the All-Union Scientific-and-Practical Conference dedicated to automatic submerged-arc welding. In his paper «Prospects for Future Development of Automatic Welding in the USSR» Evgeny O. Paton described a wide enabling potential of welding, based on the results of the pioneering integrated research conducted by the Institute.*

A wide application of welding in many countries during the Second World War revealed along with the advantages of the process also its drawbacks, including an unexpected, unpredictable fracture or cracking of welded structures (e.g. all-welded ships of the type of «Liberty» in the USA). As early as in 1943, Evgeny O. Paton began thinking about conversion of the automatic welding technology, endeavouring to apply new technologies to rapidly restore destroyed structures and speed up construction of ships, buildings and bridges. New problems had to be solved on a firm scientific basis. Soon after the Second World War, E.O. Paton used a system approach to addressing the problem of construction of all-welded structures. He united the scientific search, investigations and development of welding consumables, automatic devices and even special steels into a single package consisting of 25 subjects.

Boris E. Paton, Head of the Electrical Engineering Department, continued investigations initiated in 1943 to study the processes of arcing and melting within the welding zone, and peculiarities of operation of devices and power supplies in submerged-arc weld-

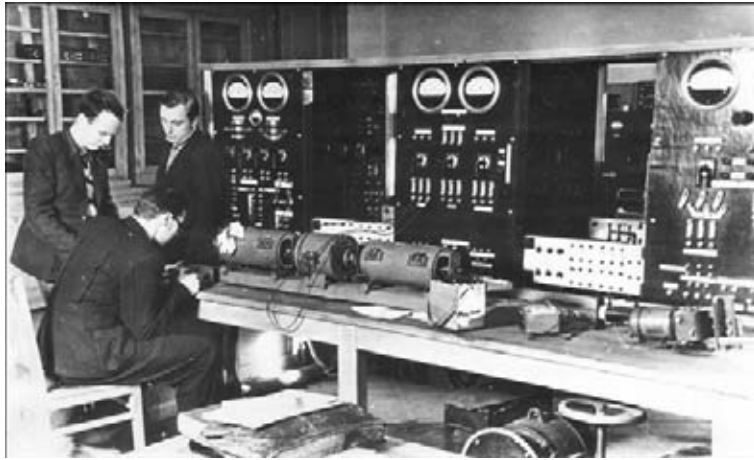
ing (including by filming using the X-ray apparatus). By the end of 1947, he identified conditions for providing the stable arc, specified the calculation formulae for consumable electrode temperature fields, and adjusted theoretical background for development of welding power supplies. Generalisation of these results served as a basis for the development of a new generation of welding units.

E.O. Paton realised that the scientific-and-technical progress would put forward increasingly higher requirements to service properties of materials. Therefore, an insufficient attention to evaluation of their weldability could lead to failure of the attempts to fabricate a reliable welded structure.

In the middle of the 1940s, the Electric Welding Institute, N.E. Bauman Moscow State Technical University and some other USSR institutions deployed the fundamental research to study causes of fracture of welded structures (E.O. Paton, G.A. Nikolaev, N.O. Okerblom, V.V. Shevernitsky, B.S. Kasatkin), establish dependence of strength of the joints on the processes of melting and solidification of the weld pool metal and distribution of temperatures (N.N.



Academician Evgeny O. Paton with participants of the Conference, 1947



At the electrical engineering laboratory of the Electric Welding Institute

Rykalin, K.V. Lyubavsky, V.I. Dyatlov, I.I. Frumin, D.M. Rabkin, A.M. Makara, B.I. Medovar, V.V. Podgaetsky, I.V. Kirdo, N.V. Shamanin, N.N. Prokhorov, A.A. Alov, G.L. Petrov et al.), and evaluate the effect of methods used to make steels and their chemical composition on weldability (A.M. Makara, A.E. Asnis, B.S. Kasatkin, S.A. Ostrovskaya, K.V. Lyubavsky, M.Kh. Shorshorov et al.). It should be noted that in that period the research in the above areas was carried out also in the USA, Great Britain and France.

Investigations into compositions, structures and properties of steels (mechanical tests, chemical analyses, determination of corrosion resistance, etc.) were conducted at a very high level. The assumption made by E.O. Paton on the negative effect of sulphide inclusions on the quality of a welded joint was confirmed. The nature of formation of hot cracks and causes of brittle fracture of welded structures were determined, and methods for comparative evaluation of weldability of steels were worked out. A result of this package of metallurgical and physical-chemical investigations was also the development of a metal featuring increased cold resistance and resistance to ageing, i.e. steel M16St3 (M.M. Dobrokhotov, B.S. Kasatkin, A.E. Asnis et al.). Metallurgists for the first time agreed with the requirement of welders to decrease the maximal content of carbon, sulphur and phosphorus in rolled steel. That created premises for selection of a rational welding technology, further improvement of welded joints and submerged-arc welding procedure, and for development of new arc welding methods. At that same period a series of fluxes were developed for automatic welding of steels (V.V. Podgaetsky, K.V. Lyubavsky, E.I. Lejnachuk, I.I. Frumin et al.). High-manganese flux of the AN-348 grade developed in 1947–1948 by a team of associates of the Electric Welding Institute and TsNIITMash is in use up to now and served as a prototype for the development of a number of new welding consumables.

In parallel with the research aimed at improvement of the quality of the weld metal, much effort was made to upgrade welding procedures. E.O. Paton posed the tasks to widen the range of structures welded and raise many times the speed of welding for their fabrication. Commercial production required immediate solutions to these tasks. A large quantity of vertical welds in restoration and construction of blast furnaces, bridges, tanks and other large-size structures were made manually. Productivity of pipe welding mills was limited only by the capabilities of the welding technology, and mainly by the welding speed. Results of investigations of the magnetic-hydrodynamic phenomena taking place in high-current arc processes were used for the development of submerged twin-arc welding with a speed of 160–200 m/h (B.E. Paton, V.K. Lebedev, S.L. Mandelberg).

In October 1947, the All-Union Conference on automatic welding was held in Kiev, at which E.O. Paton presented paper «Prospects for Future Development of Automatic Welding in the USSR». By that time the key areas of the welding science began to be formed, and requirements to the new welding equipment were identified. Welding production had the possibility to address the problems of assuring the high quality of weldments on a scientific basis with minimal expenditures. In compliance with the Resolution of the Council of Ministers of the USSR, it was planned to open new welding chairs at institutes of higher education and courses of training of operators. The Electric Welding Institute was assigned to provide the scientific and organisational support to all welding operations in the country. In 1948, a team of associates of the Electric Welding Institute published the «Automatic Submerged-Arc Welding» book, which summed up results of the first stage of elaboration of the domestic theory of submerged-arc welding.

*A.N. Kornienko, Dr. Sci. (History)*